Order Number 1333274

Software modification and implementation for, and analysis of, lidar data

Apte, Madhav Vasudeo, M.S.

The University of Arizona, 1988

U·M·I
300 N. Zeeb Rd.
Ann Arbor, MI 48106

PLEASE NOTE:

In all cases this material has been filmed in the best possible way from the available copy. Problems encountered with this document have been identified here with a check mark __✓__.

1. Glossy photographs or pages _____
2. Colored illustrations, paper or print _____
3. Photographs with dark background _____
4. Illustrations are poor copy _____
5. Pages with black marks, not original copy _____
6. Print shows through as there is text on both sides of page _____
7. Indistinct, broken or small print on several pages ✓
8. Print exceeds margin requirements _____
9. Tightly bound copy with print lost in spine _____
10. Computer printout pages with indistinct print _____
11. Page(s) _____ lacking when material received, and not available from school or author.
12. Page(s) _____ seem to be missing in numbering only as text follows.
13. Two pages numbered _____. Text follows.
14. Curling and wrinkled pages _____
15. Dissertation contains pages with print at a slant, filmed as received ✓
16. Other _____

_____

_____

SOFTWARE MODIFICATION AND IMPLEMENTATION FOR, AND ANALYSIS OF, LIDAR DATA

by

Madhav Vasudeo Apte

A Thesis Submitted to the Faculty of the

DEPARTMENT OF ELECTRICAL AND COMPUTER ENGINEERING

In Partial Fulfillment of the Requirements
For the Degree of

MASTER OF SCIENCE
WITH A MAJOR IN ELECTRICAL ENGINEERING

In the Graduate College

THE UNIVERSITY OF ARIZONA

1 9 8 8

STATEMENT BY AUTHOR

This thesis has been submitted in partial fulfillment of requirements for an advanced degree at The University of Arizona and is deposited in the University Library to be made available to borrowers under rules of the Library.

Brief quotations from this thesis are allowable without special permission, provided that accurate acknowledgment of source is made. Requests for permission for extended quotation from or reproduction of this manuscript in whole or in part may be granted by the head of the major department or the Dean of the Graduate College when in his or her judgment the proposed use of the material is in the interests of scholarship. In all other instances, however, permission must be obtained from the author.

SIGNED: Madhav Vasudeo Apte

APPROVAL BY THESIS DIRECTOR

This thesis has been approved on the date shown below:

John A. Reagan — April 20, 1988

J. A. REAGAN
Professor of Electrical and
Computer Engineering

Date

ACKNOWLEDGMENTS

Thanks are due to many past and present faculty, staff and students at the University of Arizona for their support of my efforts. Special thanks are due to Professor John Reagan for his continuing guidance, encouragement and patience over the years. Additionally, thanks are due him for his meticulous reading of the thesis manuscript and the numerous suggestions he made which improved it. Thanks are due to Professor Gerald Peterson, who provided access to computers at the University of Arizona, and to Dr. Theodore Williams, who provided the database software used in this work. The initial data acquisition for this work was partially funded by the Army Research Office Grant DAAG-29-78-G-0195 and follow-on contract DAAG-29-82-K-0081.

Thanks are due to present and past fellow graduate students for their support and many helpful discussions. These include Ian Scott-Fleming, John Garcia, Kurt Thome, John Chang, Tom Bruhns and David Buchhauser. The work builds directly on the efforts of previous graduate student James Spinhirne. Some of the staff members who have provided timely help are Juanita Maier, Sandy Sledge, and Barbara Jones. A note of appreciation goes to Erika Louie, who ensured that this work is in a form acceptable to the Graduate College. Kate and company are gratefully acknowledged for assistance in motivation and personal growth. I am indebted to many friends who have provided moral support during the course of this work.

This work could not have been completed without support from my family, notably my parents, Mr. V. K. Apte and Mrs. S. V. Apte, and my uncle and aunt, Mr. V. K. Apte and Mrs. V. V. Apte. Finally, special thanks are due to Denise Wieland, who put up with the strange hours, and without whom this past year would have seemed a lot longer.

TABLE OF CONTENTS

Page

LIST OF ILLUSTRATIONS 6

LIST OF TABLES. 8

ABSTRACT. 9

CHAPTER

1. INTRODUCTION. 10

1.1 The Advantages of a Lidar 11
1.2 Components of a Lidar System 11
1.3 The Operation of a Lidar 12
1.4 Background of the University of Arizona Lidar System 13
1.5 The Objectives of this Thesis. 15

2. THE LIDAR SOFTWARE 18

2.1 Data Acquisition 18
2.2 The Software 21
2.3 Program EDIT 26
2.4 Program AIMLESS 27
2.5 Program PIT 42
2.6 Program AER3 49
2.7 Program CAL. 57

3. RESULTS 65

3.1 The Concept of a Database and Its Capabilities 66
3.2 The Lidar Database: Categories of Data Sets. 67
3.2.1 A Typical Form for the Lidar Database 68
3.2.2 Number of Data Sets in Various Categories 72
3.3 Results of the Lidar Data Analysis . . 74
3.3.1 The S Ratio 76
3.3.2 Monthly Statistics of the S Ratio and the Optical Depth . 79

TABLE OF CONTENTS--Continued

		Page
	3.3.3 Height of the Mixing Layer (HMIX)	87
	3.3.4 Normalized Optical Depth and the S Ratio	87
	3.4 The Calibration Database	91
4.	CASE STUDIES	93
	4.1 Assessment of Horizontal Inhomogeneity	93
	4.1.1 Variation in the Gain-removed, Energy-and-Range Normalized Signal	94
	4.1.2 Variation in the Backscatter Coefficient	98
	4.1.3 Variation in the Sum of Backscatter Coefficient	102
	4.1.4 Assessment of Inhomogeneity Results	105
	4.2 A Classification of Extinction Profiles	110
	4.3 Effects of Input Parameters on the Integrated Slant Path Solution	123
	4.3.1 The Effect of the Calibration Constant as an Input	123
	4.3.2 The Effect of HMIX and S Ratio Estimate as Inputs	128
	4.4 Assessment of Particulate to Rayleigh Extinction Ratios above the Mixing Layer	129
5.	CONCLUSION AND RECOMMENDATIONS	134
	5.1 Conclusions	134
	5.2 Recommendations	135
	APPENDIX 1: THE DATABASES	138
	APPENDIX 2: FLOWCHARTS OF PROGRAM AER3	158
	LIST OF REFERENCES	171

LIST OF ILLUSTRATIONS

Figure		Page
2.1	University of Arizona monostatic lidar hardware block diagram.	19
2.2	Lidar data processing program order block diagram	24
2.3	Form of raw data (input to program EDIT). . . .	25
2.4	Form of data (output of program EDIT)	28
2.5	Plot of a shot return in the input to program AIMLESS at a zenith angle of 78.6^{o} on 21 May 1984.	30
2.6	Plot of a gain-removed, averaged shot return in the output of program AIMLESS, for 11 May 1981 at a zenith angle of 77.2^{o}	35
2.7	Slant range and effective vertical range for a zenith angle of 73.4^{o}	44
2.8	PSIG profile for a zenith angle of 0^{o} for 17 April 1980	47
2.9	PSIG profiles for all slant angles for 17 April 1980	48
2.10	Calibration plot for 23 April 1982, group II shots	61
3.1	A histogram of S ratio values	77
3.2	The standard deviation of the S ratio as a function of the S ratio	80
3.3	Average HMIX values per generic month	83
3.4	Inverse variance weighted average of S ratios per generic month	84
3.5	Average normalized TAUP at HMIX per generic month	85

LIST OF ILLUSTRATIONS--Continued

Figure		Page
3.6	Correlation between HMIX values (in Km) as deduced from PIT plots and AER3 plots	88
3.7	Normalized TAUP at HMIX as a function of TAUP at HMIX	89
3.8	Normalized TAUP at HMIX as a function of the S ratio	90
4.1	%SD of PSIG for all slant angles from program PIT for 12 May 1981	96
4.2	%SD of PSIG for the angles used in AER3 solution, from program AER3 for 12 May 1981 . .	97
4.3	%SD of BETAP for 12 May 1981 using method 1 . .	103
4.4	%SD of BETAP for 12 May 1981 using method 2 . .	104
4.5	PSIG profiles for 12 May 1981	112
4.6	Extinction cross-section profile for 12 May 1981.	113
4.7	PSIG profiles for 27 March 1980	115
4.8	Extinction cross-section profile for 27 March 1980.	116
4.9	PSIG profiles for 4 April 1980.	117
4.10	Extinction cross-section profile for 4 April 1980.	118
4.11	PSIG profiles for 23 January 1980	120
4.12	Extinction cross-section profile for 23 January 1980	121

LIST OF TABLES

Table		Page
2.1	Angle, sampling rate and range values for a typical lidar slant path data set	22
2.2	Definitions of acronyms used in the thesis. . .	33
2.3	Gainswitch index values for 9 shots at a zenith angle of 78.6 Degrees for 11 May 1981, as determined by program AIMLESS	40
3.1	List and definitions of field names in a lidar database record	69
3.2	A sample record from the lidar database	71
3.3	The number of data sets in each category of the lidar database	73
3.4	A sample record from the calibration database and definitions of the field names.	75
3.5	Arithmetic and inverse variance weighted means of lidar parameters	78
3.6	Monthly averages of lidar parameters.	81
4.1	Inhomogeneity computations.	106
4.2	Effect of varying calibration constant as input to AER3 for 21 May 1984	124
4.3	Effect of varying calibration constant as input to AER3 for 12 May 1981	127
4.4	Particulate/Rayleigh extinction ratio results .	132

ABSTRACT

The software system to process integrated slant path lidar data has been debugged, modified, documented, and improved in reliability and user-friendliness. The substantial data set acquired since 1979 has been processed and a large body of results has been generated. A database has been implemented to store, organize, and access the results. The lidar data set results--the S ratios, the optical depths, and the mixing layer heights are presented. The seasonal dependence of the lidar solution parameters has been explored. The assumptions made in the lidar solution procedure are investigated. The sensitivity of the S ratio and the particulate extinction coefficient to the system calibration constant is examined. The reliability of the calibration constant is demonstrated by examining the particulate to Rayleigh extinction ratio values above the mixing layer.

CHAPTER 1

INTRODUCTION

The earth's atmosphere consists of gases and aerosols. The distinction between gases and aerosols is primarily one of size. Aerosols are much larger than air molecules and range in diameter from about 0.01 micron to several microns. They may consist of dust, pollen, by-products of various man-made processes, and other airborne particles. Because of their size, aerosols interact rather strongly with visible and near-visible radiation. With manmade aerosol production increasing worldwide, they exert an increasing influence on the radiative transfer of solar radiation through the earth's atmosphere. To understand the radiative effects of atmospheric aerosols requires knowledge about their spatial extent and their physical properties. The distribution of aerosols as a function of height, along with their scattering and absorption parameters, are some of the key elements required in characterizing the radiative effects of aerosols.

Information about the atmosphere in general, and aerosols in particular, can be obtained via direct measurements, such as sampling from an aircraft or a balloon, or via remote sensing, such as by lidars. The acronym lidar stands

for LIght Detection And Ranging. A lidar is similar to a radar in principle, but it operates in the visible, or near-visible region of the electromagnetic spectrum. As the name implies, it gives information about the "range" of the sensed object. A signal is obtained which varies as a function of time, and, through the speed of light relation, distance. The signal may be analyzed to obtain information about scattering and extinction properties of the atmosphere.

1.1 The Advantages of a Lidar

With a lidar, the wavelength is short enough to be sensitive to scattering by aerosols and air molecules. Data may be acquired along a given path essentially "instantaneously," and repeated measurements may be taken along various azimuth and elevation angles to scan a volume of the atmosphere. With portable lidars, data may be taken from almost any location, including from aircraft and satellites. A well designed lidar system built with current technology can operate reliably for long periods of time. While a lidar system can be automated to a great extent, a certain amount of technical knowledge on the part of the operator is necessary to maintain intelligent control over the data acquisition process.

1.2 Components of a Lidar System

A typical lidar system consists of the following:

1. A laser transmitter with its attendant electronics;
2. Receiving optics, such as a telescope;
3. A photo detector, such as a photo multiplier tube, and normal signal conditioning elements, e.g., amplifier, analog-to-digital converter;
4. Signal recording and display devices, such as disk drives, solid state memory, cathode ray tubes;
5. Intelligent controller, such as a microprocessor-based computer, and the various sensors and drivers it uses;
6. Peripheral equipment, such as printers, off-line tape drives, power supplies.

1.3 The Operation of a Lidar

For lidar operation, a laser transmitter emits a monochromatic, well collimated light pulse of extremely short duration into the atmosphere. The atmospheric constituents absorb and scatter this propagating pulse and a portion of the pulse energy is scattered back in the direction of the transmitter where it is collected by the optical receiver. The collected light is converted into electrical energy by a photodetector, thereby yielding a time-varying electronic signal. As the range from which the photons are being returned from increases, the loss in light energy due to scattering and absorption increases, and the time varying received signal decreases in amplitude. This signal may be

recorded and analyzed to gain knowledge of atmospheric aerosols.

1.4 Background of the University of Arizona Lidar System

The Atmospheric Remote Sensing Laboratory (ARSL) at the University of Arizona, headed by Dr. John A. Reagan, first began work on a lidar system in the late sixties. Webster (1971) developed a combination monostatic-bistatic lidar in its skeletal form. A bistatic lidar differs from a monostatic lidar in that the receiver is in a geographically separate location from the transmitter. The system he designed was used to take some preliminary data, and he demonstrated that it worked in both the monostatic and bistatic modes. Fernald (1972) carried out further work on the monostatic lidar. Fernald acquired data at varying elevation angles, and the lidar returns were recorded on 35 mm film. He analyzed lidar data in conjunction with solar radiometer data. He developed a solution approach (Fernald et al., 1972) to extract aerosol extinction and backscatter cross sections from the lidar data.

The monostatic lidar at the University of Arizona continued to evolve in form and capability. Spinhirne (1974) improved the data-handling capabilities of the lidar system through the installation of a high-speed gain-switching amplifier and a signal digitizer. He continued his work with

lidar, making quantitative measurements of aerosol properties via a slant-path monostatic lidar sensing technique, which he described in his Ph.D. dissertation (Spinhirne, 1977). At this point, the University of Arizona monostatic lidar system was capable of acquiring digitized records of lidar returns which were recorded on punched paper tape. The data was subsequently processed at the University Computer Center. Spinhirne's multi-angle solution technique to the lidar equation was an extension of the S ratio approach developed earlier by Fernald. This scheme eliminated the need for auxiliary inputs, such as those supplied by the solar radiometer, to extract aerosol extinction and backscatter coefficients from the lidar data. Spinhirne determined aerosol extinction and backscatter profiles for several days, and he also inferred particulate absorption indices of the aerosols using auxiliary solar radiometer data (Spinhirne et al., 1980).

The University of Arizona monostatic lidar system was further modified by Bruhns (1985). He upgraded the data acquisition system substantially. An Interdata 7-16 computer was installed as the user interface, and a 6502-based slave microcomputer was used for various peripheral controls. He incorporated several digital controls, installed a disc drive (8-inch floppy diskettes, Sykes 7000), modified the signal

conditioning electronics, and wrote the software for data acquisition.

The last few years of Bruhns' work was done in absentia, with Bruhns making several visits to the University to install and check his modifications. At the same time, a number of people were working intermittently on both the lidar system hardware and the data processing software. Among these are Gail Box, Daniel D'souza and Alan Anderson. Gail Box is credited with the division of program AER3 into various subroutines. A substantial lidar data acquisition program was also being conducted during this time. The core of the data processing software was a set of programs left by Spinhirne (1977). Much of the software was undocumented. Over the years, the body of information regarding the proper use of the data processing software had deteriorated. During this time, data may have been processed inaccurately and some errors may have been introduced in the software. The author's original assignment was to examine the data processing software and debug it. This task evolved into the larger problem of working with the lidar system, analyzing the lidar data, and modifying the system software. The results of this effort eventually led to this thesis.

1.5 The Objectives of this Thesis

The major thrust of this thesis can be summarized in four parts.

1. The Software: Spinhirne (1977) did not specifically discuss the data processing software for the monostatic lidar. As such, there was a need to better document the software, and explain/assess the methods of analysis employed in the software. This work will strive to show the main features of the software, describe how it runs, and discuss the necessary modifications that have been made to it. This will be presented in Chapter 2. Most of the software is now documented, and anyone with an understanding of lidar can run the programs.
2. The generation of results: As mentioned before, much more data has been acquired since the departure of Spinhirne. Most of it has been successfully processed, and a large body of results is now available. These will be presented in Chapter 3.
3. The database: Key results from each data run have been catalogued into a database. The discussion of the database and its advantages will also be presented in Chapter 3. The relationships between some of the lidar parameters will be explored using the database.
4. Case studies: Some of the assumptions made in the multi-angle lidar solution procedure have been

examined. The results of these studies will be discussed in Chapter 4.

Finally, some of the future possibilities for lidar data analysis will be discussed in Chapter 5.

CHAPTER 2

THE LIDAR SOFTWARE

This chapter discusses the software used in processing lidar data. Several programs are presented in the order in which they are used in processing a typical data set. Some discussion of the key aspects of the integrated slant path solution, which forms the core of the analysis, is also presented at appropriate junctures within the discussion of the software. To understand the basis of the lidar data processing software, it is advantageous to have an understanding of the data acquisition process. A brief review of this is presented here as well. For an in-depth look at the lidar hardware, the reader is referred to the Ph.D. dissertation by Bruhns (Bruhns, 1985), and for aspects of the lidar hardware as well as theory, to Spinhirne's M.S. thesis (Spinhirne, 1974) and Ph.D. dissertation (Spinhirne, 1977).

2.1 Data Acquisition

The lidar data is acquired with a ruby laser lidar system (wavelength of 694.3 nanometers), which is located at the University of Arizona farm near Roger Road and Campbell Avenue in Tucson, Arizona. A block diagram of the data acquisition hardware is shown in Figure 2.1. The data is

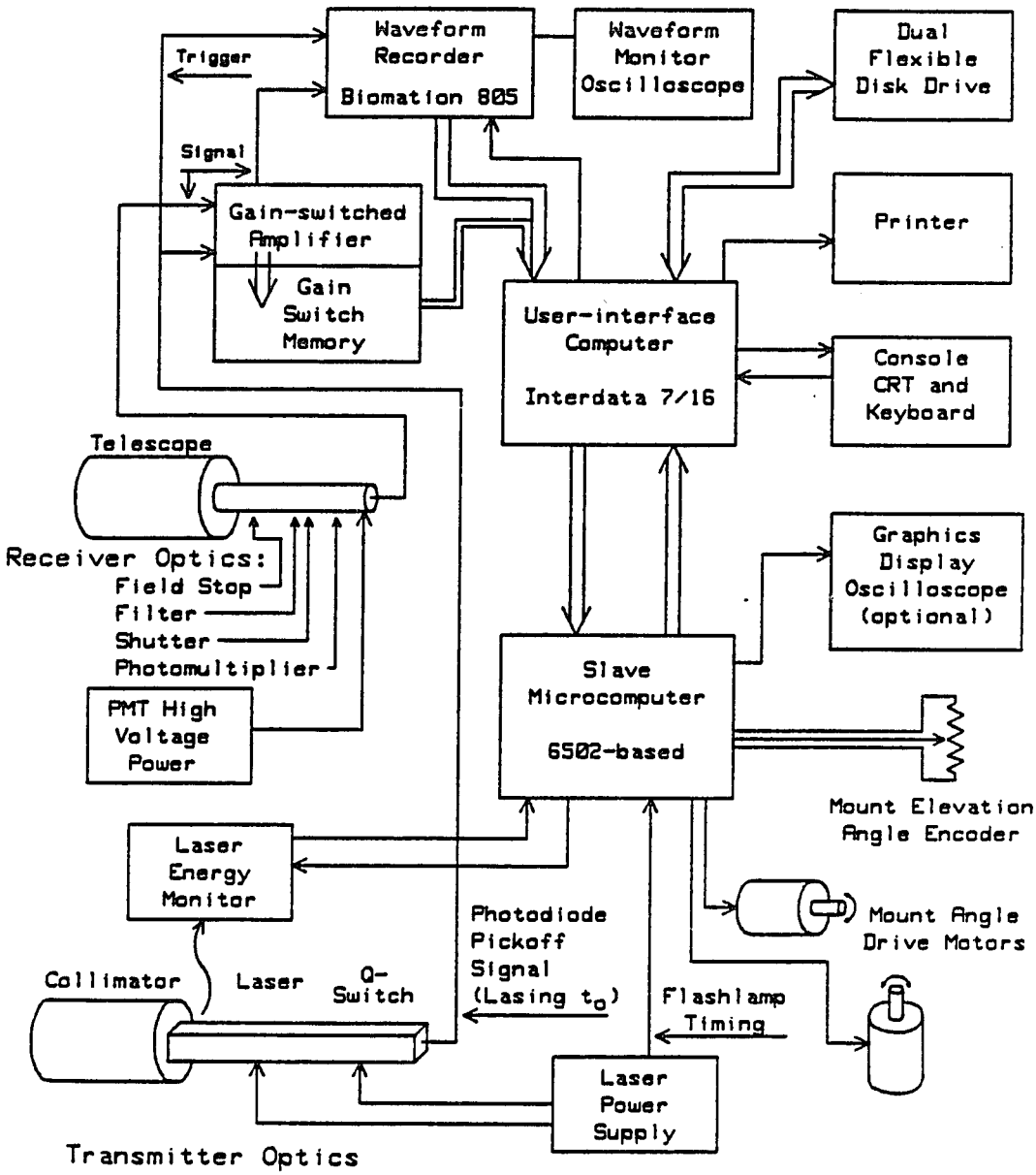

Figure 2.1. University of Arizona monostatic lidar hardware block diagram.

taken primarily at night because, if data acquisition is attempted during the day, background radiation from the sky increases the noise in the returned signal to unacceptable levels. One data set is usually acquired on any given night. In a typical data run, several shots are fired with the laser at varying zenith angles. Each shot constitutes a record of data. Data is acquired in groups of shots, one group at each zenith angle, starting at the largest zenith angle and ending with a zenith angle of zero, which is the vertical position. Ten shots are generally fired at each zenith angle and at each sampling rate. The sample rate is usually the same for all slant angle shots. At the zenith (vertical), two sets of shots are fired. One set is taken at the same sample rate that was used for all the slant angles (typically 0.5 microseconds) and the other at a faster sample rate (typically 0.2 microseconds). The signal returns from the atmosphere are recorded on an 8-inch floppy disk, and the disk is then transported to the University of Arizona's CCIT (Center for Computing and Information Technology) for processing.

If a sample is recorded at time "t" after the laser has been fired, the distance travelled by the signal during that time is "C*t," where "C" is the speed of light. This, though, is the "round trip" distance from the transmitter to a scattering volume at a range "r" and back to the receiver. The one way distance, or range "r," is given by "C*t/2."

Given that the speed of light is 0.3 km per microsecond, the ranging relation of the lidar is 0.15 km per microsecond. The resolution, or step size, or distance travelled per sample, for any sample rate in microseconds, is given by

$$\text{step size (km)} = 0.15 \text{ km/microsecond} * \text{sample rate} \quad (2.1)$$

For a sample rate of 0.5 microseconds the step size is 75 meters, or 0.075 km. At a 0.2 microsecond sampling rate, resolution is obtained down to 30 meters, or 0.030 km. For shots fired at zenith angle equal to zero (vertical shot) and 256 samples per shot, this means that data are obtained out to 19.2 km for a 0.5 microsecond sample rate and to 7.68 km for a 0.2 microsecond sample rate. The zenith angles typically used in a data run are shown in Table 2.1, which also lists the effective vertical range for each angle and sample rate.

2.2 The Software

Processing of the lidar data recorded on a floppy disk begins with it being read at the CCIT where the data is transferred to the mainframe computer's memory (CYBER 175). Until recently, the writing, revising and updating of programs, as well as of job control files were done on the DEC-10 computer of the CCIT, and the programs were executed on the CYBER 175 computer. The DEC-10 computer is scheduled

Table 2.1. Angle, sampling rate and range values for a typical lidar slant path data set.

Elev. Angle (degrees)	Zenith Angle (degrees) theta	Secant theta	Sample rate (micro-seconds)	Slant Range (km)	Effective Vertical Range (km)
11.54	78.46	5.0	0.5	19.2	3.84
12.84	77.16	4.5	0.5	19.2	4.27
14.48	75.52	4.0	0.5	19.2	4.8
16.60	73.40	3.5	0.5	19.2	5.49
19.47	70.53	3.0	0.5	19.2	6.4
23.58	66.42	2.5	0.5	19.2	7.68
30.00	60.00	2.0	0.5	19.2	9.6
41.81	48.19	1.5	0.5	19.2	12.8
90.00	0.0	1.0	0.5	19.2	19.2
90.00	0.0	1.0	0.2	7.68	7.68

for termination in 1988, and the software has been moved to a VAX computer at the CCIT. The ARSL facilities now include an AT&T 6300, which is being used for program development as well as for communicating with the VAX. The software development is now done jointly on the VAX and the AT&T 6300, but the lidar software is executed on the CYBER 175, as before.

Figure 2.2 shows the order in which lidar data processing programs operate, starting with the raw data in a CYBER disk file and continuing until final results are generated. These include various plots, printouts, and magnetic tape storage of the derived parameters. Lidar data is processed through programs EDIT, AIMLESS, PIT and AER3. Program MONAV is for averaging the results of several days of data. Program CAL is used to process calibration data to determine the system calibration constant.

The form of the raw data is shown in Figure 2.3. This is how the data is stored on the floppy disk and on the CYBER disk file. Each data set has a header, which contains a system header record, followed by a record containing the information about that data run: month, day, year, start time (of the data run), finish time, photomultiplier tube voltage (PMT), temperature in degrees Celsius. What follows next are two groups of information, which are repeated for each shot in the data set. The first group is simply the alphanumeric string "record," followed by a number, which is

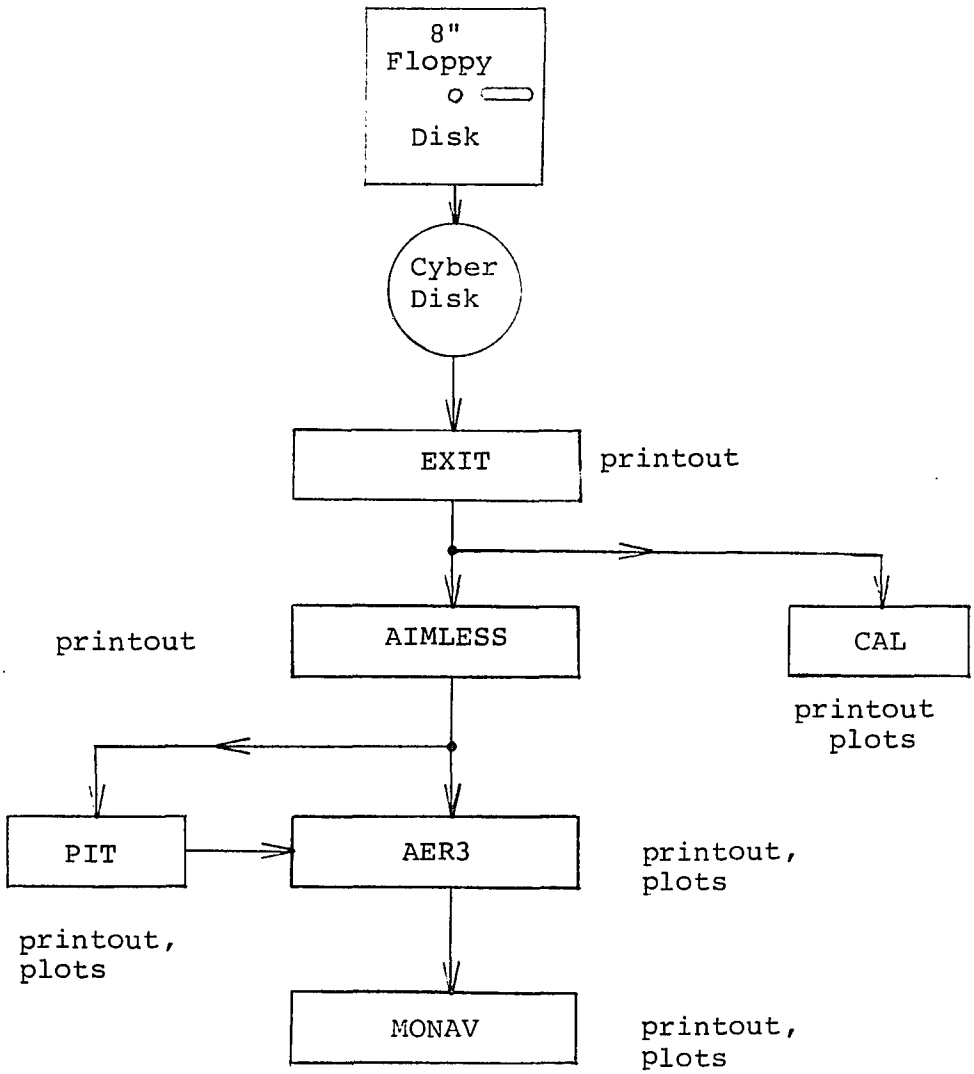

Figure 2.2. Lidar data processing program order block diagram.

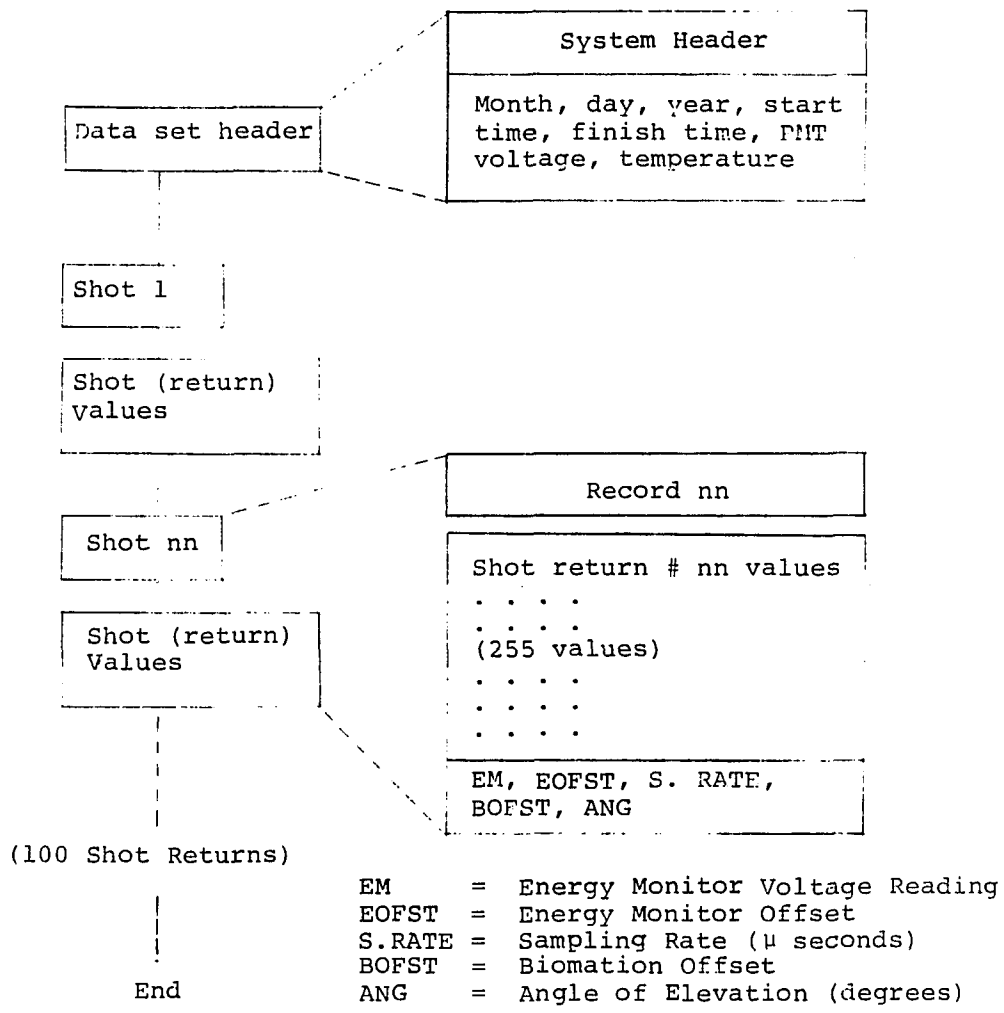

Figure 2.3. Form of raw data (input to program EDIT).

the "shot number" for the record. Increasing positive integers are assigned as shot numbers. The second group has the signal in digitized form, 255 integer samples, or values. This is followed by five numbers that relate to the shot: energy monitor value in volts, energy monitor offset, sample rate in microseconds, Biomation offset (Biomation is the brand name of the signal digitizer), and elevation angle in degrees. These are written as real numbers.

2.3 Program EDIT

The program EDIT reads the raw data and slightly modifies and rearranges it. Figure 2.4 shows the output of EDIT. Note that there is no overall header record. The shot number record is replaced by a record that contains a logical tape unit number, month, day, year, start time, finish time, photomultiplier tube (PMT) voltage, and temperature. The second segment in each group pair is 300 elements long, and it contains the original shot signal, followed by values of energy monitor, energy monitor offset, sample rate, etc., converted to integers.

As noted above, program EDIT only slightly rearranges the data. In the raw data, information about the day, date and month of the data run is available only at the beginning of the data set. To protect against inadvertent loss of this information, program EDIT inserts this record in between every two successive shots. Thus, even if part of the data

set is accidentally lost, the rest of the data set remains identifiable and useful. The data set that is read by program EDIT is sometimes in the EBCDIC format, as opposed to ASCII. This reportedly results in the loss of a "carriage return" character between records. The program has been modified to accommodate either form, the indicator being an integer flag that is entered at the end of the job control language for the program to process in one of the two ways. Occasionally the data in an isolated shot is corrupted, due to a hardware glitch, or an item of information, such as the sample rate has been entered incorrectly, due to operator error. In such cases, the mistakes are corrected manually at this stage.

2.4 Program AIMLESS

The real data processing begins in program AIMLESS. The output of EDIT is the input for AIMLESS. This program removes the gain changes in the signal introduced by the lidar hardware, as well as normalizes out the shot-to-shot variations in the transmitted pulse energy. It then averages the shots that have identical sample rate and zenith angle.

The first operation performed by program AIMLESS is to replace the integer values (between 0 and 255) for each shot sample by a corresponding voltage value based on a full scale voltage of 2 volts. The numbers thus change from integers to real numbers representing voltages.

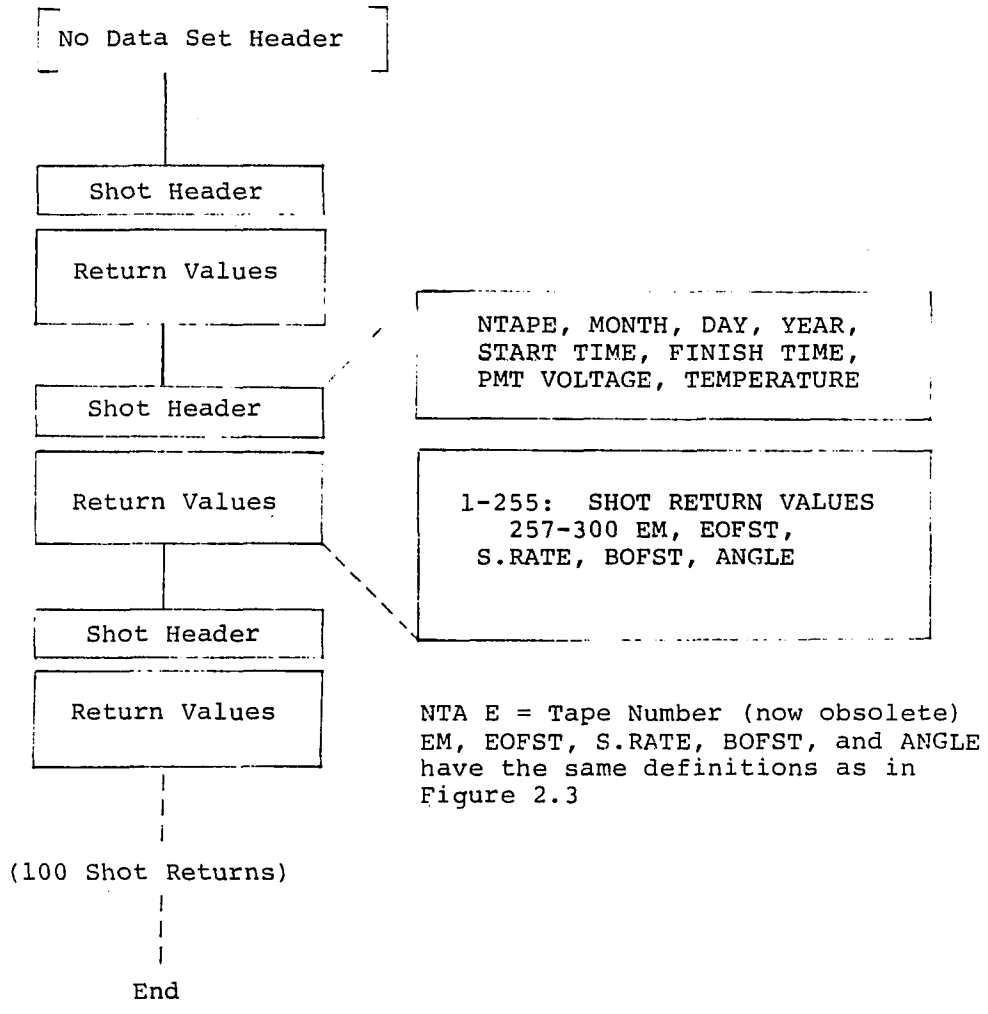

Figure 2.4. Form of data (output of program EDIT).

The overlap distance is the distance from the lidar transmitter at which the fields of view of the transmitter and the receiving telescope fully overlap. Partial overlap occurs at 404 meters and full overlap at 673 meters, as reported by Bruhns (1985). Spinhirne (1977) reports full overlap as being at 800 meters. In either case, it may be safely assumed that full overlap has occurred after about 900 meters. Program AIMLESS detects and marks the first "peak" in magnitude for each shot. From then on, the signal drops in a dominantly (1/r**2) fashion, where "r" is the range, or distance. Data is assumed valid only for distances greater than the "peak" index in each shot record.

After each laser shot is fired, the lidar hardware records the signal backscattered from the atmosphere. As the signal drops below a minimum threshold, the gainswitching amplifier switches to a new gainstage, so as to maintain the signal in an acceptable range for subsequent digitization and recording. This point in the shot record is called the gainswitch location, or simply, the "gainswitch." The signal goes through eight such gainstages, or seven gainswitches. Each gainstage provides a gain of about 3.0. Figure 2.5 shows the plot of a gainswitched lidar return for a zenith angle of 78.6 degrees. It is this type of a record which program AIMLESS operates on to remove the various gains and produce a gain "unswitched" record. The gainswitches can be

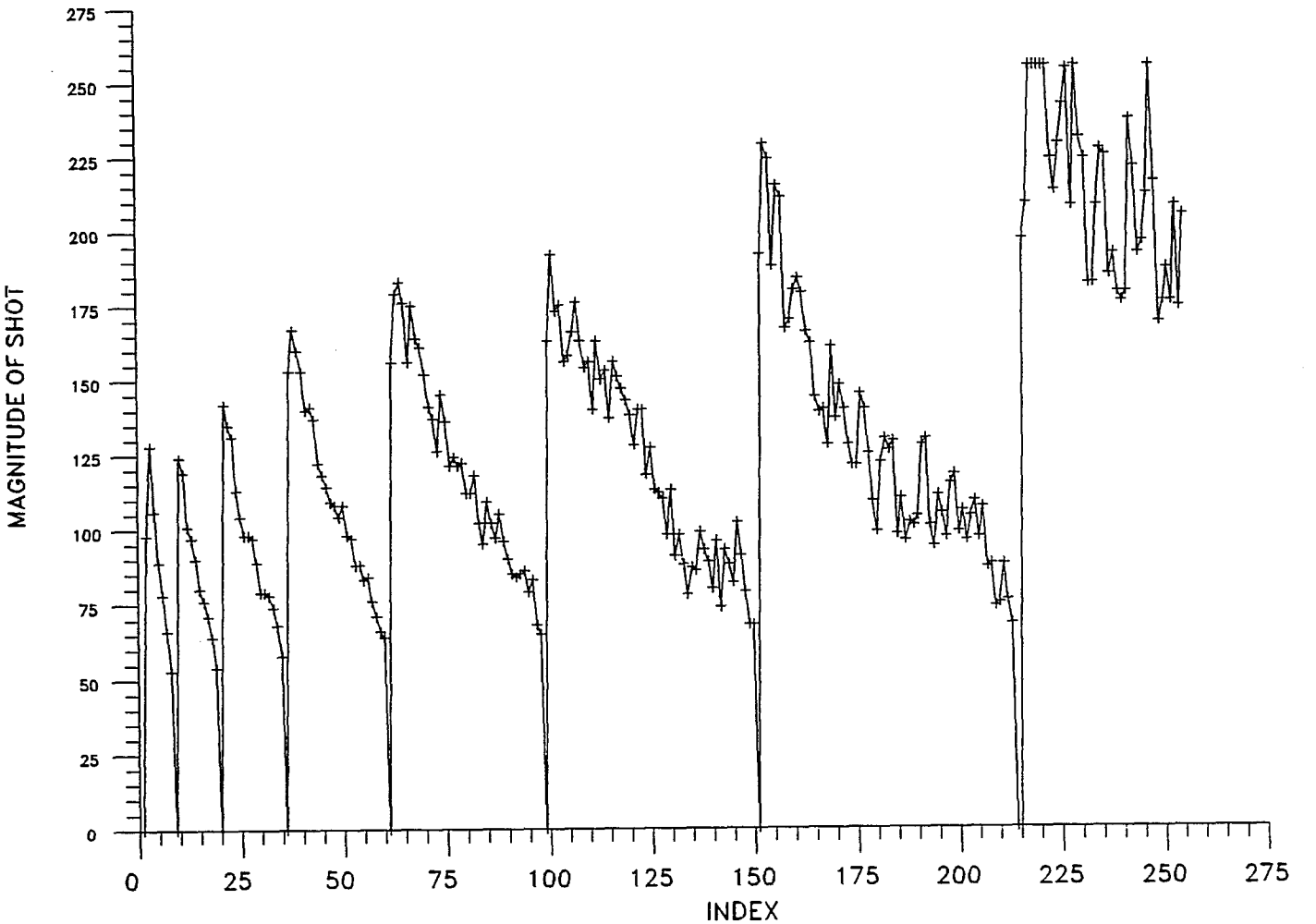

Figure 2.5. Plot of a shot return in the input to program AIMLESS at a zenith angle of 78.6^{O} on 21 May 1984.

clearly seen in this figure. These gainswitches must be detected in order to remove the gain changes from the shot and restore the signal to its true range variation.

For a shot fired at a zenith angle of theta, the signal at an effective vertical height of z km is given by

$$V(z,\theta) = \frac{CE}{z^2 \sec^2\theta} [\beta_P(z,\theta) + \beta_R(z)][T_P(z)T_R(z)]^{2\sec\theta} \tag{2.2}$$

where

$V(z,\theta)$ = instantaneous measured return signal in volts

β_P = particulate volume backscatter cross section

β_R = Rayleigh volume backscatter cross section

T_P = effective vertical path one-way particulate transmission

T_R = effective vertical path one-way Rayleigh transmission

C = system calibration constant

E = transmitted pulse energy reference

The energy normalized signal is given by

$$Q(z,\theta) = \frac{V(z,\theta)}{E} \tag{2.3}$$

Substituting for v(z,theta),

$$Q(z,\theta) = \frac{C}{z^2 \sec^2\theta} [\beta_P(z,\theta) + \beta_R(z)][T_P(z)T_R(z)]^{2\sec\theta} \tag{2.4}$$

The transmission to an altitude z km is a function of the atmospheric volume extinction cross section, as given by

$$T(z) = e^{-\int_0^z 6(z')dz'} \tag{2.5}$$

where

6(z) = the atmospheric volume extinction cross section

The integral of the volume extinction cross section from the surface to a height z is known as the optical depth, or the optical thickness, at height z. The transmission to a height z can be now restated as

$$T(z) = e^{-\tau(z)} \tag{2.6}$$

where the optical depth is

$$\tau(z) = \int_0^z 6(z')dz' \tag{2.7}$$

Throughout the rest of this thesis, a number of acronyms will be used in the discussion of the lidar parameters. They are listed in Table 2.2. Most of them are taken from the Greek symbols used to denote the parameters in mathematical equations. Some, such as PSIG, are identical to the

Table 2.2 Definitions of acronyms used in the thesis.

sigmap	=>	the particulate extinction
sigmar	=>	the Rayleigh extinction
sigmat	=>	the total extinction
sdsigmap	=>	the standard deviation of the particulate extinction
varsigmap	=>	the variance of the particulate extinction
betap	=>	the particulate backscatter
betar	=>	the Rayleigh backscatter
betat	=>	the total backscatter
varbetap	=>	the variance of the particulate backscatter
sdbetap	=>	the standard deviation of the particulate backscatter
taup	=>	the particulate optical depth
taur	=>	the Rayleigh optical depth
taut	=>	the total optical depth
vartaup	=>	the variance of the particulate optical depth
sdtaup	=>	the standard deviation of the particulate optical depth
PSIG	=>	the gain removed, energy-and-range normalized, average signal return at a given zenith angle and sampling rate.
%sd	=>	the standard deviation of a quantity, expressed as a percentage of the average
HMIX	=>	the height of the mixing layer, in kilometers.

names of arrays used in the lidar software to store the quantities they represent.

To energy normalize the signal, each voltage is divided in AIMLESS by E, the energy monitor value. This is necessary to compensate for the shot-to-shot variations in the energy output of the lidar laser transmitter. In a given data set, several shots are fired at each zenith angle. Shots fired at any given slant angle typically have the same sample rate. Thus, the shots fall into natural groups. In AIMLESS, all the shots that form a group are averaged. The output of AIMLESS is a gain removed, energy normalized, averaged signal. Figure 2.6 shows the output of AIMLESS, for a zenith angle of 78.6 degrees, which may be contrasted with the input to AIMLESS depicted earlier in Figure 2.5.

Various problems were encountered in program AIMLESS to properly condition the lidar returns. For each shot, it is necessary to find the "peak" in the shot response. Sometimes this peak is rather small in magnitude (relative to the magnitude in one gainstage) and difficult to detect. If undetected, this may result in a gainstage being unrecognized. The code has been modified so that the threshold used in finding the peak is low enough to detect a low peak. Another important point is how early in the shot return this peak may occur. We have documented cases where the peak occurred so early that it was overlooked, leading to a whole

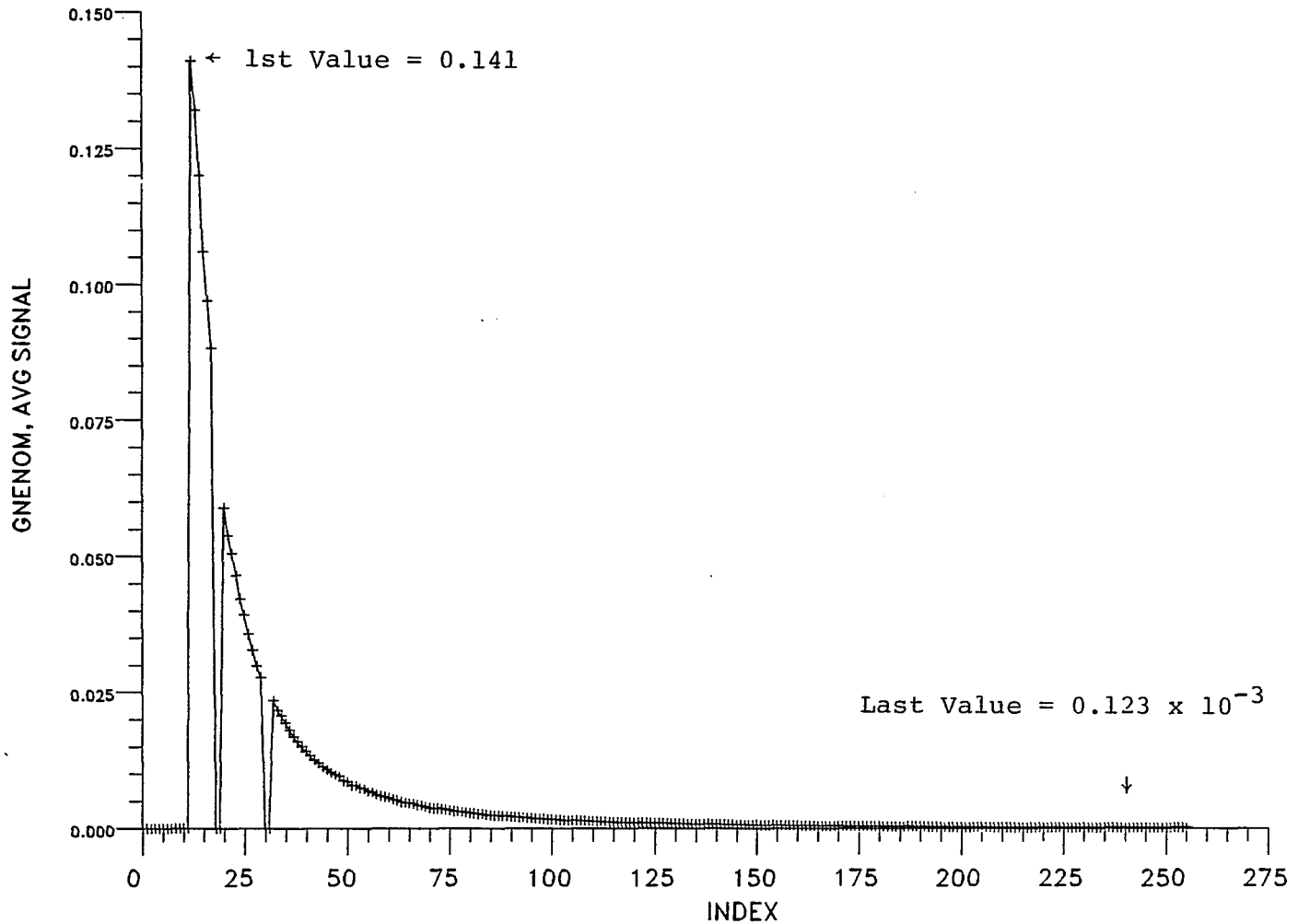

Figure 2.6. Plot of a gain-removed, averaged shot return in the output of program AIMLESS, for 11 May 1981 at a zenith angle of 77.2°.

gainstage not being recognized. Whether these unrecognized "peaks" were in reality peaks in the shot responses or whether they were due to noise generated by the hardware is not known. Such instances, when they occur, are judged on a case by case basis.

The gainswitches, as mentioned above, are detected via software, and the signal is adjusted to remove the gain. For a gainswitch to have occurred, the signal must show a drop in magnitude, followed by a sudden jump, followed again by a generally decreasing signal as shown earlier in Figure 2.5. When the gain switching amplifier switches to a new gainstage, sometimes a little "ringing" may occur; that is, the return value may oscillate a little before a complete transition is made to the new gainstage. A new gainswitch, must, therefore, be far enough away from last detected gainswitch so as to avoid detecting the ringing as a gainswitch. Stray zeroes that are occasionally seen in the returns, must also not be falsely detected as gainswitches. These conditions are searched for in each shot record in the data set, and the gainswitches are detected. Two thresholds are used, NTA and NTB. The threshold NTA is intended as a lower threshold. The signal must fall below it for a gainswitch to occur. The exact reason for using the second threshold, NTB, is not known. It seems to be used as a variant of NTA. Its

value is set a little higher than NTA. The conditions used to identify a gainswitch point are as follows:

A gainswitch is supposed to have occurred at a sample point if

1. the signal is less than that at the next sample,
2. it is at least the third sample from the previous gainswitch,
3. it is below the threshold NTA, and
4. the signal at the second sample from it is greater than twice the value of NTA

or

1. it is at least the fifth sample from the previous gainswitch,
2. the signal is less than that at the next sample
3. the signal at the third sample from it is greater than twice the value that would have been obtained by extrapolation in the absence of a gainswitch,
4. the third sample from it is greater than the threshold NTA, and
5. it is below the threshold NTB.

Once a gainswitch is detected, a zero is inserted at that index and at adjacent indexes on either side of the gainswitch index. The signal from that point on is divided by 3.0 to remove the gain introduced by the gainswitching amplifier. This procedure is performed at each consecutive

gainswitch, so the shot return in the second gainstage is divided by 3, the return in the third gainstage is divided by 9, and so on. The shot return in the last, or eighth, gainstage is divided by (3**7), or 2187.

The lidar instrumentation has a piece of hardware called the gainswitch marker which, when used, puts a zero in the data when a gainswitch occurs. Attempt was made to use a zero detect mechanism (in program AIMLESS) to locate the gainswitches, but, there were problems with this scheme. First, it would detect stray zeroes, which are occasionally found in the data, as being gainswitches. Secondly, there was no guaranteed way of a priorily determining which data runs had used the marker and which ones had not. This approach was therefore abandoned.

Monitoring the magnitude variation of the shot response has proven to be sufficiently reliable means for the detection of gainswitches. To check on the operation of gainswitch detection, another simple idea was introduced; namely, a record was kept of where the gainswitches occurred, and the indexes of gainswitches for each shot were printed out. This was a valuable tool, because after running program AIMLESS, one can scan the printout or screen display of index values of gainswitches for a group of shots with the same zenith angle and same sample rate. Normally, each shot would show 7 index values, one for each gainswitch. The variation

in the output energy of the laser transmitter will introduce some fluctuation as to the exact index point in each shot that a gainswitch is detected; however, the gainswitches for identical gainstages in successive shots should still occur in fairly tight groups of index values. For some data sets, the gainswitch locations detected by this scheme were compared with the locations determined by manually examining the printouts of raw data. It was found that the software was detecting all 7 gainswitches, and the index values determined by the software differed by less than 2 or 3 from the corresponding index values determined manually. Table 2.3 shows the printout of gainswitch locations for nine shots at a zenith angle of 78.6 degrees for 11 May 1981. It can be seen that the index values did not vary by much from shot to shot.

In AIMLESS the shots having the same sample rate and same elevation angle are averaged to yield noise reduction. In subsequent processing, the averaged shot response is then treated as if it represents the signal obtained from a single shot fired at that zenith angle. It is crucial, therefore, to keep track of the sample rate and angle for each shot and to separate the shots into correct groups. In this regard, faulty angle readouts or sample rate values have caused trouble in the past. The hardware now reads the angles correctly. Even small variations in the angle can be

Table 2.3. Gainswitch index values for 9 shots at a zenith angle of 78.6 degrees for 11 May 1981, as determined by program AIMLESS.

GSW -> SHOT	1	2	3	4	5	6	7
1	19	30	49	76	121	172	239
2	18	29	47	75	117	176	232
3	17	28	46	73	112	168	230
4	18	30	49	77	120	176	243
5	18	30	48	76	116	177	238
6	18	30	48	78	115	178	239
7	18	30	48	75	116	178	240
8	17	29	45	70	109	172	235
9	17	28	45	70	110	170	233

significant in terms of the difference in the volume of the atmosphere sampled by the propagating laser pulse as the range increases. Thus, it is important to not group two shots together if they differ in zenith angle by more than 0.1 or 0.2 degrees. There have been times when the lidar hardware recorded varying zenith angles for two successive shots when, in fact, the angle had not changed. Only when it was known with certainty that this was the case was the correct angle later written into the data.

AIMLESS does further checking within each group of shots before performing the averaging. At each index value, the deviation of each shot value from the average value for the group is checked. If a shot is smaller than half the average value or greater than twice the average value, it is assumed to have missed a gainswitch, and it is corrected. If this happens for more than 33% of the shots, a warning is printed. Frequently the last gainstage of a shot is noisy, and this can be seen by the warning printouts of program AIMLESS. When averaging the shots, if the fractional standard deviation of the group is more than $\simeq 0.16$, the shot causing it is omitted from the average. There is a provision to use a flag which, when set, allows the program to compensate for a missed or improperly detected gainswitch by checking the magnitude variation of each shot. However, this feature may tend to corrupt the data instead of improving it.

As such, it has seldom been used in the past and it has been altogether abandoned in the recent past.

All conditions that cause the program to terminate, whether normal (end of data file reached) or not (unexpected value in a field) are trapped and printed out. The output of AIMLESS is in the form of four arrays written out to a file on the CYBER 175. Array JD(10) contains information common to the entire data set, such as the month, day, year, etc. ASEC(15) contains the secants of zenith angles that are used in a given data run. The secant of the zenith angle is a quantity often used in these programs. DSMP (15) is an array that contains the step size for each angle. PSIG (15,255) is the array that contains the gain removed, energy normalized, averaged signal.

2.5 Program PIT

Program PIT performs range normalization for all slant paths. From Equation 2.2, given earlier, the gain removed and energy-and-range normalized signal is given by

$$P(z,\gamma) = \frac{V(z,\theta)z^2\sec^2\theta}{E} \qquad (2.8)$$

By substituting for V(z,theta),

$$P(z,\gamma) = C[\beta_P(z,\gamma)\beta_R(z)][T_P^{\gamma}(z)T_R^{\gamma}(z)] \qquad (2.9)$$

In both of these equations,

$$\gamma = 2 \sec\theta \tag{2.10}$$

The signal in array PSIG coming into program PIT is a gain removed, energy normalized, averaged signal at various slant ranges. It is necessary to first compute the signal at effective vertical heights and then (vertical) range square normalize it. Vertical heights from 0 to 7.68 km at 0.03 km intervals are used. This can be accomplished in a combination step, instead of two steps, as shown next. Consider a slant zenith angle of 73.4 degrees. The secant of the zenith angle is 3.5. As depicted in Figure 2.7, for a slant range of 19.2 km, the effective vertical range is 5.49 km.

Now suppose that it is desired to determine the signal for this angle at an effective vertical height of 2.01 km. This corresponds to a slant range of 7.035 km. However, because a sample rate of 0.5 microseconds (a step of 0.075 km) is typically used for the slant angles, a value of the signal is not available at exactly 7.035 km. What is available is the signal at 6.975 km (index 93) and 7.05 km (index 94). In such a case, the effective (vertical) PSIG at slant ranges of 7.05 km and 6.975 km is computed first, and the effective (vertical) range normalized signal at a vertical range of 2.01 km is then computed by interpolation. The effective vertical range resolution available in the data

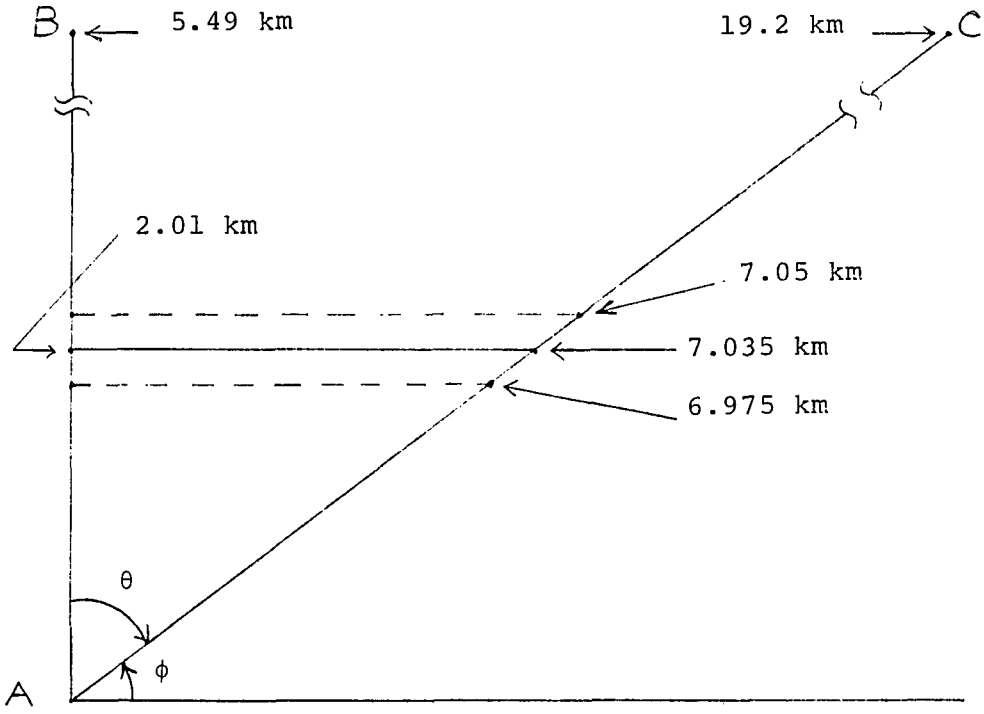

(Diagram Not to Scale)

ϕ = Elevation Angle = 16.6° Sample Rate

θ = Zenith Angle = 73.4° = 0.5 μS

Secant θ = 3.5

AC = 19.2 km = Total Slant Range

$AB = \frac{AC}{\text{Sec } \theta}$ = Total Effective Vertical Range

Slant Index	Slant Range
93	6.975
94	7.05

Figure 2.7. Slant range and effective vertical range for a zenith angle of 73.4°.

set ranges from 0.05 km for a zenith angle of 48.19 degrees to 0.015 km for a zenith angle of 78.46 degrees. Thus, the interpolation is always over a distance of less than or equal to 0.05 km, except for those occasions where a zero is inserted by program AIMLESS. In this way, effective vertical PSIG signal is determined for all angles from 0.0 km to 7.68 km at 0.03 km intervals. Program PIT removes the zeroes inserted in the shot records by program AIMLESS and substitutes interpolated values. If there is an excessively long string of zeroes, this indicates a problem with that shot and it is zeroed out for all distances greater than where the zeroes occurred.

To perform the range normalization as discussed above, it is important to keep track of the angle and sampling rate of each shot and to use it properly to determine the appropriate interpolated signal. There had been problems in this regard in the past, where, due to the use of incorrect sample rates, the height of the signal being printed out was erroneous for some angles. This has been corrected, and the printouts now show the correct heights for all signals. The vertical angle at 0.5 microsecond sampling rate provides information out to 19.2 km, and the averaged returns acquired at the vertical angle are printed out separately. Also, the graphs for all angles were not being printed out, and there was no provision to specify any combination of angles to be

plotted. The graphics portion of the program PIT now works, and it is possible to have one or more angles plotted, either on separate graphs or in any combination on the same graph. Figure 2.8 shows the PSIG profile versus height for a zenith angle of 0 degrees (vertical) for 17 April 1980, and Figure 2.9 shows the PSIG profiles for all slant angles for the same day. Plots such as the one in Figure 2.9 make it convenient to assess the value of PSIG, because all the PSIG profiles may be seen at once. Currently, all the slant angles are plotted on one graph, and the vertical angles are each plotted on a separate graph. The way the angles were previously being manipulated in the array PSIG there was a danger of existing information being overwritten. This has been corrected so information is not accidentally erased.

As shown in Equation 2.9, the range squared, energy normalized signal contains the product of the calibration constant, the total backscatter, and the total transmission. Atmospheric transmission is an integral function of particulate and molecular extinction over distance, and it varies only slowly with range. In contrast, the particulate volume backscatter cross section is, to a first approximation, proportional to particulate concentration, and it may vary significantly from point to point. A plot of PSIG versus height can yield a good approximation of the vertical distribution of particulates in the atmosphere at that time,

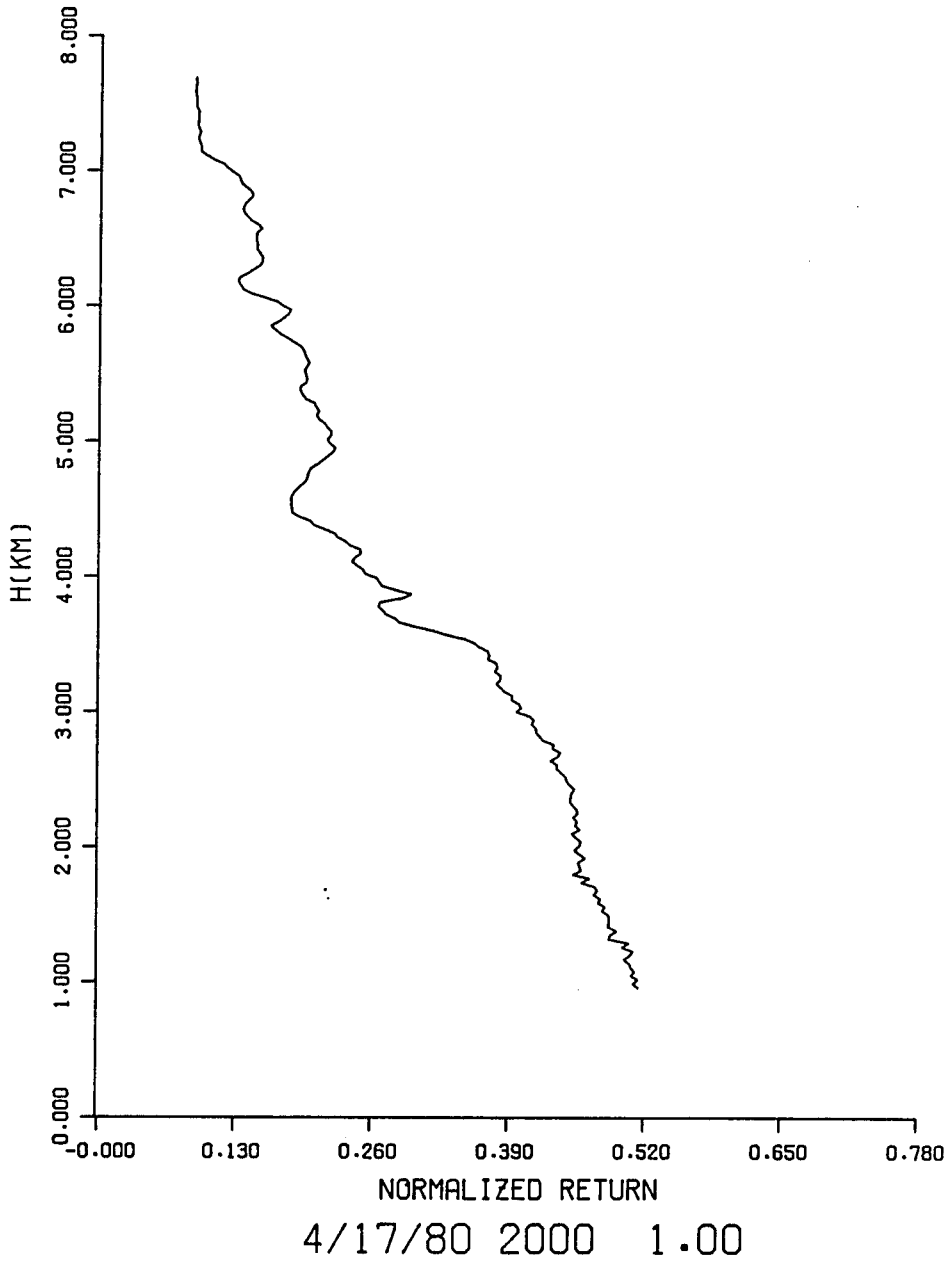

Figure 2.8. PSIG profile for a zenith angle of 0^{o} for 17 April 1980.

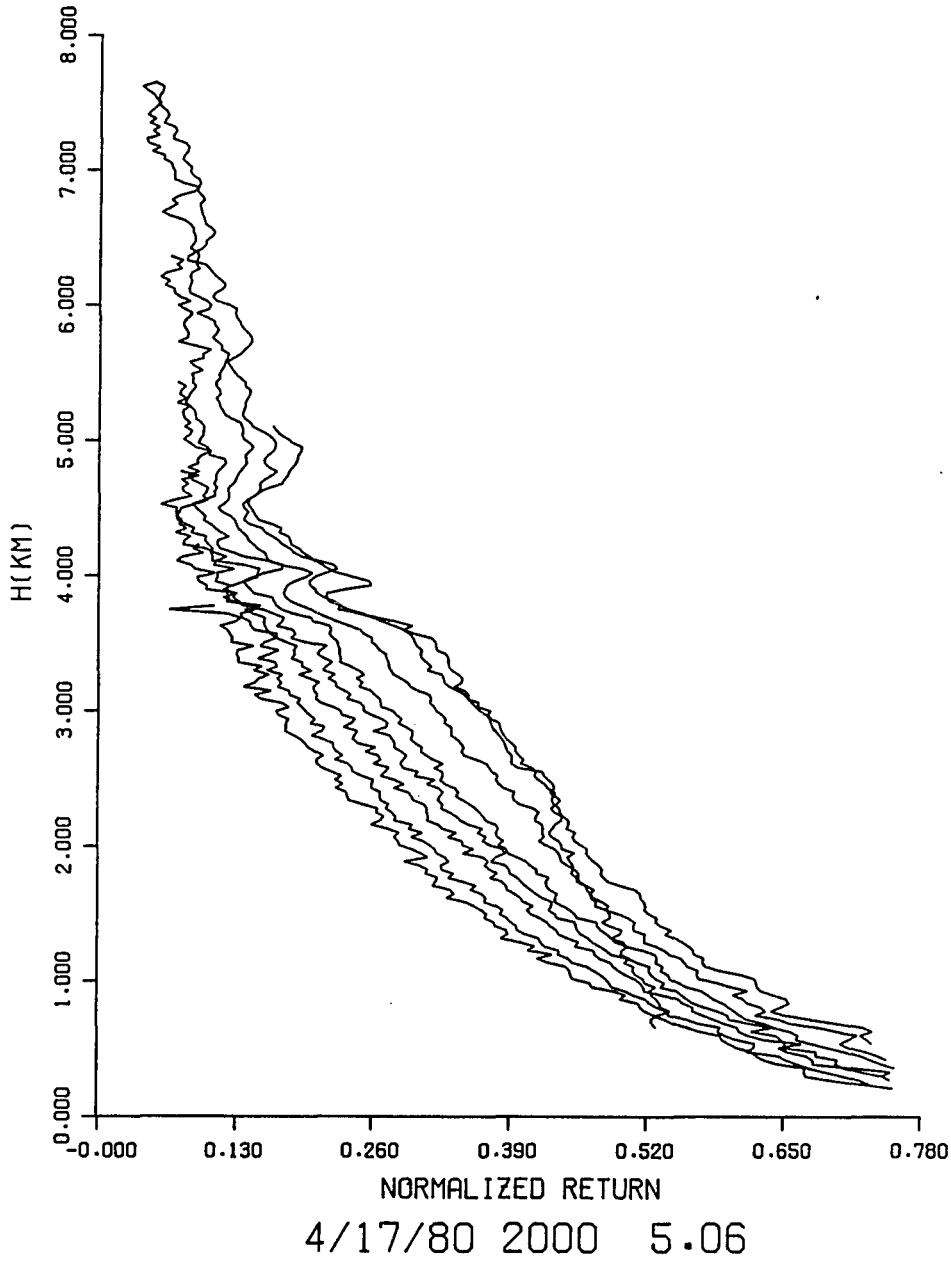

Figure 2.9. PSIG profiles for all slant antles for 17 April 1980.

and an estimate of the height of the aerosol mixing layer can be obtained directly from this plot. This estimate is used in the solution to the integrated lidar slant path equations in program AER3.

2.6 Program AER3

Program AER3 solves the integrated lidar slant path equations, as described by Spinhirne (1977), to extract a value of the S ratio (particulate extinction over particulate backscatter) for the mixing layer. The output of program AIMLESS is the input to program AER3. A plot of particulate extinction as a function of height is produced as part of the output of AER3. Various parameters, such as particulate backscatter, particulate optical depth, and total optical depth, are also computed as a function of height. An overview of program AER3 is given in Appendix 2.1, and the operation of AER3 is described below.

First, the input variables and the data are read in the subroutine READIN (Appendix 2.2). The variables include switches to determine which profiles to plot, as well as lidcal (the lidar system calibration constant--to be discussed later); tprad, the radiometer optical depth (if available); hnurd, a number used in the computation of the mass concentration factor; hmix, the height of the mixing layer; and sinit, the initial value for the S ratio. Additionally, an array mcut(20) is read in which has index

values for each zenith angle. The signal for each zenith angle is cut off above the corresponding index value from array mcut. This is used when the output of AIMLESS or PIT indicates there is excessive noise beyond a given gainstage in a shot return.

It was mentioned before in section 2.4 that for the lidar considered here, full overlap between the transmitter and receiver field of view does not occur until about 700 to 800 meters. Below this range, the data is not accurate. For this reason, in subroutine NORM, for each angle, data below 900 meters is zeroed out. Subroutine NORM (Appendix 2.3) then performs range square normalization on the signal. This procedure is identical to that performed by program PIT.

The integrated slant path lidar equation was shown earlier in Equation 2.9. Spinhirne (1977) discusses the derivation of this equation and further manipulation of it to solve a system of equations, one equation for each slant path, from a height z1 to a height z2, to solve for the transmission and the S ratio. The application of the integrated slant-path solution requires that the particulate optical depth to the bottom of the mixing layer and the lidar system calibration constant be known, and an initial estimate of the S ratio be made. Additionally, the height of the mixing layer is required as an input. A value of 20 is typically used as the initial estimate for the S ratio. The

mixing layer height is judged from the PSIG plots from program PIT. The aerosol optical depth at any height z is the integral of the aerosol extinction cross section from ground to height z. Thus, the taup at the bottom of the mixing layer (the surface, or 0 km) is unity. However, due to the overlap problem, there is no signal available below a vertical height equivalent to a slant range of 900 meters. For each zenith angle, data is available down to a vertical height equal to the overlap range (900 meters) divided by the secant of the zenith angle.

Subroutine GROUND (Appendix 2.5) is used to extend the signal to ground using available data. The three largest zenith angles are selected. For each of these angles, using taup values from an assumed low altitude atmosphere, the product c*betat is computed for the first nine indexes at which the signal is nonzero. The average c*betat product is used in extrapolating the signal values to ground. This extrapolation is linear in backscatter.

The integrated slant path lidar solution procedure also requires Rayleigh coefficients, which are computed in subroutine RAYLEE (Appendix 2.4). Rayleigh extinction, backscatter, and transmission are calculated from 0 km to 7.68 km at 0.03 km intervals, using known pressure-temperature - height distributions.

Throughout the rest of the program, it is necessary at several times to compute taup between two heights. Subroutine INT is used for this. It works in one of two ways. Given two height values, the S ratio for the atmosphere between those two values, and the taup at one of the two boundary heights, one may obtain either (1) the taup at the other boundary only, or (2) the taup at the other boundary as well as at all intermediate height indexes (interval of 0.03 km). A linear regression scheme, as described by Spinhirne (1977, p. 35, Equation 2.27), is used to compute this.

In subroutine SOLVE (Appendix 2.6), the integrated slant path lidar equation is finally solved. By initially assuming a value of the S ratio, and a surface optical depth of 0, subroutine INT (Appendix 2.7) is used to obtain a taup value at 1 km; "z1" will be used to denote 1 km from here on. The integrated slant path solution is applied from z1 to the top of the mixing layer (z2), and a new value of the S ratio and optical depth at z2 are obtained. Using the new value of S, the optical depth at 0.03 km is again calculated (subroutine INT). If this value of taup at 0.03 km is acceptable, then the subroutine INT is used again to obtain all the intermediate values of taup from z1 to 0 km. The signal is again extended to ground for the 3 largest zenith angles, this time using the newly computed values of taup. The integrated slant path solution is redone, with the new value

of optical depth at z1. These steps are repeated until the optical depth at z1 converges. The solution procedure is continued for the layers above height z2, if this is requested. For each new layer, the solution from the previous layer provides the value of particulate optical depth at the top of the previous layer as a starting point for the new one. Subroutine ERRORS (Appendix 2.8) computes the errors in the S ratio and particulate optical depth for each layer.

In subroutine VERTPRF (Appendix 2.9), with the optical depth values at the top of the solution layer and the S ratio known, taup is calculated at intermediate heights from the lowest available signal height to the top of the highest layer for which the solution procedure was used. For a single layer, which is most often the case, this would be at z2. Sigmap and betap values are also derived for these heights.

The highest effective vertical height for which signal is available is called the "top of the data," or "ztop." The computations for parameters above z2, or above the top of the highest layer solved for, are performed by subroutine TOPLYER (Appendix 2.10). A model of betap/betar is assumed for the upper atmosphere. The model is used to estimate the integral of betap from top of data to infinity. Betat, sigmat, and taup values are computed from 7 km to 19 km at 0.5 km intervals. If the solar radiometer total

optical depth (TPRAD) is supplied, then the following method is implemented.

For the height interval from z2 to ztop, the S ratio is assumed identical to the value determined for the topmost layer below z2. Taup, sigmap, and betap are calculated from the z2 to ztop. An improved S ratio for the upper atmosphere is calculated, using a relation developed by Spinhirne (1977, p. 62, Equation 3.2), given by Equation 2.11 here

$$S = \frac{\tau_P(\infty) - \tau_P(z_2)}{\int_{z_2}^{z_{TOP}} \beta_P(z')\,dz' + \int_{z_{TOP}}^{z_\infty} \beta_P(z')\,dz'} \qquad (2.11)$$

The new value of the S ratio obtained with this relation is used to recompute the values of taup, sigmap and betap. The S ratio is computed iteratively until it converges.

If the solar radiometer total optical depth is not supplied, a second method is implemented. The values of taup, sigmap, and betap are calculated just as in method one above, but only once; i.e., no iterations are performed. Also, instead of calculating a new S for the upper atmosphere, the value of S derived for the topmost layer is used to compute total particulate optical depth. This is done using the relation (Spinhirne, 1977, p. 62).

$$\tau_P(\infty) = \tau_{P_{TOP}} + S \int_{z_{TOP}}^{z_\infty} \beta_P(z')dz' \qquad (2.12)$$

In subroutine PRINTF (Appendix 2.11) the product (C*betat) is calculated from the lidar equation at each height for each angle, from the lowest available signal to the top of the data (ztop). The average betat is then obtained from the average C*betat product by dividing out the calibration constant (C). Using the average betat, the average betap is calculated at each of these heights, and betat, varbetap, sigmap, sigmar, sigmat, varsigmap, sigmap/sigmar, betap/betar, and pml (= sigmap * smf) are also computed. An extinction cross section profile (sigmap versus height) is then plotted.

Average values of betap, varbetap, sigmap, varsigmap, taup, vartaup from 0.2 km to 7 km are calculated and printed. They are also written to a logical file to be stored so that they can be used by program MONAV. Values of betap, betar, varbetap, sigmap, varsigmap, and taup from ground to top of data are written to another logical file to be available for further plotting. This is done in subroutine AVERAG (Appendix 2.12).

The division of the original AER3 program into subroutines was done by Gail Box. However, the revised program was still largely undocumented. As an example, most of the

variables used in the programs were uncommented. The program has now been well documented, and word definitions have been provided for most of the variables used in it. Subroutines have also been added to the program to calculate the horizontal homogeneity in terms of the range square normalized signal (PSIG) and in terms of betap, where betap is obtained for individual angles. The discussion of these is postponed until Chapter 4, where case studies are presented.

The integrated slant path solution procedure as described in AER3 assumes that the atmosphere is horizontally homogeneous. A further constraint imposed by the AER3 solution procedure is that the ratio of aerosol extinction to backscatter is constant within the mixing layer. These are the only direct constraints applied in AER3. The value of the S ratio obtained by the program AER3 depends upon the shape or form of the aerosol size distribution and on the aerosol particle refractive index. For interpretive analysis, the assumptions applied are that the individual particles are spherical and homogeneous and that they have a single, average refractive index over all the particle sizes. A discussion of the relationship among the refractive index, size distribution, and extinction to backscatter ratio of aerosols can be found in Spinhirne (1980) and Reagan et al. (to be published, 1988).

The program MONAV uses the information created and stored by AER3 to compute averages of various parameters over several data runs. MONAV operates on the results generated by program AER3 for more than one data run. The dates of the results to be used by MONAV can be specified. MONAV generates average profiles of particulate extinction, backscatter, and optical depth. Average mixing layer height and the S ratio are also computed, and all these parameters are printed out. A plot of the average profile of the particulate extinction is also plotted. MONAV is used to obtain monthly, seasonal, or yearly averages of the scattering parameters.

2.7 Program CAL

The term "C" in the integrated lidar slant path equation shown previously (Equation 2.9) is the system calibration constant, referred to variously as CALCON or LIDCAL in the data processing programs. Program CAL determines this constant by processing data from a special data run, called the calibration data run. The laser is fired at a target 100 meters away from the lidar optics. A standard target calibration technique is used, similar to the one used by Hall and Ageno (1970). Our technique is described in detail by Reagan et al. (1976) and Spinhirne (1977).

Spinhirne (1977) has shown that the system calibration constant, C, is given by

$$C = C_A R_L \left(\frac{r_A}{r_T}\right) \left(\frac{P_{TV}}{E}\right) \left(\frac{C\pi R_T^2}{2\rho T_f T_T^2 \cos\theta}\right) \qquad (2.13)$$

This equation can be rewritten as

$$C = C_A R_i \left(\frac{r_A}{r_T}\right) \left(\frac{P_{TV}}{E}\right) \left(\frac{C\pi R_T^2}{2\rho T_f T_T^2 \cos\theta}\right) \left(\frac{R_L}{R_i}\right) \qquad (2.14)$$

where

C_A = capacitive load on the pmt

R_L = load resistance on the pmt

R_i = input resistance of amplifier after pmt

r_A = pmt responsivity for the atmosphere

r_T = pmt responsivity for the target

P_{TV} = peak integration signal voltage

E = transmitted pulse energy (relative measure)

c = speed of light

R_T = distance to the standard target

ρ = diffuse reflectance of the standard target

T_f = transmission of the target calibration neutral density filter

T_T = atmospheric transmittance to the standard target

θ = angle between the receiver line of sight and the target normal

In this equation, everything is known except the product (Ca*Ri) and the ratio (PsubTV/E). These are the two quantities determined from a calibration run.

The signal voltage obtained on the pmt load resistor in a calibration run, V(t), can be expressed as

$$V(t) = P_{TV} e^{\frac{-t}{C_A R_i}} \tag{2.15}$$

This can be rewritten as

$$V(t) = A^{-\frac{t}{tau}} \tag{2.16}$$

where

$$A = P_{TV}$$

$$tau = C_A R_i$$

The equation for V(t) can be rewritten again as

$$\frac{V(t)}{A e^{-(t/tau)}} \simeq 0 \tag{2.17}$$

To implement the solution procedure, an initial estimate is made for A and tau. The left hand side of Equation 2.17 is evaluated as a function of time. Iterative minimization of the slope and intercept of this function, by successively modifying guesses for A and tau, yields the correct values of A = PsubTV and tau = (Ca*Ri). The system calibration constant, C, is then computed.

A typical calibration run has about 100 shots. The Biomation digitizer voltage range is typically set to one value for the first 50 shots, and to a different value for the second 50 shots. This is done so that data may be acquired for a range of energy monitor values. Each group of 50 shots is processed separately, and a calibration constant is computed for each group. Values of calibration constant and the error estimated for it are printed out for each group. Plots of the energy monitor value versus the integrated target return voltages are also plotted. As an example, Figure 2.10 shows the results for group II shots from a calibration run performed on 23 April 1982.

It was found that in program CAL the computed value of the calibration constant was being divided by a number to derive the final value. This number was either five or ten. No documentation was available as to why this was done. The explanation requires a second look at program AIMLESS, which processes normal data runs. In it, the signal is assumed to range from 0 volts to 2 volts when the conversion is made from an analog value to a digitized value. The data is actually taken with a full scale value of 10 volts. Thus there is a 1/5 scaling factor in the normal slant path lidar data.

In a calibration run, the Biomation voltage range is set to either 2, 5, or 10 volts for a group of 50 shots.

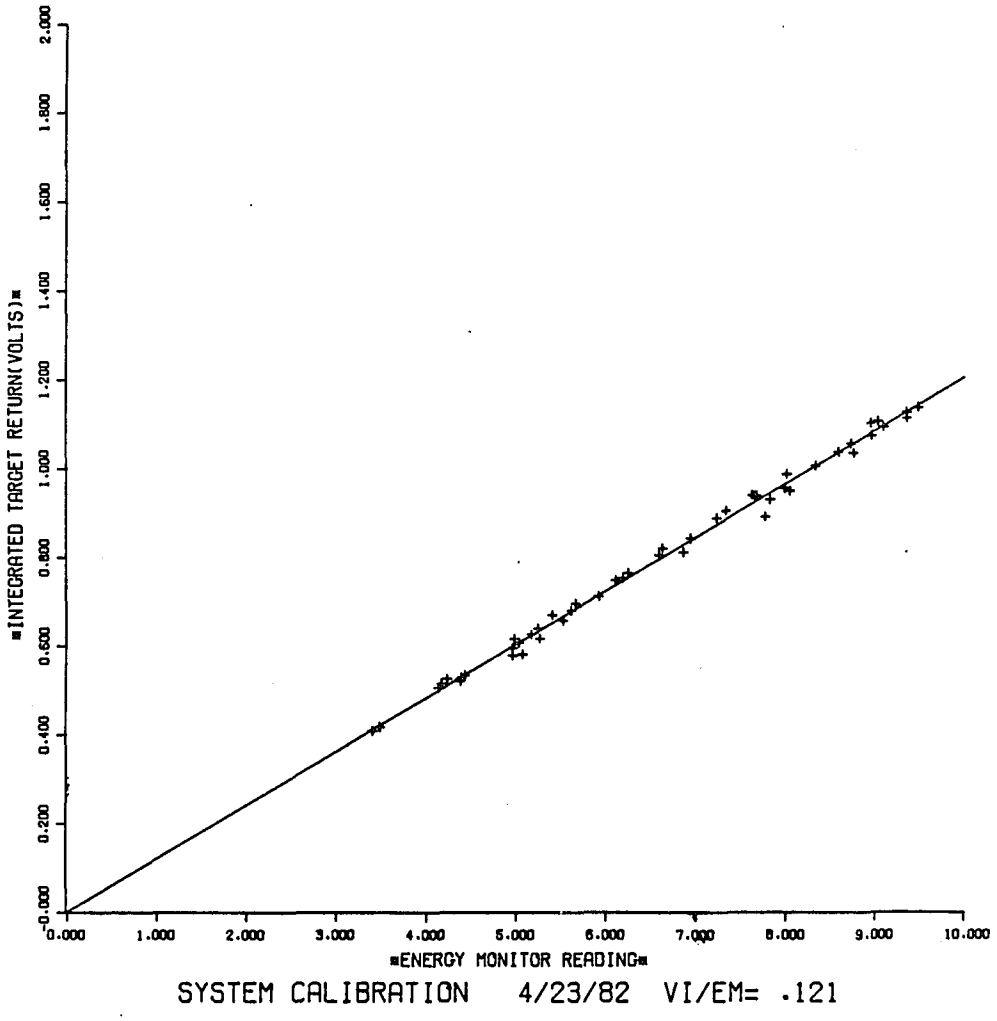

Figure 2.10. Calibration plot for 23 April 1982, Group II shots.

However, the calibration data is processed as if it were a 2 volt range, just as in AIMLESS. Thus, depending upon the Biomation setting, the computed calibration constant may have a scaling factor of 1, 2/5, or 1/5, but it should be the same as in the atmospheric data. Therefore, the computed constant should be divided by 5, 2, or 1, respectively. This would assure that the calibration constant as well as the slant path lidar data have a factor of 1/5. This was not clearly understood in the past and has resulted in erroneous values for the calibration constant. The Biomation voltage for each group of shots is now taken into account to insure that the proper scaling factor is used.

Another problem noted with program CAL encompasses programs CAL, PIT, and AER3. It was noted that in PIT and AER3 the signal was being divided by a quantity called GRATIO. This was supposed to be a ratio of PMT voltage divided by 1800, the quantity raised to a power of 11.212. The usual PMT setting is 1600 volts, so GRATIO is equal to (1600/1800)**11.212, or 0.267. Dividing by this meant effectively boosting the signal by a factor of 3.7456. This did not make sense until an examination of program CAL revealed that the quantity (ra/rt) is taken to be 3.7456. This is because the calibration runs were taken at a PMT voltage of 1600 volts, but data runs used to be taken at 1800 volts. The PMT voltage for the data runs was later changed to 1600

volts. Once this was done, the quantity (ra/rt) should have been entered as unity (1), but it was not. Thus, the calibration constant was boosted by a factor of 3.7456, and the signal was also boosted by a factor of 3.7456 in PIT and AER3. These two factors effectively cancelled each other out.

Sometimes the data in a calibration run shows a constant offset of about 1.3 volts. That is, the plot of energy monitor values against integrated target voltage returns does not pass through the origin, but shows an intercept on the target voltage axis. The reason for this is unknown to the author. It is assumed that this is some sort of a bug in the hardware, and an intermittent one at that. The remedy employed is to simply subtract the offset from all data points.

Calibration data runs have been taken periodically, and program CAL has been used to obtain a system calibration constant. For processing any data run, the latest value available for Calcon should be used. The value of Calcon is extremely important in that an error in it can have a significant impact on the solution. An error in the value of Calcon can produce roughly the same relative error in the total backscatter cross section. In the upper troposphere, where the particulate backscatter cross section can be less than 15 percent of the total backscatter cross section, a

small error in Calcon can result in a large error in the particulate backscatter cross section. In the past, attention was not always paid to what value of Calcon was used, and there was some confusion about the value of Calcon itself. As a result, different values of Calcon were at times used in an attempt to get a solution for some of the data runs. As noted above, this can significantly affect the retrieval of particulate backscatter; the effect of varying Calcon value in the input to program AER3 will be discussed in Chapter 4.

CHAPTER 3

RESULTS

It was mentioned in the introduction that an extensive amount of data has been collected since the departure of Spinhirne. Currently data from about 1979 to 1985 are available. Much of the collected data has been analyzed and, as discussed in Chapter 2, results consist of printouts and plots from program PIT and AER3. Outputs of program EDIT and AIMLESS are intermediate results. The data and results are currently available on a variety of media: plots and text outputs of programs on paper, data (in various degrees of processing) stored on magnetic tapes, raw data on magnetic tapes and on floppy diskettes.

Lidar data analysis results in the generation of a number of profiles and parameters. Interpretation of the results involves synthesis of much information including: conditions at the time of the data acquisition, input conditions used in the programs, and parameters that emerged in the outputs of the programs. It is a difficult task to deal with a large collection of such results on paper and give it the careful consideration that it deserves. It was evident to the author that there was a need for a tool whereby pertinent information about each data set and the results thereof

could be stored in a manner suited for easy access. A database, which is a generic name for a particular type of software, is such a tool.

3.1 The Concept of a Database and Its Capabilities

A database is an organized collection of information. It allows one to create what are commonly referred to as "records." Each record has a number of "fields" in it, each "field" being an item of information about the "record." Each field has a name, and the same type of information about each record is entered into the same field. Thus a "record" may have different "fields," each field holding a value for a different item; each field has values, each value corresponding to a different record. For example, in the lidar database, each data set forms a record. For each record, many fields have been created, such as "date," "time," and "fpnum." For a given data set, "date" holds the date of when the data was acquired, "time" has the start time of the data set, and "fpnum" has the number of the floppy disk on which the data for that set was originally recorded. Once the information has been entered, it is relatively easy to sort the information in various ways, and to create new fields based upon the values of existing ones. Having information in a database means that the information is organized, it is easy to examine any of it quickly, different items that are

interrelated by a commonality may be readily accessed, and various conditions may be applied to the database, the results of which may be seen immediately. Some database programs come with a built-in graphics package which allows one to display the relationship between two or more parameters in the database. A database program known as "REFLEX" has been used in organizing the results of lidar data analyses.

3.2 The Lidar Database: Categories of Data Sets

Data sets acquired by the laser radar operated by ARSL fall into four different categories, depending upon what type of data was acquired. These are as follows:

1. Slant path data set: this means that shots were fired at varying zenith angles. This is the most common category of data acquisition. Usually, the azimuth angle was not changed, and two sets of shots were fired at a zenith angle of zero degrees.
2. Vertical data set: all shots were fired at a zenith angle of zero degrees.
3. Calibration data set: the laser was fired at a calibration target, to acquire information needed to calculate the lidar calibration constant.
4. Simulation data set: the laser was not actually

fired; instead, a simulator was used to generate data similar to that acquired in a real data set.

3.2.1 A Typical Form for the Lidar Database

Information about all the data sets acquired by ARSL from 1979 to present has been entered into the database. As mentioned above, each data set constitutes a "record." Table 3.1 shows the names of various fields used in the lidar database and their definitions. Table 3.2 shows what a typical record in the lidar database looks like, with values included. Each record has information that may be categorized as follows:

- information about data acquisition conditions (for example: date, time, floppy number);
- the input parameters for programs like AER3 (for example: Sguess, Calcon); results of the programs (for example: S_hml, taup_hml);
- what types of results are available on paper (for example: praw, pedit);
- the identification number for magnetic tapes that have data or results recorded on them, for example: mt8473g, mt8449k; and
- comments made about the data set, in fields com1 through com9.

Table 3.1. List and definitions of field names in a lidar database record.

Date:	the date of data acquisition
Time:	time of data acquisition
Trynum:	a number assigned to denote each attempt to analyze the data
Fpnum:	floppy number, a number assigned by CCIT to each floppy on which data is recorded
Ournum:	a number assigned by us (ARSL) to each data floppy
Flags:	a code to denote the nature, and the outcome of the data run. The codes are as follows: r = ran (aer3 worked) f = failed (did not get all the way to, or through, AER3) a = aborted data acquisition s = data was slant path v = data is vertical z = data is simulated e = equipment malfunction noted while attempting to process data A combination flag is often noted, for ex: RS means that the data was slant path, and it was successfully analyzed.
Sguess:	input guess for S ratio (to program AER3)
Calcon:	input value for the calibration constant
hml:	height of the mixing layer, input to aer3
pithml:	height of the mixing layer, assessed from PIT
hml_gr:	height of the mixing layer, assessed from the AER3 extinction plot
S_hml:	the S ratio computed from AER3, for the lst mixing layer
Sdev_hml:	the standard deviation of S for the lst mixing layer

Table 3.1--Continued

pes:	standard deviation as a percentage of S for the lst mixing layer
taup_hml:	particulate optical depth for the lst mixing layer
taup_stdl:	the standard deviation of particulate optical depth for the lst mixing layer
petpl:	the std. dev. as a percetage of taup_hml
taup_tot:	total particulate optical depth
taup_ttstd:	std.dev. of taup_tot
praw:	printout from raw data available (y or n)
pedit:	printout from program edit available (y or n)
paim:	printout from program aim available (y or n)
ppit:	printout from program pit available (y or n)
gpit:	graph from program pit available (y or n)
paer3:	printout from program aer3 available (y or n)
gaer3:	graph from program aer3 available (y or n)
mtxxxxx:	if the data is on a magnetic tape in raw or partially processed form, its position on the magnetic tape is noted in ynn format, where nn is the position.
coml.... .. com8:	comment lines for remarks

Table 3.2. A sample record from the lidar database.

```
Date: 3/17/80    Fpnum: 213      Trynum: 1            Time: 1905
month: 3         Ournum: 1054    Flags: rs

Calcon: 452      Sguess: 20      ntaul: 8.412E-03      praw: n
                                                       pedit: n

pithml: 2.50     S_hml: 21.53    taup_hml: 0.02128     paim: y
hml: 2.50        Sdev_hml: 6.27  taup_stdl: 0.00710    ppit: y
hml_gr: 2.50     pes: 29         petpl: 33             gpit: y
                                                       gaer3: y
taup_tot: 0.03390                                      paer3: y
taup_ttstd:
petpt:

pithm2:          S_hm2:          taup_hm2:
hm2:             Sdev_hm2:       taup_std2:
hm2_gr:

mt8473g:   mt8413g:yl4    mt8449k:yl5    mt8462h:
mt8433d:y3 mt3283d:

com1: Pit plot hmix 2.5 km, aer3 plot hmix 2. 5 km.
com2: Aer3: parti. ext stays < raylee above 2.3 km.
com3: ok run.
com4:
com5:
com6:
com7:
com8:
```

Note that in Table 3.1 the "trynum" field shows a trial number for each data set. Many data sets were analyzed a number of times, and although results of all the multiple attempts of all the trials has not been recorded, some data sets do show multiple attempts. Typically, a trial number of 1 ("trynum" = 1) was assigned for the set that showed the optimum results, and other sets were assigned integer values greater than or equal to 2.

3.2.2 Number of Data Sets in Various Categories

The Table 3.1 shows a field named "flags," and as explained in the definitions, the field can have seven different alphabetical designations for a given data set, depending upon the type and the outcome of the data set. Table 3.3 shows the number of data sets in each category. It shows that out of a total of 104 slant path data sets that could have been analyzed, 83 have been successfully processed ("flags=rs"), a ratio of almost 80 percent, or four out of five. Appendices 1.1 through 1.5 show the lidar database for all the slant path data sets that were processed and had a trial number of 1. Note that some field names appear in more than one appendix. This is done so that closely related parameters may be seen on a single page. Note also that each of Appendices 1.1 through 1.5 are two pages long. The slant path data sets that could not be successfully processed

Table 3.3. The number of data sets in each category of the lidar database.

Flags	Category Description	Number
RS	ran, slant path	83
FS	failed, slant path	21
ES	equipment failure, slant path	11
S	not processed, slant path	14
C	calibration run	13
Z	simulation run	6
V	vertical data run	8
	Total	156

("flags"=fs) are listed in Appendix 1.6. The slant path data sets that had some type of equipment (hardware) failure associated with them ("flags"=es) are listed in Appendix 1.7. There are some slant path data sets that have not yet been processed ("flags"=s), and for future consideration, these are listed in Appendix 1.8. The vertical path data sets and the simulation data sets ("flags"=v and "flags"=z, respectively) are listed in Appendix 1.9 and Appendix 1.10. Finally, the calibration data sets are listed in Appendix 1.11. The calibration data involves a set of parameters that is different from the slant path data set. Therefore, although the calibration data sets have been listed in the lidar data set list, they have also been entered separately into another database, called the Calibration database. A table showing the form of a typical Calibration database "record," along with definitions of the field names, is shown in Table 3.4. The calibration database itself is listed fully in Appendices 1.12 through 1.14. Results of the calibration data sets will be discussed later in this chapter.

3.3 Results of the Lidar Data Analysis

Successful analysis of a slant path data set produces two important visual results: a profile of the energy-and-range normalized return, and a profile of the extinction coefficient. The extinction profiles vary a great deal from one another, and it is instructive to look at them for clues

Table 3.4. A sample record from the calibration database and definitions of the field names.

A Sample Calibration Record	
Date: 7/06/85	Time: 1040
Fpynum:	Ournum:
RsubL: 1000	Tubrs: 3.7456
GrIBioFSvolts: 5	GrIIBioFSvolts: 10
GrICalcon: 549	GrIICalcon: 625
AvgCalcon: 587	
8473G:	8413G:
8449K:	8462H: y
8433D:	3283D: y

Definitions	
Date	date of data acquisition
Time	time of data acquisition
Fpynum	floppy number, assigned by CCIT
Ournum	our floppy number, (assigned by ARSL)
RsubL	load resistance on the pmt
Tubrs	tube responsivity ratio
GrIBioFSvolts	full scale Biomation volts, group I
GrIIBioFSvolts	full scale Biomation volts, group II
GrICalcon	calibration constant computed from group I shots
GrIICalcon	calibration constant computed from group II shots
AvgCalcon	average calib. constant (of group I and II
xxxxy:	data on magnetic tape xxxx (y or n)

about the structure of the lower troposphere on a given day. In view of this, examples of the normalized return profiles and corresponding extinction profiles should be presented. However, in order to obtain a cohesive presentation, this discussion is postponed until Chapter 4, where these profiles are shown, following a discussion of horizontal inhomogeneity effects. Other results of lidar data analysis include the heights of the mixing layers, the Sratio values and the optical depths. Discussions of the result for these quantities, using the lidar database, are presented next.

3.3.1 The S Ratio

The lidar slant path results may be discussed in various ways. A histogram of S ratios from Appendix 1.2, with a class interval of 5, shown in Figure 3.1, illustrates which S ratio values have occurred most frequently. It can be seen that the values of S have ranged from about 5 to 100. The primary concentration is seen to be from 10 to 40, accounting for 73 percent of all the values. Roughly 19 percent of S ratios were over 40, showing a secondary concentration mode, and about 7 percent were less than 10. The histogram clearly shows that the most representative values of S, for the conditions in Tucson, on an annual basis, range between 10 and 40, with a clear domination of values in the 20 to 30 range. Various averages may be computed over a yearly or monthly basis. Table 3.5 shows a

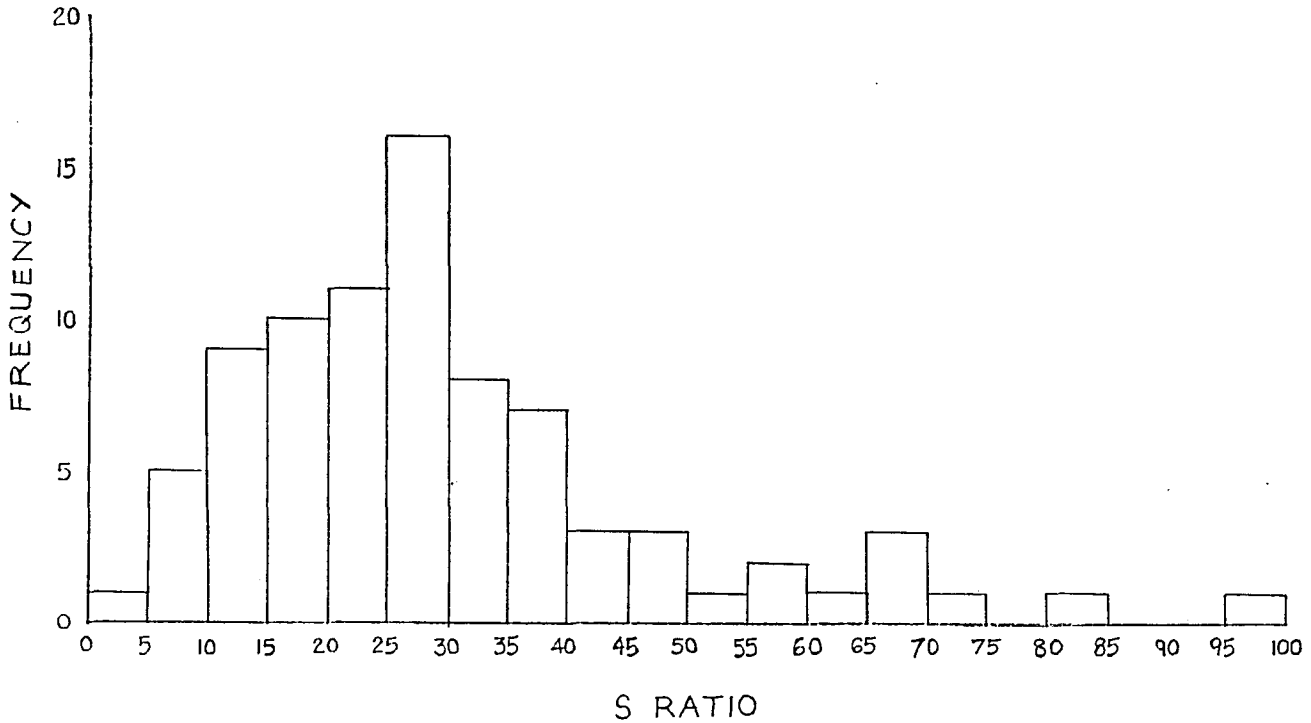

Figure 3.1. A histogram of S ratio values.

Table 3.5. Arithmetic and inverse variance weighted means of lidar parameters.

Parameter		Arithmetic Mean ± Sdev	E.S.wtd Mean
S Ratio			
All values	(83)	30.14 ± 17.74	24.47
thru(10,50)	(67)	26.67 ± 9.78	23.23
thru(10,40)	(61)	24.84 ± 8.17	22.36
≥ 50	(10)	67.50 ± 12.73	64.26
≥ 40	(16)	59.15 ± 14.90	57.65
Particulate Optical Depth @ Mixed Layer			
All values		0.04307 ± 0.02434	0.03856
thru S (10,50)		0.04329 ± 0.02393	0.0379
thru S (10,40)		0.04119 ± 0.02295	0.0377
s ≥ 50		0.05730 ± 0.02033	0.0599
s ≥ 40		0.06005 ± 0.02175	0.0555
Total Particulate Optical Depth			
All values		0.07504 ± 0.04637	
thru S (10,50)		0.07287 ± 0.04313	
thru S (10,40)		0.0677 ± 0.0376	
s ≥ 50		0.11944 ± 0.04281	
s ≥ 40		0.11841 ± 0.04979	
Height of Mixed Layer (km)			
From Pit plots		2.65	
Input to AER3		2.67	
From AER3 Plots		2.80	

variety of arithmetic and inverse variance weighted means (the "weight" is the reciprocal of the variance of a parameter), and standard deviations. It can be seen that the arithmetic mean of all S ratios is 30.14, but the error square weighted mean of all S ratios is somewhat lower, 24.47. The arithmetic mean of the primary group of S ratios, (10 to 40) is 24.84, and the error square weighted mean for this same grouping is 22.36. These values are not significantly different from those previously reported by Spinhirne [1977], Spinhirne et al. (1980), and Reagan et al. (to be published, 1988).

A plot of absolute values of the standard deviation of the S ratio versus the S ratio is shown in Figure 3.2. It can be seen that, except for three cases, the absolute standard deviation of S never exceeds 20, while the S ratio varies from about 5 to about 80. This leads to larger percent error values in S for smaller S ratios.

3.3.2 Monthly Statistics of the S Ratio and the Optical Depth

It is of interest to determine whether the values of the S ratio, optical depth and mixing layer heights show a long term temporal or seasonal dependence. Table 3.6 shows the average mixing layer height (from AER3 extinction plots), the inverse variance weighted averages of S and of the optical depth at mixing layer height, on a generic-month

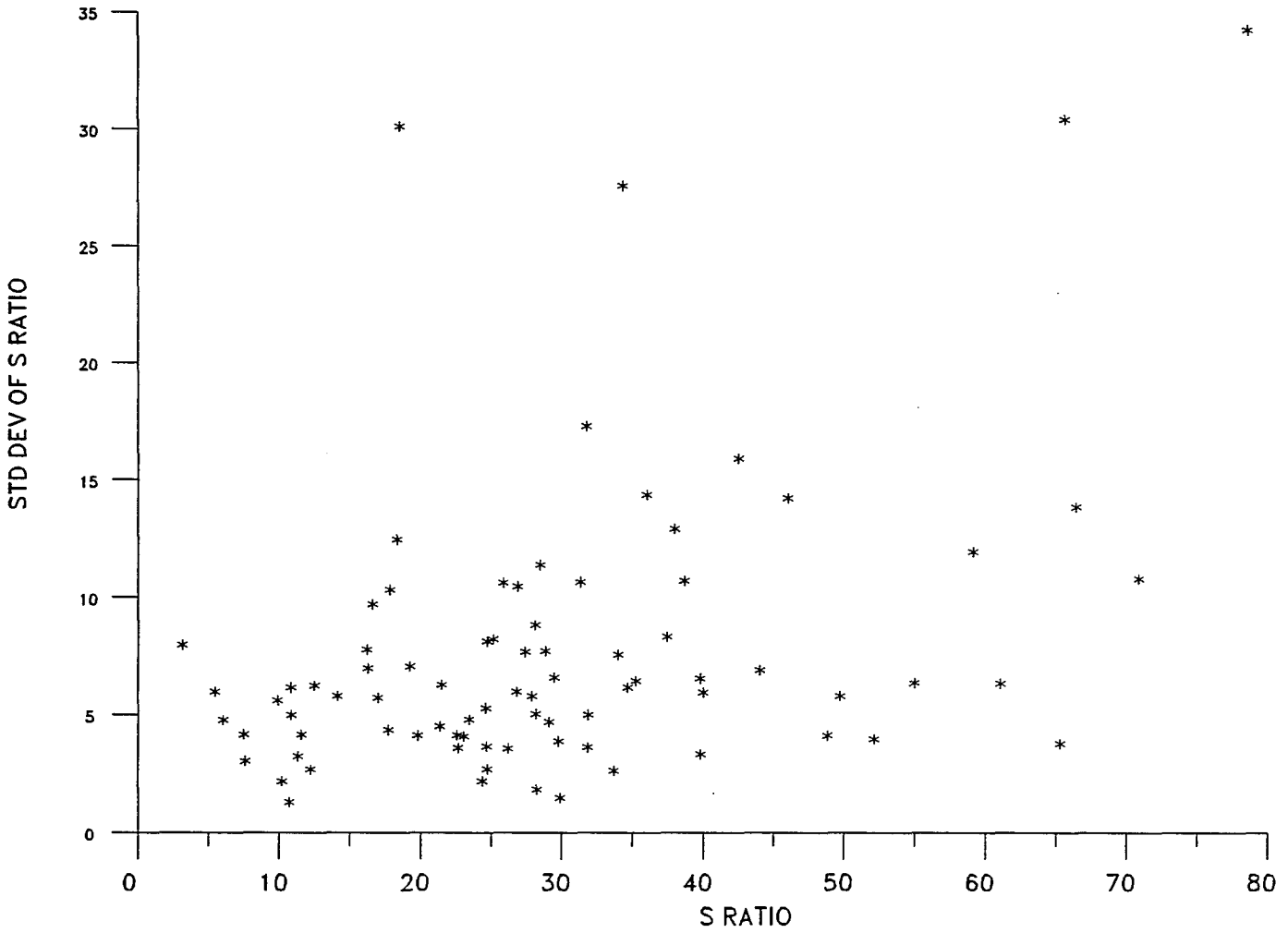

Figure 3.2. The standard deviation of the S ratio as a function of the S ratio.

Table 3.6. Monthly averages of lidar parameters.

ahmlam = aer3 hmixl, arithmetic mean

ihmlam = input hmixl to aer3, arithmetic mean

sram = s ratio, arithmetic mean

srewm = s ratio, inverse variance wtd. mean

tplam = tau parti. for hmixl, arithmetic mean

tplewm = tau parti. for hmixl, inverse variance wtd mean

Labels may be truncated to fit columns.

MON	#DAYS	AHMl	IHMlA	SRAM	SREWM	TPlAM	TPlEWM
1	4	1.78	2.23	45.63	25.11	0.03855	0.01666
2	7	2.54	2.6	26.9	24.49	0.03034	0.02686
3	14	2.56	2.55	31.94	30.77	0.03599	0.03265
4	14	2.89	2.81	30.48	28.05	0.05437	0.065
5	21	3.08	2.73	28.05	22.97	0.04436	0.03901
6	12	3.4	2.92	30.14	14.9	0.04202	0.03473
7	1	3.3	2.5	7.64	7.64	0.02346	0.02346
10	2	1.8	2.5	10.42	14.35	0.01835	0.02773
11	3	2.17	2.37	40.28	43.31	0.05491	0.06234
12	5	1.8	2.43	31.37	30.87	0.05654	0.04842

basis. Note that no values are available for the months of August and September, and less than 5 data sets are available per month from July through January. The average HMIX and inverse variance weighted average of the S ratio are plotted versus a generic year in Figures 3.3 and 3.4 respectively, where the x axis is in months, starting from January (1) to December (12). Figure 3.5 shows TAUP in a "normalized" form plotted against a generic year. The normalization is performed by dividing the TAUP for each data set by the HMIX (as judged by SIGMAP plot) for that day. These values were averaged on a monthly basis to obtain the points shown in Figure 3.5. The normalized optical depth is, in effect, an average extinction coefficient for the mixing layer, as TAUP is the integral of SIGMAP over distance.

Figures 3.3 through 3.5 demonstrate that the parameters do have a seasonal dependence. The HMIX reaches an annual summer high of 3.4 km in June, and is down in the winter, at $\simeq$ 1.8 km in October, December and January. The S ratio is at its lowest in June and July (15 and 8, respectively) and is above at least 24 in the winter, from November through February. The normalized TAUP displays a behavior similar to the S ratio. In Figure 3.5, the per kilometer TAUP is down to about 0.013 in June and is above 0.020 from November through January. It does go down to 0.012 in

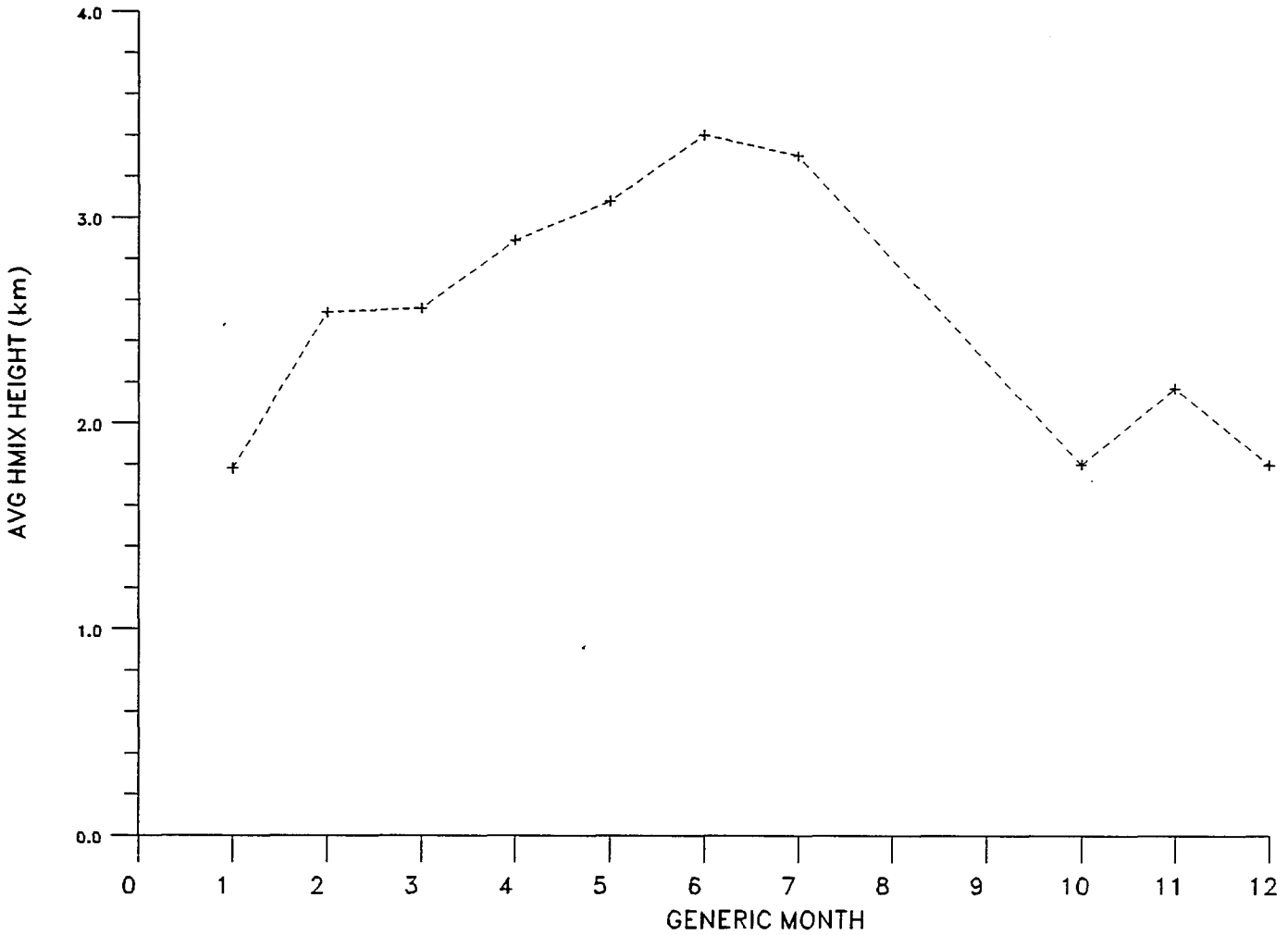

Figure 3.3. Average HMIX values per generic month.

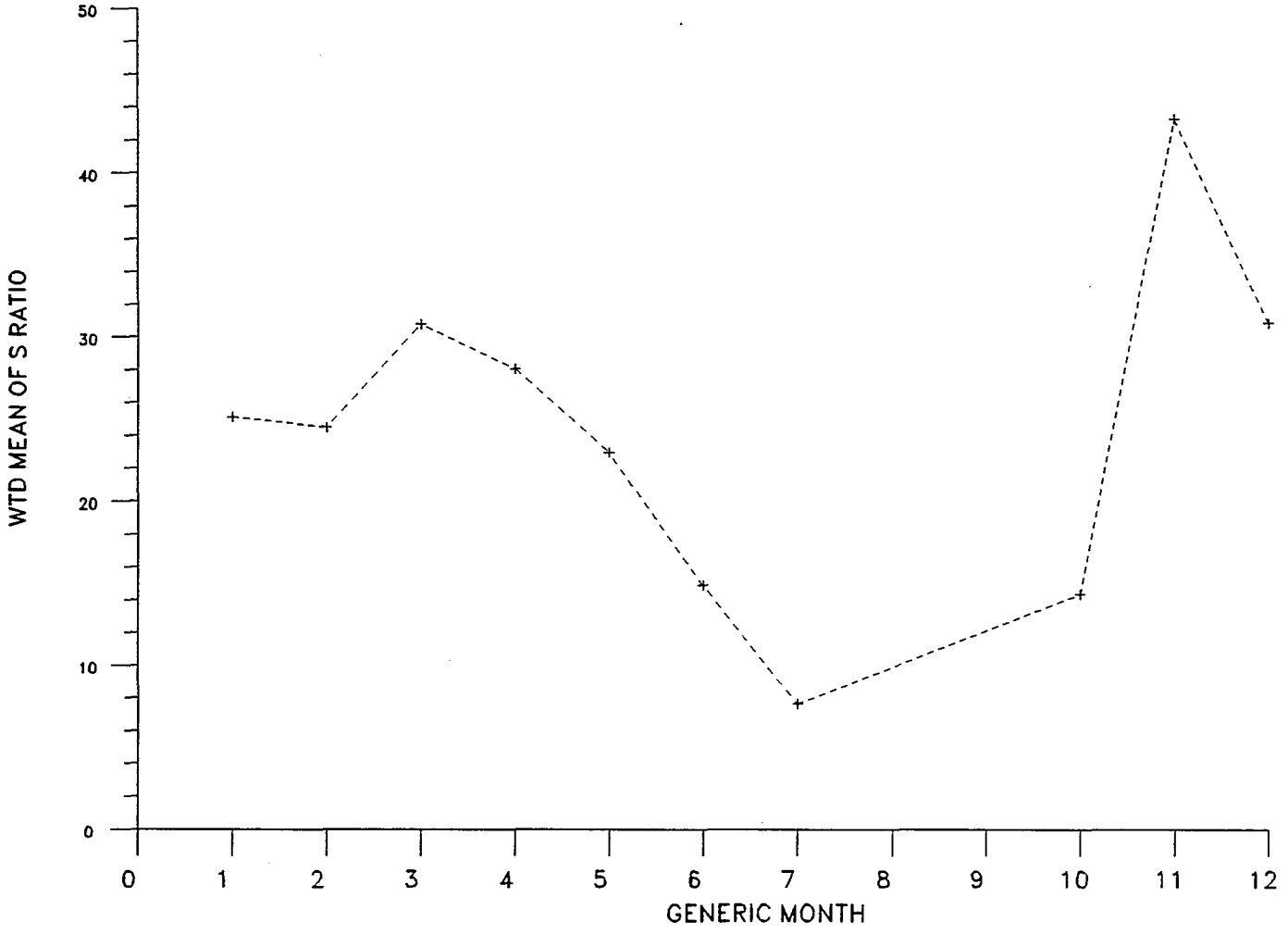

Figure 3.4. Inverse variance weighted average of S ratios per generic month.

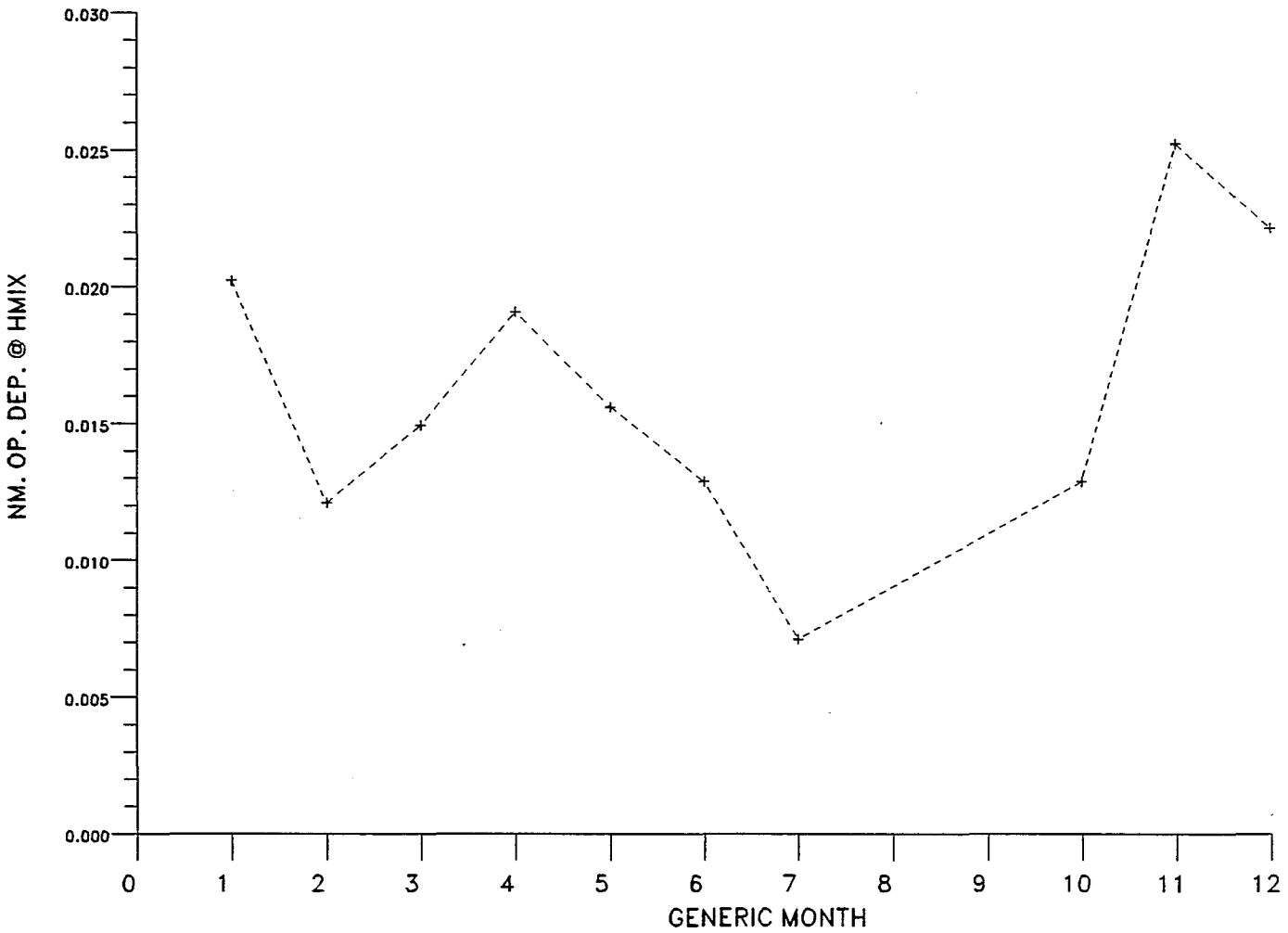

Figure 3.5. Average normalized TAUP at HMIX per generic month.

February, but increases again to 0.015 and 0.020 in March and April.

A likely explanation for the behavior of HMIX may be that in winter the low temperatures cause the HMIX to drop. As winter turns into spring and the temperatures increase, the mixing layer height starts to increase, reaching a high in summer. High values of HMIX in summer mean that the aerosols are distributed over a larger height interval, whereas low values of HMIX in winter indicate a denser distribution of aerosols. This may be the reason that the S ratio and the TAUP per kilometer are in general the inverse of HMIX, namely, low in the summer and high in the winter, although there can be seasonal deviations, as indicated by the case for February in Figure 3.5. Table 3.6 indicates that the absolute values of TAUP during the winter time are among the highest for the year. This is most likely due to the strong temperature inversions that tend to occur around this time of the year which trap a major proportion of particulate matter in the lower troposphere below the mixing layer height. It should also be noted that there are more data sets available in spring than at any other time. Data sets should be equally distributed throughout the year to provide a good statistical base for a more detailed assessment of the seasonal trends in the data.

3.3.3 Height of the Mixing Layer (HMIX)

It was noted in Chapter 2 that plots of gain removed, energy-and-range normalized signal can give a good indication of the height of the mixing layer in the lower troposphere. This value is typically used as an estimate for the mixing layer height used as an input to program AER3. As the plot of HMIX as judged from program PIT versus HMIX as judged from program AER3 in Figure 3.6 illustrates, there is very good correlation between HMIX as deduced by plots of PSIG from program PIT and by the extinction profile produced by program AER3. This will again be illustrated in Chapter 4, where a classification of SIGMAP profiles will be presented.

3.3.4 Normalized Optical Depth and the S Ratio

A plot of the normalized optical depth versus optical depth at HMIX is shown in Figure 3.7. The data sets included here are restricted to those with S ratios of less than 50 and optical depths of less than 0.1. Since only 4 sets have optical depths at the mixing layer height of greater than 0.1 and almost 90 percent of the sets have S ratios of less than 50, this is a reasonable restriction. The plot in Figure 3.7 indicates that as optical depth increases, the optical depth per kilometer increases in a fairly linear fashion. The dashed lines on the graph show that the majority of cases do fall in this linear "band." Another plot, shown in Figure

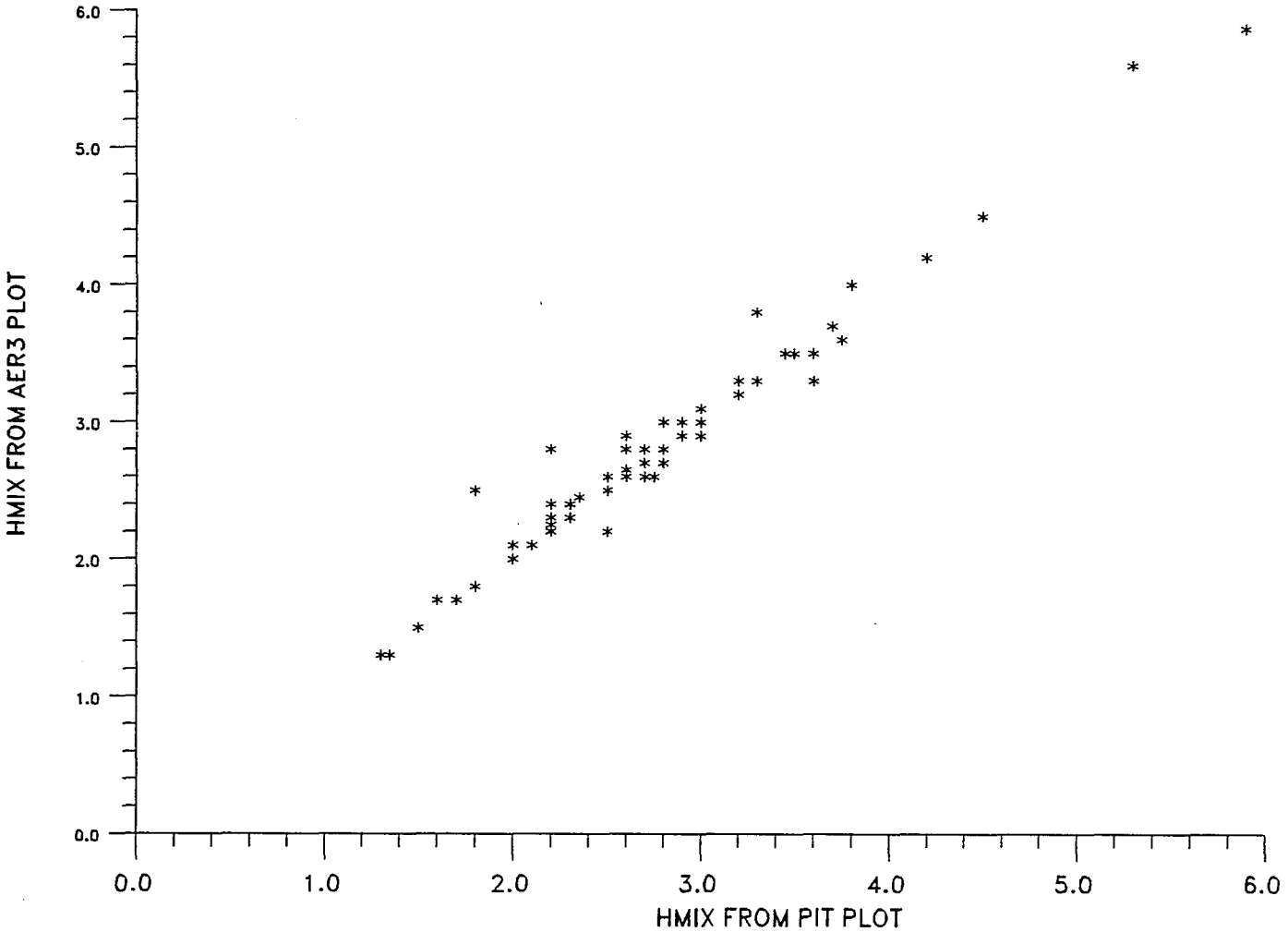

Figure 3.6. Correlation between HMIX values (in km) as deduced from PIT plots and AER3 plots.

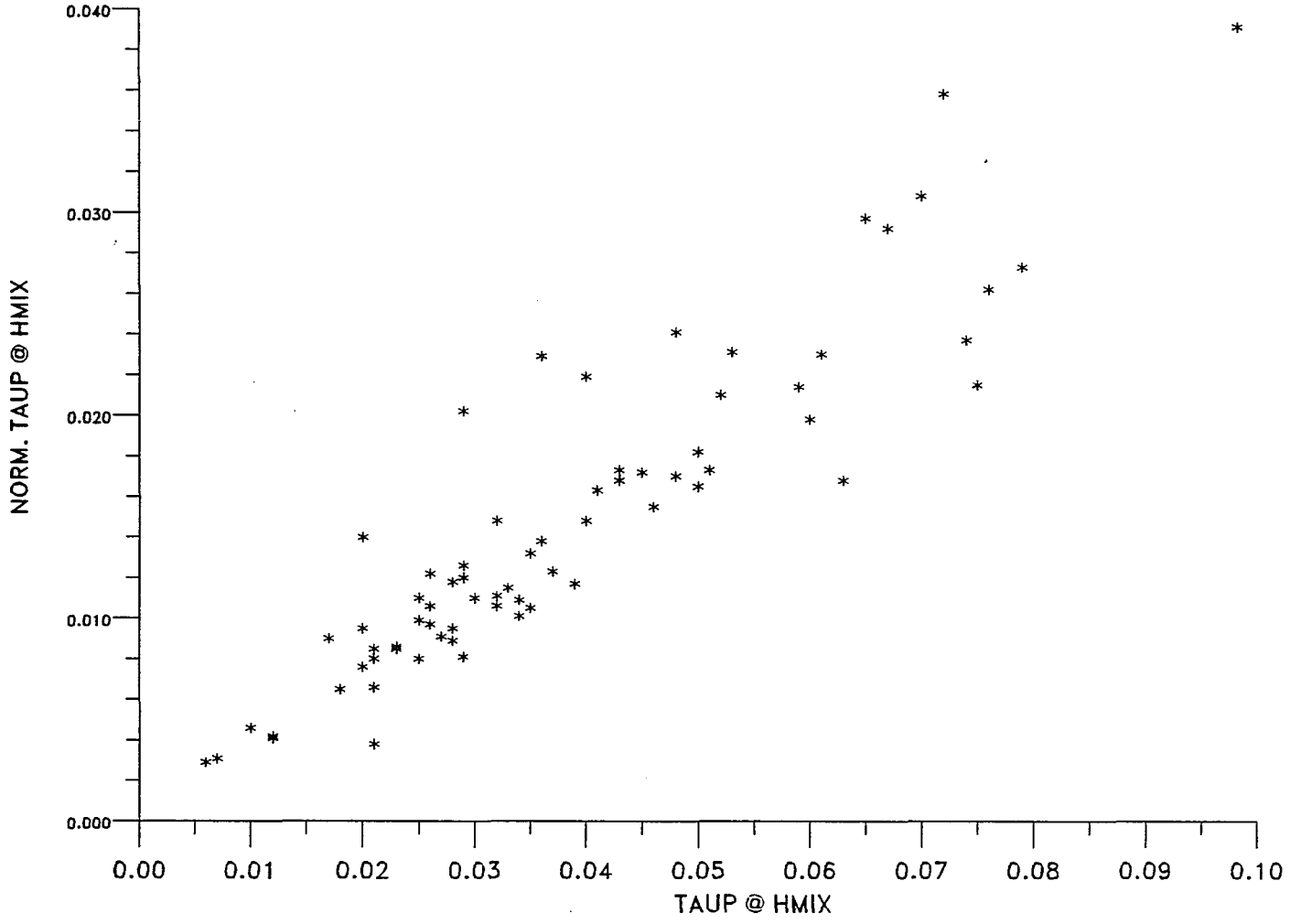

Figure 3.7 Normalized TAUP at HMIX as a function of TAUP at HMIX.

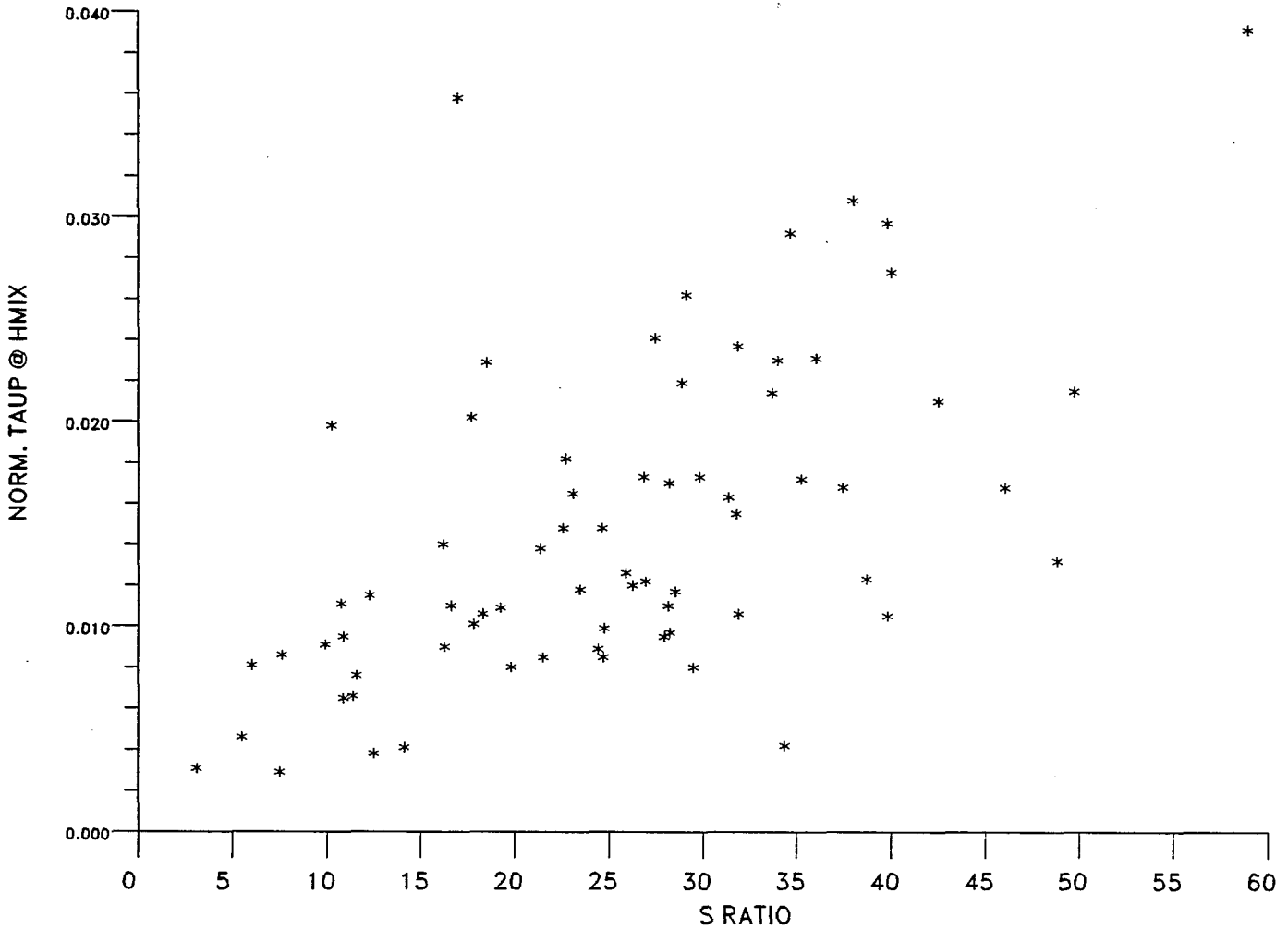

Figure 3.8. Normalized TAUP at HMIX as a function of the S ratio.

3.8, illustrates that the S ratio also increases in general as the normalized optical depth increases. This plot shows more scatter in the data, and there is also some saturation in the normalized TAUP at larger S ratio values. This behavior is not unexpected, because the S ratio is dependent upon both SIGMAP and BETAP, whereas TAUP is dependent only upon SIGMAP. Thus there can be two data sets that produce identical or nearly identical S ratio values, but have different optical depths. This effect is also shown in the results previously reported by Spinhirne (1977).

3.4 The Calibration Database

The calibration data results are important to lidar data processing; they provide values of the calibration constant required as an input to successfully run program AER3. Over the years a number of calibration data sets have been acquired, as can be seen in Appendices 1.12 through 1.14. Out of the 13 sets, 10 sets have been analyzed to produce values of the calibration constant, 2 have not been accessed and 1 has apparently been lost. From 1979 to 1984 the calibration constant values can be seen to decrease slowly from about 600 to about 235. However, the bulk of the lidar data that has been collected and analyzed in this work has been for a calibration constant between about 400 to 500. In 1985 this value is seen to have reverted back to 625. However, the author does not have confidence in this value.

Lidar data collected since 1985 has proven to be problematic in terms obtained an AER3 solution. Values of the calibration constant in the range indicated (549 to 625) have failed to yield a solution. In some cases, as can be seen in Appendix 1.2, calibration constant values of 325 to 450 have been used to obtain successful solution. It is possible that the lidar hardware setup is no longer in optimal condition; additionally, the target used for the calibration data has degraded over the years. It would be more reasonable to assume that the calibration constant value in 1985 was somewhere between 250 and 350, which would be in line with the trend seen over the years.

CHAPTER 4

CASE STUDIES

The integrated slant path solution procedure for analyzing lidar data and the results obtained from it may be examined in several ways. This chapter examines some of the assumptions made in implementing the integrated slant path solution procedure. The impact of variations in the input parameters to program AER3 is assessed and results of particulate to Rayleigh extinction ratios above the mixing layer, which relate to the lidar system calibration constant, are discussed. A classification of particulate extinction profiles is also presented.

4.1. Assessment of Horizontal Inhomogeneity

An assumption made in the integrated slant path solution procedure is that the atmosphere is horizontally homogeneous. The solution is developed to allow for some variation, but large variations in a horizontal slice of the atmosphere can have an adverse effect on the solution. The homogeneity assumption can be tested by examining the horizontal variation in the gain removed, energy-and-range normalized signal (PSIG). Another approach is to extract, by one or more means, the particulate backscatter for different

angles at a given height. The variation in these values with angle may yield a clue as to the source of errors in the integrated slant path solution. Various techniques that have been employed to investigate the homogeneity assumption are presented below.

4.1.1 Variation in the Gain-removed, Energy-and-Range Normalized Signal

At a given height, the variation in PSIG for different zenith angles is indicative of variation in the product of total backscatter and transmission. Two ways of computing this have been devised. First, in program PIT, the horizontal variation in PSIG is computed. After the signal has been range normalized, the average of the values of PSIG for the different slant angles at each effective vertical height is computed. The standard deviation, the percent standard deviation (% of the average), the minimum deviation from the average, and the maximum deviation from the average of PSIG are also computed as various measures or indicators of horizontal inhomogeneity. The percent standard deviation of PSIG versus height is also plotted. These steps are performed in a new subroutine, HOMGEN, in program PIT. It is useful to have a measure of horizontal variation of PSIG that includes only those angles which are used in the slant path solution angles. This is the second way of computing inhomogeneity in

PSIG, currently done in program AER3 using a subroutine also named HOMGEN, called from within subroutine SOLVE.

Additionally, this provides an indication of the horizontal variation of the signal even when program AER3 fails, thereby providing a possible clue as to why it may have failed.

Figure 4.1 shows a plot of the percent standard deviation of PSIG versus height for all angles, generated by program PIT, for 12 May 1981. A similar plot is shown in Figure 4.2 except this plot was generated from AER3 using only the solution angles. The two plots are almost identical but this will not always be the case as the AER3 plot is only for the slant angles that were used in the solution. Depending upon the value of the HMIX, one or more of the slant angles may not be used in the solution, and their inclusion in the computation of horizontal inhomogeneity in PSIG would not be proper, particularly if these numbers are used as an indicator of why the solution may have failed. It should be mentioned here that at a given effective vertical height, PSIG values for small zenith angles will, and should, be slightly larger in magnitude than the PSIG values for the larger zenith angles. This is because the smaller path lengths of the returns at smaller zenith angles result in decreased transmission losses and increased magnitudes in the shot returns. Thus, some amount of deviation in PSIG at any

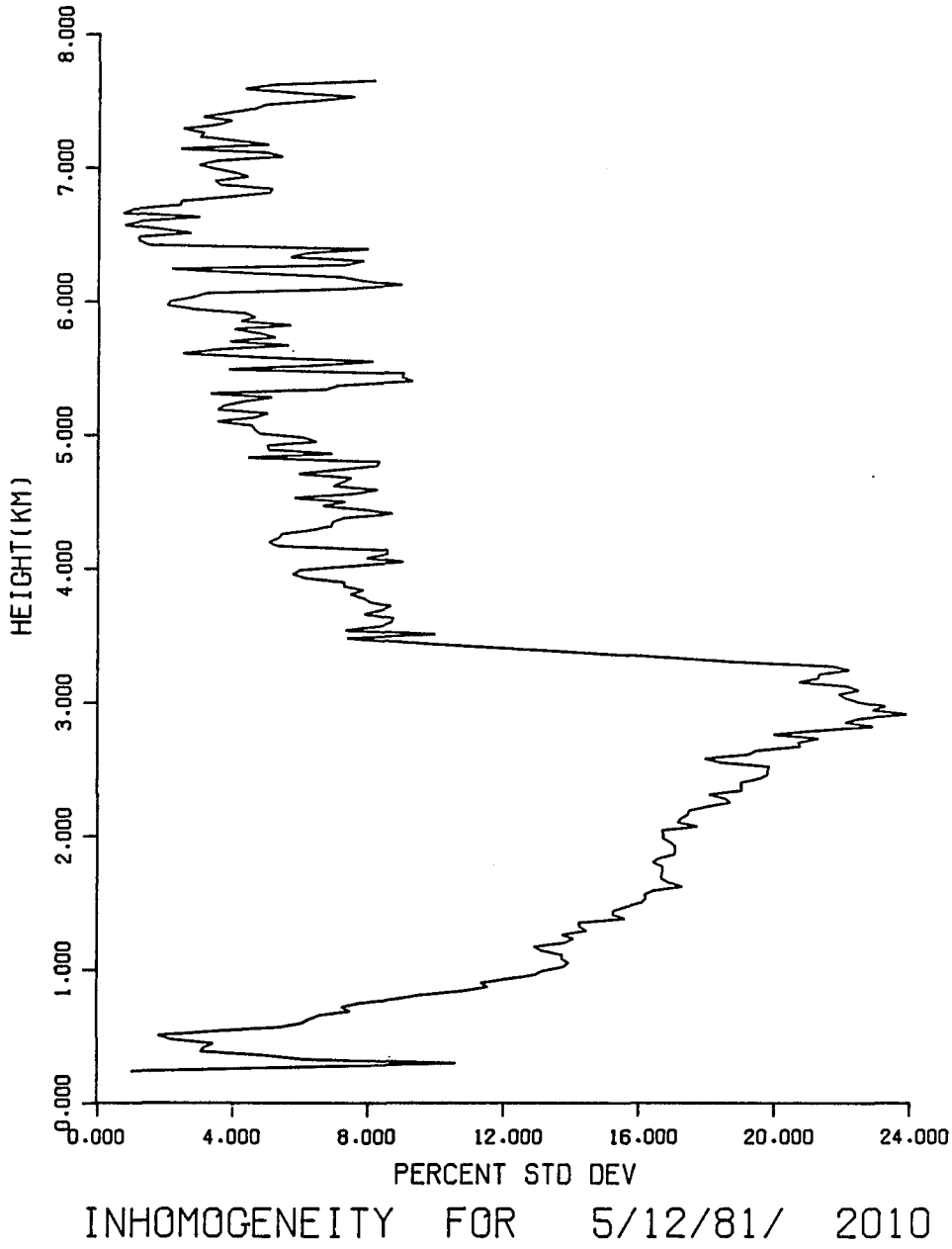

Figure 4.1. %SD of PSIG for all slant angles from program PIT for 12 May 1981.

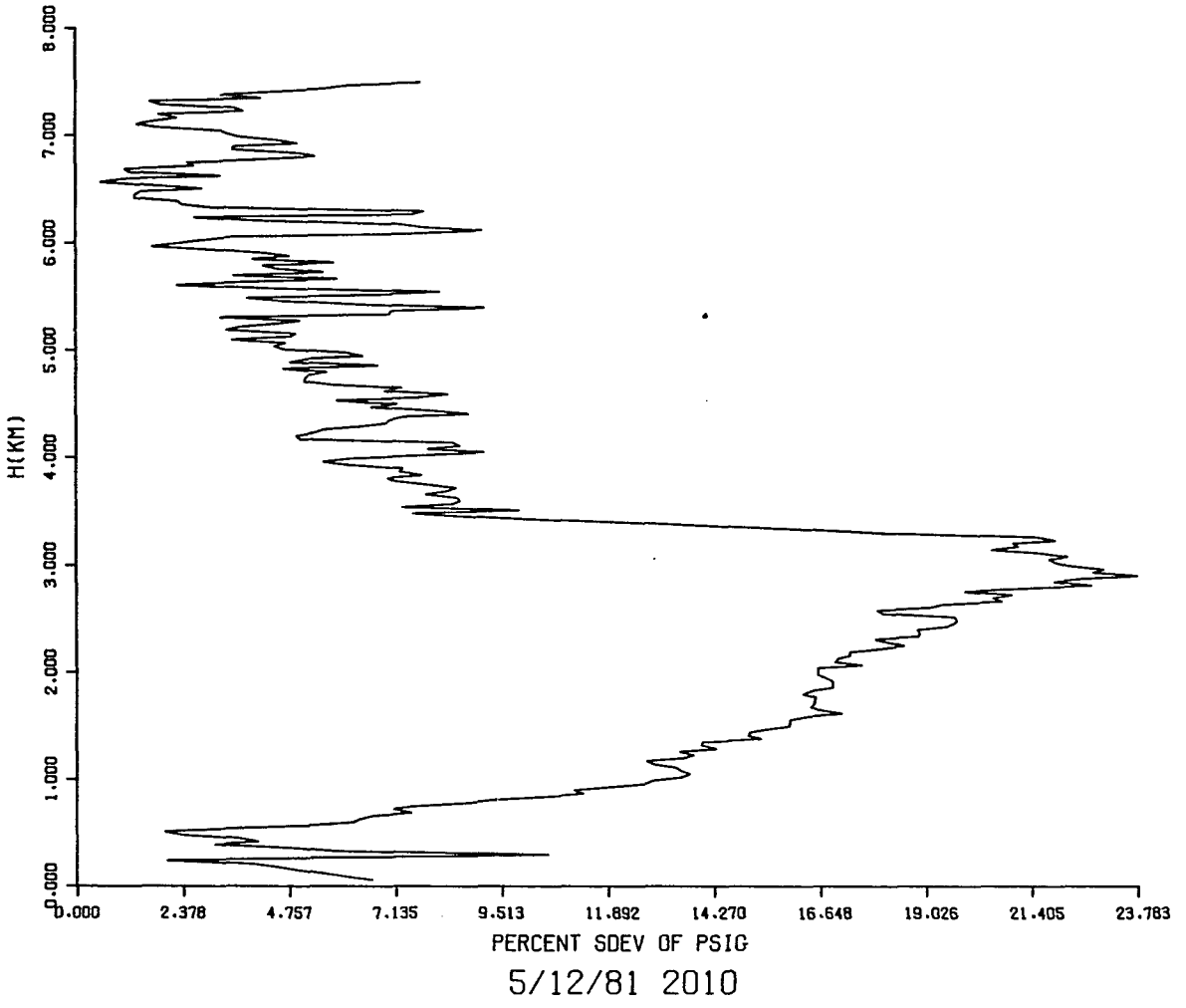

Figure 4.2. %SD of PSIG for the angles used in AER3 solution, from program AER3 for 12 May 1981.

height is always expected, and it should increase as height increases. Still, plots such as Figure 4.1 are useful in that inhomogeneity in the backscatter coefficient may still be evident, particularly if the signal return for an angle is significantly different in magnitude from others.

4.1.2 Variation in the Backscatter Coefficient

Instead of examining the variation in PSIG, the backscatter coefficient itself may be extracted in various ways. Three different techniques were explored which are as follows:

1. Once an AER3 solution has been reached and the S ratio and optical depths through the lower troposphere have been obtained, the lidar equation may then be solved for the particulate backscatter coefficient for each angle at a given height. Equation 2.6 for PSIG can be rewritten as

$$P = C\beta_{TOT}e^{-2\sec\theta(\tau_{TOT})} \qquad (4.1.2.1)$$

where

P = gain removed, energy-and-range normalized signal

C = the calibration constant

β_{TOT} = total backscatter

θ = zenith angle of the acquired data

τ_{TOT} = total optical depth

This equation can be used to derive the total backscatter for each slant angle. The particulate backscatter is then found by subtracting Rayleigh backscatter from it.

2. Once the S ratio and the particulate optical depth at the bottom of a layer is known, the integrated slant path lidar equation can be solved for the particulate transmission for each zenith angle. This form of the lidar equation (Spinhirne, 1977, Equation 2.14) is given by

$$T_P^r(z) = \frac{T_P^r(z_1)T_R^{rx}(z_1)}{T_R^{rx}(z)} - \frac{rS}{T_R^{rx}(z)}\int_{z_1}^{z} \frac{P(z',r)T_R^{r(x-1)}(z')dz'}{C} \qquad (4.1.2.2)$$

where

z_1 = the bottom of a layer, start of integration point

z = the top of the segment of height over which integration will be performed

r = (2 * secant θ), where θ = zenith angle

T_P = particulate transmission at a given height

T_R = Rayleigh transmission at a given height

S = S ratio

$X = \frac{3S}{8\pi}$

P = gain removed, energy and range normalized signal at a given height for a given angle

C = calibration constant

In this equation, every quantity on the right hand side is known so the particulate transmission for each zenith angle

can be computed. The natural logarithm of transmission yields the particulate optical depth, and differentiating the optical depth gives the extinction coefficient. Using the S ratio, S = sigmap/betap, the backscatter coefficient can then be obtained. This procedure is performed at each height starting from the bottom of the mixing layer, and particulate backscatter profiles are obtained for individual angles. Only those angles that were used in the integrated slant path solution for the mixing layer are considered in this case.

3. This method is similar to method (1) above, except, rather than computing the backscatter for each angle directly from the lidar equation, the product c*betat is calculated for each angle. Statistical computations are performed for this product, the average is derived, and the calibration constant is then divided out, yielding an average backscatter value. The particulate backscatter is then obtained by subtracting the Rayleigh backscatter. This is how particulate backscatter is usually computed in program AER3, in subroutine PRINTF. The subroutine VERTPRF of AER3 also computes particulate backscatter profiles. The difference between the two subroutines is that in VERTPRF, the subroutine INT is first used to compute the particulate optical depth values, and the extinction and backscatter profiles are then obtained. INT only uses the angles included in the AER3 solution, whereas all angles are used in PRINTF. The error

in backscatter computed according to method (3) includes the error in the calibration coefficient, because the product C*beta particulate is computed before extracting the backscatter value.

Methods (1) and (3) seem to be rather similar, but method (2) appears to be different. It is possible that the resultant backscatter values obtained from method (2) may be significantly different from values of the other two methods. The lidar solution procedure gives equal weighting to all the zenith angles that it uses. In methods (1) and (3), the betat value at each effective vertical height is obtained using the optical depth values derived by subroutine INT, which also gives equal weighting to all the zenith angles. In contrast, method (2) starts out using a value for optical depth at the bottom of the mixing layer that has been obtained by the lidar solution. But at the next height, the transmission is computed separately for each angle, and for all successive heights the values of transmission computed at previous heights are used. Therefore the same weighting as that used in the lidar solution and in methods (1) and (3) would not necessarily result.

In practice it was found that the beta particulate profiles derived using these methods were not greatly different from each other, although there were some differences in the error calculation results. Methods (1) and (2) were

performed in subroutines ANGLE1 and ANGLE2 of program AER3. These are called from a subroutine GTBETA. In each method the particulate backscatter is calculated for each angle. The average, standard deviation, and the percent standard deviation are calculated, and printouts are generated. Plots of the percent standard deviation versus height are also generated. Figures 4.3 and 4.4 show profiles of the percent standard deviation by method (1) and (2), respectively, for 12 May 1981. Notice that the percent error increases rather dramatically just above 3 km, just as it reaches the top of the mixing layer. A likely reason is the behavior of the various returns near the top of the mixing layer. As the top of the mixing layer is approached, the return for each zenith angle drops in magnitude dramatically, a large drop over a small height increment. The average of these returns, then, would show an increased standard deviation near the top of the mixing layer. Since methods (1) and (2) solve for particulate backscatter for individual angles, it would be reasonable to see an increase in the percent standard deviation of betap among the angles at about the mixing layer height.

4.1.3 Variation in the Sum of Backscatter Coefficient

Another assumption made in the integrated lidar slant path solution is that the effective vertical transmission

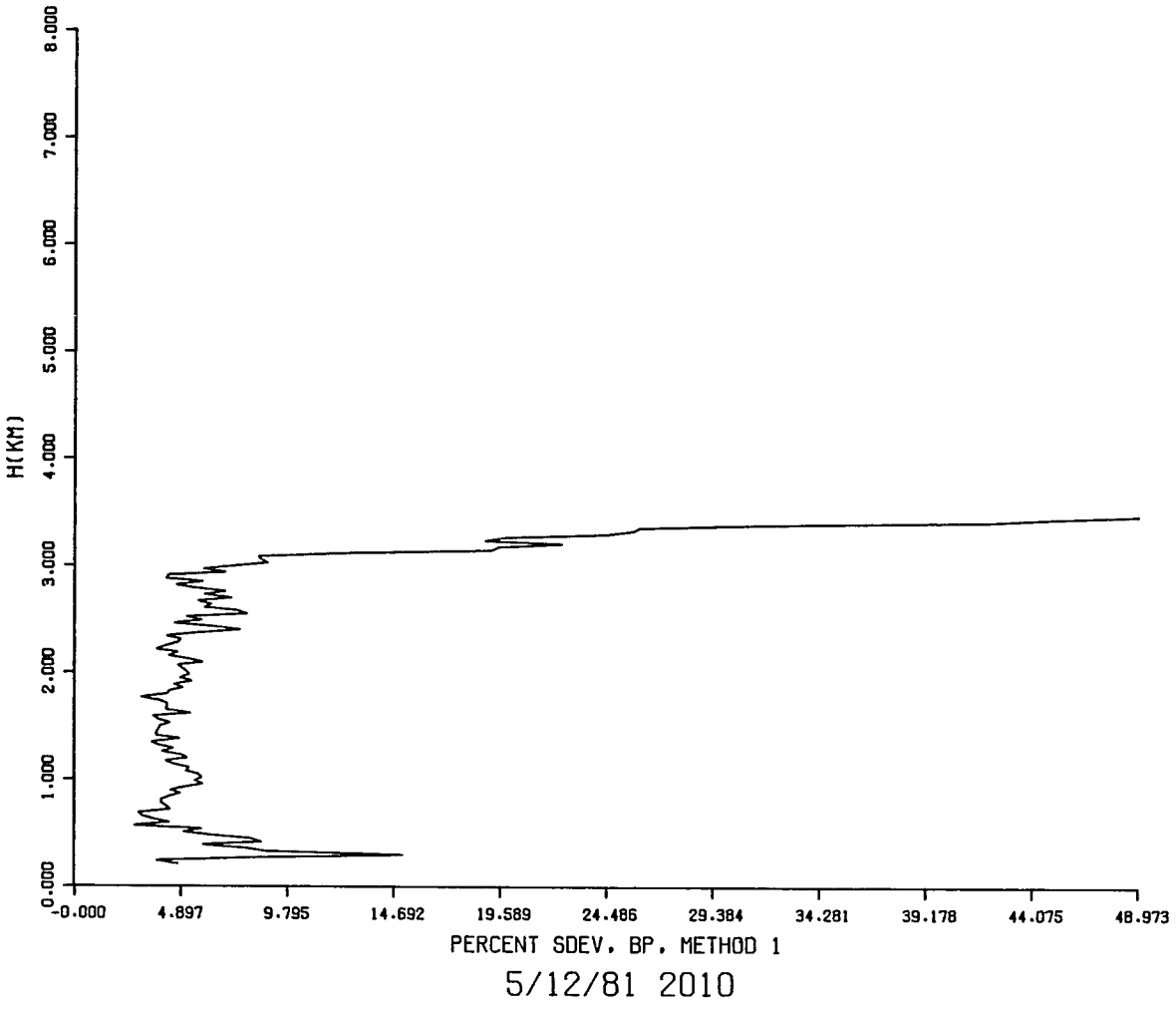

Figure 4.3. %SD of BETAP for 12 May 1981 using method 1.

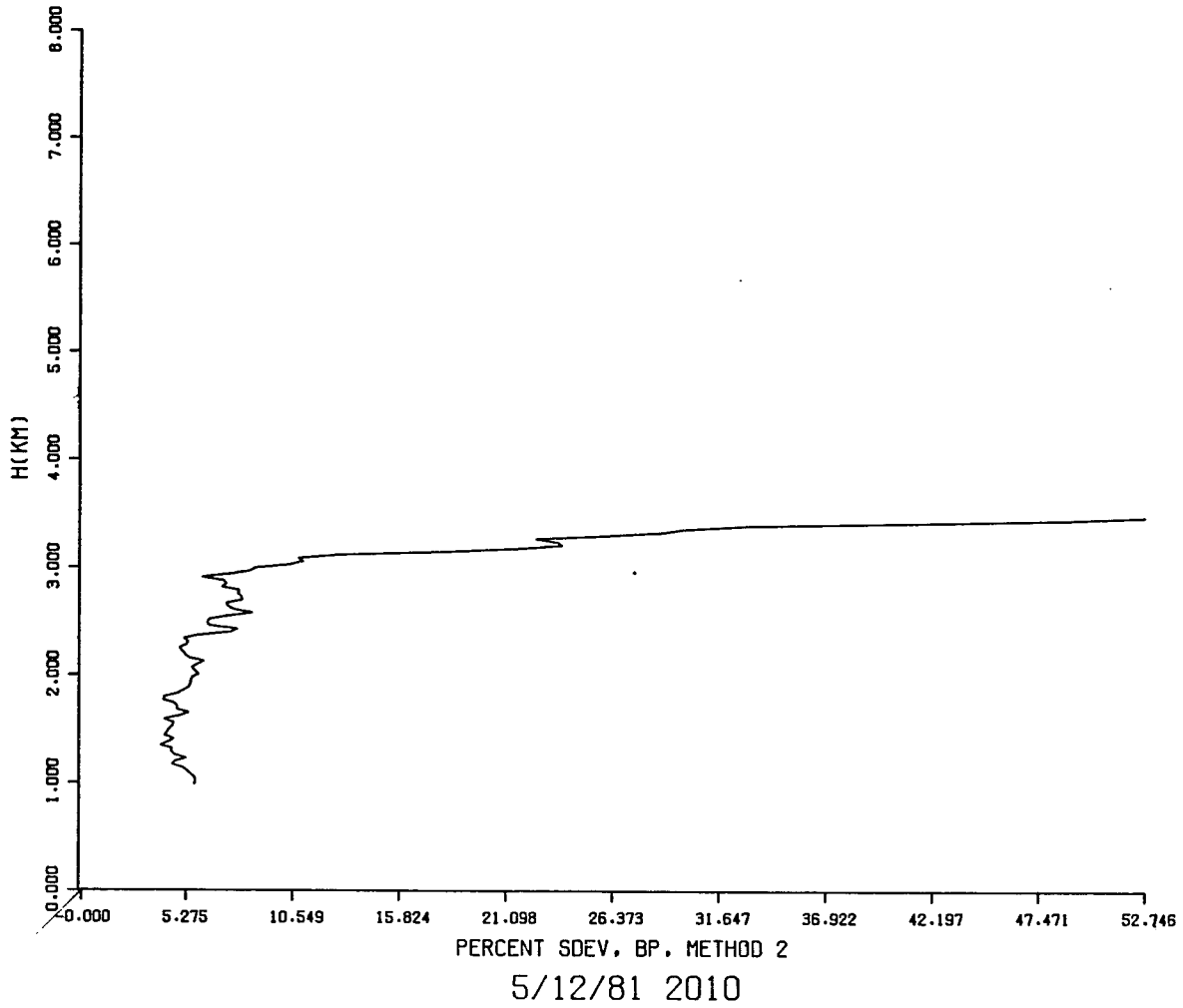

Figure 4.4. %SD of BETAP for 12 May 1981 using method 2.

through the mixing layer is constant for all slant paths through the layer. This assumes that the integral of the extinction coefficient from the bottom to the top of the mixing layer, evaluated at equivalent vertical height increments, is constant from one slant angle to the next. This has the effect of smoothing over any eddy scale fluctuations which may be present in the atmosphere. Of course, it is possible that an eddy may exist at the edge of the layer, which would throw the integral off. This can be avoided by first looking at plots generated by program PIT to make an intelligent assessment of the height of the mixing layer.

Since the extinction coefficient is related to the backscatter coefficient by a constant (the S ratio), the assumption noted above can be tested by summing the backscatter cross-section over the mixing layer for each slant angle, and then examining the variation in this sum for the different slant angles. Currently, this sum, and the percent standard deviation of it, are calculated from the particulate backscatter values obtained by method (1) in section 4.1.2, and the result is printed out from subroutine GTBETA mentioned above.

4.1.4 Assessment of Inhomogeneity Results

An examination of AER3 runs, incorporating the above changes, was made for several test data sets. Table 4.1

Table 4.1. Inhomogeneity computations.

Day, HMIX (km)	PIT %SD in PSIG Range	AER3								
		%SD in PSIG Range, AVG	%SD in BETAP1 (Method 1) (range)	%SD in BETAP2 (Method 2) (range)	%SD in BETAP (Original) (range)	AVG %SD BETAP1 in HMIX (method 1)	AVG $\Sigma\beta_p$ $\pm$ %δ	S $\pm$ δS, % δS	τ_p @ HMIX $\pm$ $\delta\tau_p$, % $\delta\tau_p$	τ_{ptot}, $\pm$ $\delta\tau_{ptot}$, % $\delta\tau_p$
5/11/81 3.4 km	5-8-13	7-7-14 9 avg 15 max	7-12	7-13	10-15	16	0.0366 ±8.2%	12.09±7.9 65%	0.0229 ±0.0171 75%	0.0315 ±0.0191 60%
5/12/81 3.5 km	1-14-10	7-14-10 17 avg 23 max	3-9	4-11	7-10	8.65	0.0919 ±4.7%	24.77±2.7 11%	0.10308 ±0.01182 11%	0.1425 ±0.01378 9.7%
5/13/81 3.5 km	53-7-43	544-7-17 12 avg 17 max	5-12	5-13	9-12	10.04	0.0403 ±7.99%	53.96±6.15 11%	0.08129 ±0.01719 21%	0.1186 ±0.02082 18%
6/1/82 2.6 km	3-11-6	2-11-5 10 avg 13 max	5-17	7-16	11-42	13.48	0.0188 ±5.47%	35.72±6.45 18%	0.04479 ±0.00845 19%	0.1800 ±0.01114 6.2%
5/21/84 3.15 km	44-10-4	3-5-5 5 avg 13 max	2-14	2-15	8-19	13.94	0.0178 ±3.37	18.08±4.19 23%	0.01938 ±0.00608 31%	0.01992 ±0.00636 32% @ 7 km
6/16/81 3.3 km	0.6-16-5	2-15-5 11 avg 18 max	8.39	17-30	20-60	11.3	0.0302 ±11%	28.5±11.4 40%	0.03855 ±0.02335 61%	0.05048 ±0.02438 40%

Table 4.1.--Continued

Day, HMIX (km)	PIT %SD in PSIG Range	AER3								
		%SD in PSIG Range, AVG	%SD in BETAP1 (Method 1) (range)	%SD in BETAP2 (Method 2) (range)	%SD in BETAP (Original) (range)	AVG %SD BETAP1 in HMIX	AVG $\Sigma\beta_p$ $\pm$ %δ in HMIX (method 1)	S $\pm$ δS, % δS	τ_p @ HMIX $\pm$ $\delta\tau_p$, % $\delta\tau_p$	τ_{ptot}, $\pm$ $\delta\tau_{ptot}$, %$\delta\tau_p$
4/17/80 4.0 km	3-9-27	0.6-9-32 19 avg 32 max	1-8	1-6	5-11	3.79	0.0912 ±1.2%	29.89±1.5 5%	0.12035 ±0.00452 4%	0.1721 ±0.0054 3%
1/2/80 2.0 km	1-20-17	10-15-19 16 avg 25 max	8-40	8-33	12-43	24.9	0.0108 ±14.2%	18.53±30.1 163%	0.03565 ±0.02222 62%	0.05426 ±0.02981 55%
4/4/80 3.0	3-7-11	2-10-12 11 avg 17 max	5-17	4-13	8-18	9.8	0.0276 ±4.2	23.39±4.5 19%	0.04938 ±0.00769 15.6%	@7.2 km .5537 ±0.0086 1.6%
3/27/80 2.4 km	2-5-7	2-4-6 6 avg 9 max	3-4	3-7	8-10	5.3	0.0178 ±0.00035 1.9%	26.45 ±3.61 13.6%	0.02884 ±0.00417 14.5%	0.04720 ±0.00521 11%
4/7/80 AM 2.9 km	1-6-22	2-8-23 15 avg 27 max	5-10	5-13	8-65	8.35	0.0400 ±0.00268 6.7%	40.5 ±5.99 14.8%	0.07922 ±0.01381 17.4%	0.2326 ±0.02578 11%
1/23/80 3.0 km	0.4-6-2	1-2-3 3 avg 4 max	4-7	4-8	10-13	5.57	0.0147 ±0.000415 2.8%	6.71 ±2.96 44%	0.00522 ±0.00368 70%	0.01255 ±0.00628 50%

Note: In the %SD columns for PIT and AER3, the three numbers separated by dashes indicate the %SD near the surface (0.3 km), at 1.0 km, and at HMIX, respectively.

lists the results obtained from these days. The results show that while it is not possible to establish a direct, linear relationship between the errors in particulate backscatter and the errors in the S ratio and optical depth, some trends do seem to be apparent. In discussing the results, the acronyms as listed in Chapter 2 are used. The trends apparent in Table 4.1 may be summarized as follows

1. Large errors in betap (method 1, 2, etc.) over the mixing layer correspond in general with large errors in the S ratio and taup at HMIX. This is particularly so if the S ratio is less than 20, and the optical depth at the mixing layer is also low, less than $\simeq$ 0.04. In general, low S ratio values have larger errors associated with them. The larger the S ratio, the smaller is the effect of the error in betap on the S ratio. Also, when the errors are shown as a percentage, the large S values have a comparatively lower error percentage.
2. The %sd in the sum of betap is an indicator of how good the S ratio and taup results are. Small values of %sd in betap coincided with small errors in the S ratio.
3. Whenever %sd in PSIG (from AER3) is greater than about 22 percent, the solution (AER3) does not con-

verge, particularly when the %sd in psig towards the beginning of the mixing layer at 1.02 km is large.

4. When the AER3 solution does work, large errors in %sd of psig coincide with large errors in the S ratio and taup.

The above conclusions can be readily observed from Table 4.1. For example, 11 May 1981 had an average 16 %sd in betap in the mixing layer. It had an 8 %sd in the sum of betap while the average %sd in PSIG was only 9 percent in the mixing layer. However, it had a low S ratio (12.09) and a low taup at HMIX (0.0229), resulting in errors in the S ratio and optical depth of 65 percent and 75 percent, respectively. The 2 January 1980 case had a little higher S ratio (18.53) and taup at HMIX (0.0365), but had an average %sd in betap of 24.9%, an average %sd in psig of 15.6% over the mixing layer, and a high 14 %sd in the sum of betap. Correspondingly, the errors in the S ratio and taup at HMIX were 163 percent and 62 percent, respectively.

April 17, 1980 can be seen as a day where the %sd in psig in the mixing layer, at 19%, was not very small, but the average %sd in betap was only 4%, average %sd in the sum of betap was only 1.2%, and the S ratio was 29.89. The taup at HMIX was 0.1204. The errors in the S ratio and taup at HMIX were a very low 5% and 4%, respectively.

For 16 June 1981, the average %sd in betap was 11% and the errors in the S ratio and taup at HMIX were 40% and 61%, respectively. In contrast, for 13 May 1981, the average %sd in betap was 10%, almost the same as for 16 June 1981, but the errors in the S ratio and in optical depth at HMIX were a modest 11% and 21%, respectively. The S ratio for 13 May 1981, at a value of 53.96, was almost twice that of 16 June 1981 (28.50), and the taup at HMIX for 13 May 1981 was 0.0813 as compared to 0.0386 for 16 June 1981.

Percent standard deviations in PSIG in the mixing layer of up to 20 or 25 can be tolerated, if other conditions prove conducive to a solution for program AER3. The results display average %sd values for psig ranging from 5 to 19, and the program aer3 succeeded in solving for the S ratio and optical depth in all cases. Percent standard deviations in PSIG of much greater than 25 usually lead to a failure; a number of data sets have failed to produce results for such cases.

4.2. A Classification of Extinction Profiles

Every data set that was successfully processed resulted in, among other things, an extinction profile (from program AER3) and a range-and-energy normalized return profile (from program PIT). The extinction profiles generated for all the data sets may be loosely classified, based upon

their shape, into different categories. For each category, the PSIG profile from program PIT is shown first, followed by the sigmap profile. The purpose of including PSIG profiles along with the extinction profiles is twofold. One is to depict the correlation between the value of HMIX as indicated by the two plots, and the second is to illustrate the correlation between the shape of the PSIG profile and the sigmap profile.

May 12, 1981 was a day that had a well defined, fairly flat-topped mixing layer with large extinction values. The PSIG profile for this day is shown in Figure 4.5, and the sigmap profile is shown in Figure 4.6. The %sd in PSIG for this day ranged up to about 24% within the mixing layer, and was less than 8% above it. In Figure 4.5, the HMIX is seen to be $\simeq$ 3.5 km; the same value for HMIX is indicated by the sigmap profile in Figure 4.6. The sigmap value is greater than 0.025/km almost to the top of the mixing layer, where it then drops abruptly to less than 0.01/km above it. However, the sigmap profile still stays to the right of, or greater than the Rayleigh extinction profile up to 7 km, indicating a sustained presence of aerosols above the mixing layer. This is also evidenced by the large total particulate optical depth of 0.1425. For this large optical depth, the S ratio value, at 24.77, is still within the range of the most frequent S values.

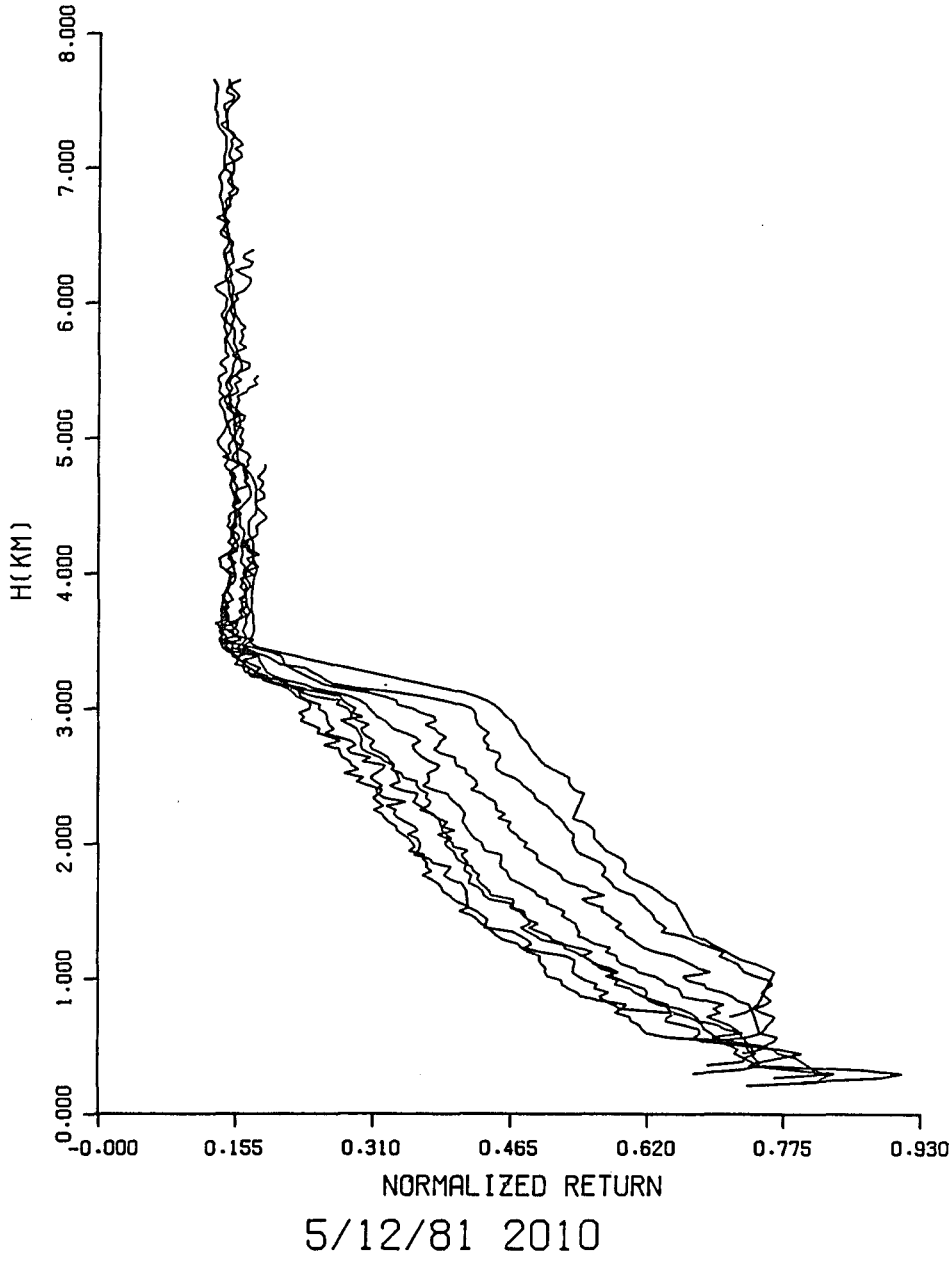

Figure 4.5. PSIG profiles for 12 May 1981.

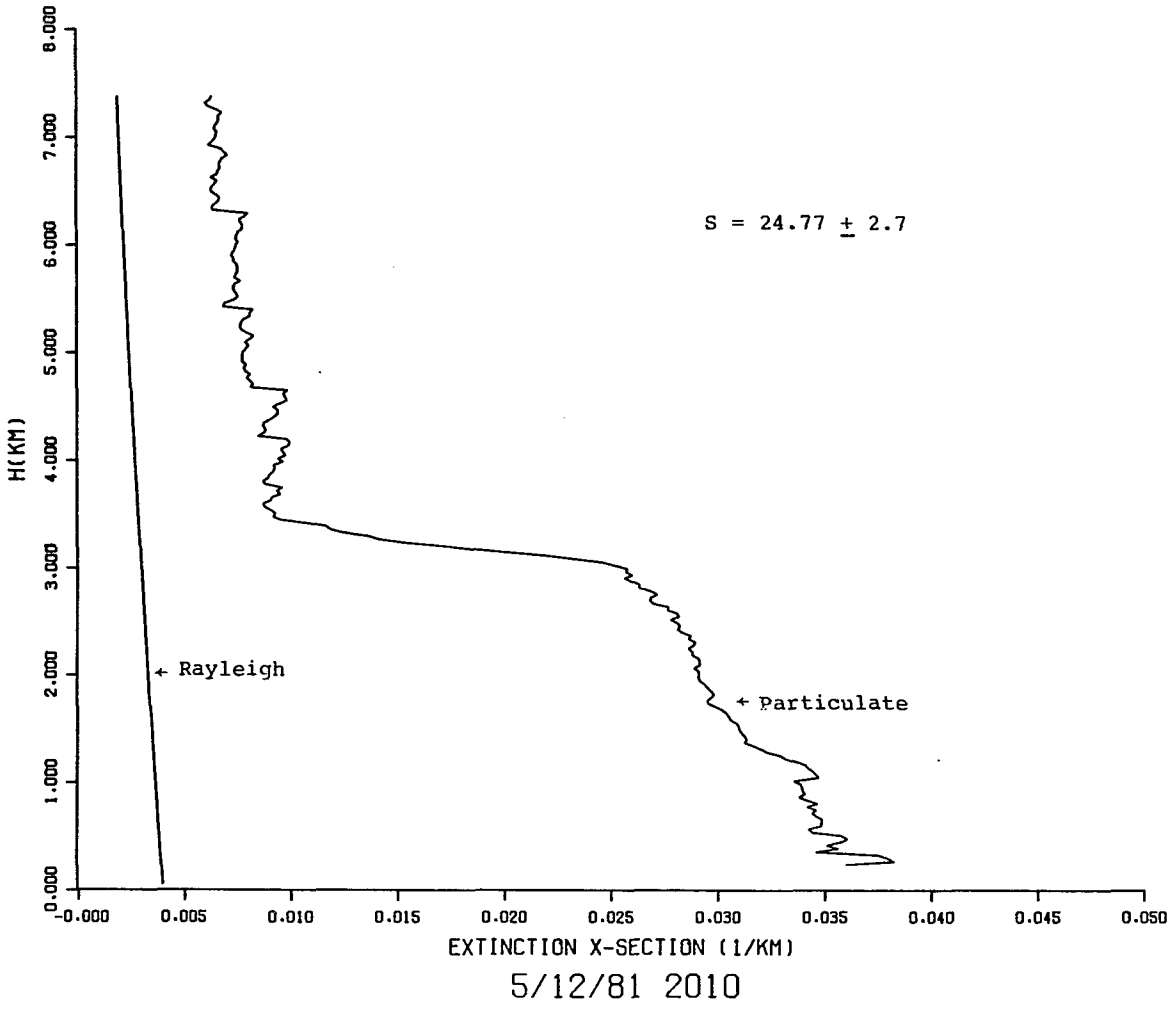

Figure 4.6. Extinction cross-section profile for 12 May 1981.

The case of March 27, 1980 is illustrated in Figures 4.7 and 4.8, which display a very well defined mixing layer, but the extinction values are notably smaller than those for 12 May 1981. The %sd in PSIG for this day was under 10% up to the top of the mixing layer and was under 14% above it. In Figure 4.7, a mixing layer height of ≃ 2.4 km is indicated by the PSIG plots, and is confirmed in Figure 4.8 by the sigmap profile. The mixing layer in the sigmap profile has a sharp, flat cap. Above the mixing layer, the extinction profile stays under, or less than the Rayleigh profile, with periodic excursions above it. The total particulate optical depth for this day was 0.0472, almost twice that at the top of the mixing layer (0.02884).

Sometimes the mixing layer is not sharp and flat but is slowly decreasing as height increases. The shape of the slope may be somewhat linear, or at times, exponential. A case in point is 4 April 1980, shown in Figures 4.9 and 4.10. The PSIG profiles are shown in Figure 4.9, where all eight zenith angles may be seen. The %sd in PSIG for this day is small, ranging from under 3 percent at 0.3 km, to no more than 11 percent at 3 km. Above 3 km, the %sd does increase to 19% at 4 km, but decreases again thereafter. An HMIX of 3 km is indicated by the PSIG profiles. The sigmap profile in Figure 4.10 indicates a corresponding HMIX of 3 km. The Figure also indicates that sigmap magnitude slowly decreased

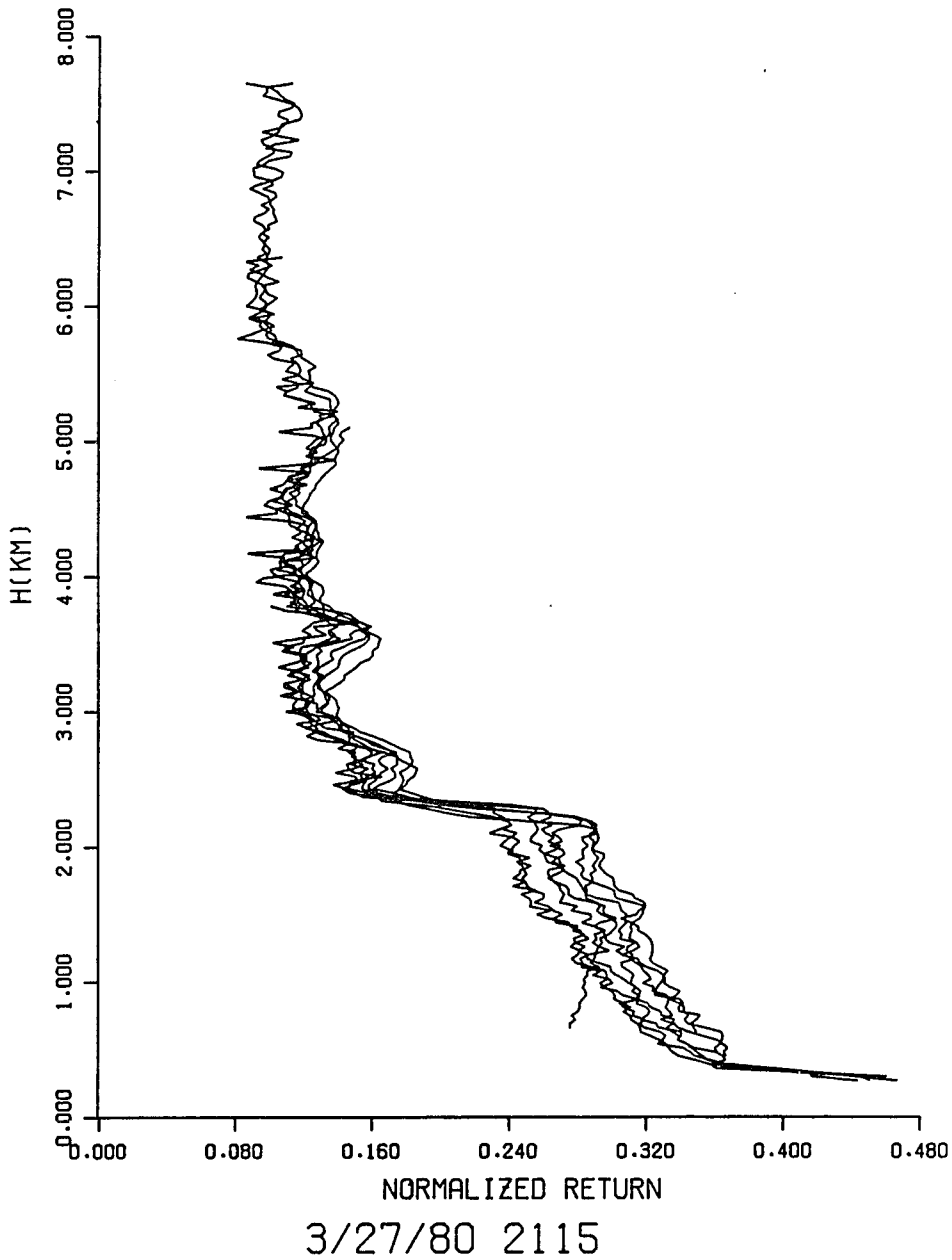

Figure 4.7. PSIG profiles for 27 March 1980.

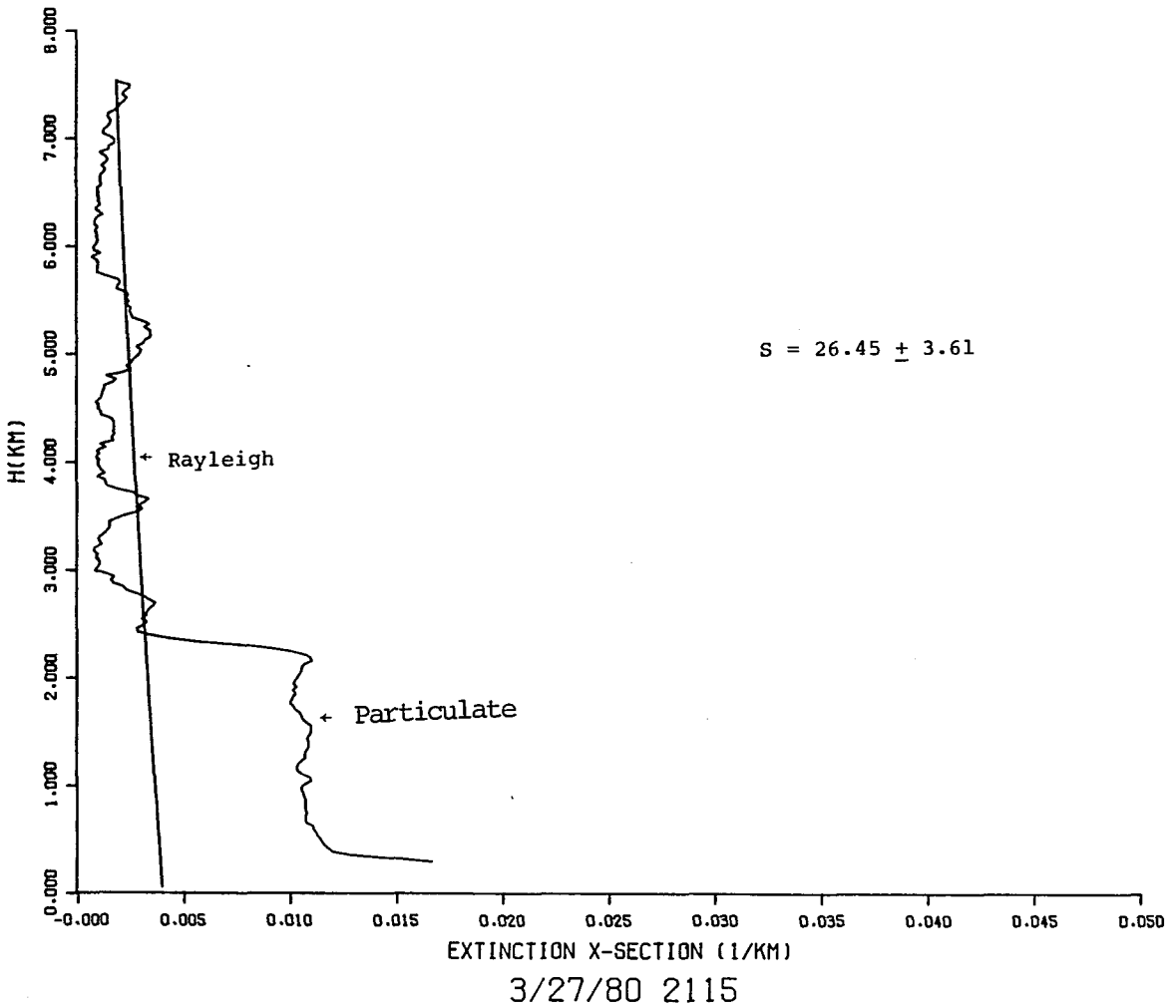

Figure 4.8. Extinction cross-section profile for 27 March 1980.

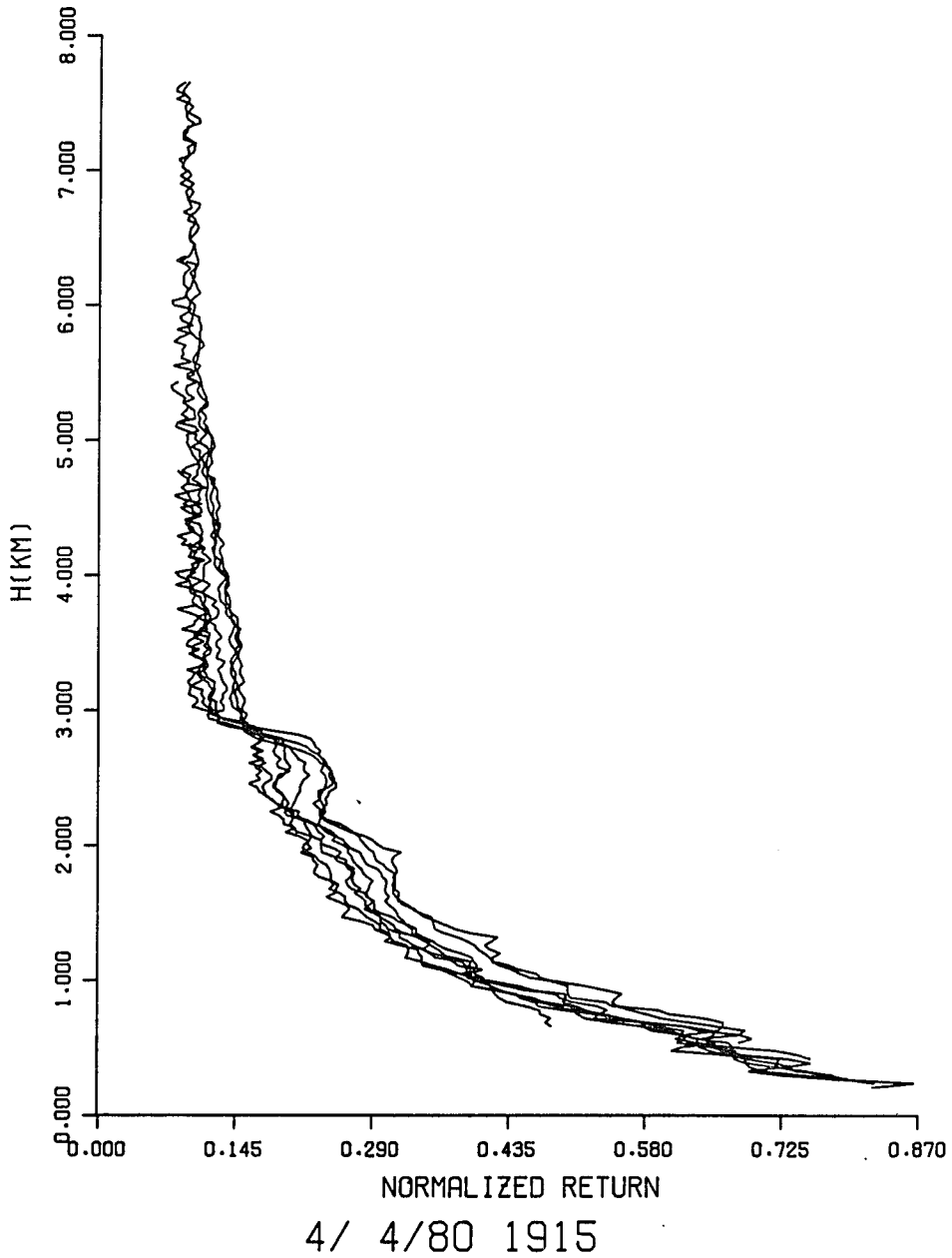

Figure 4.9. PSIG profiles for 4 April 1980.

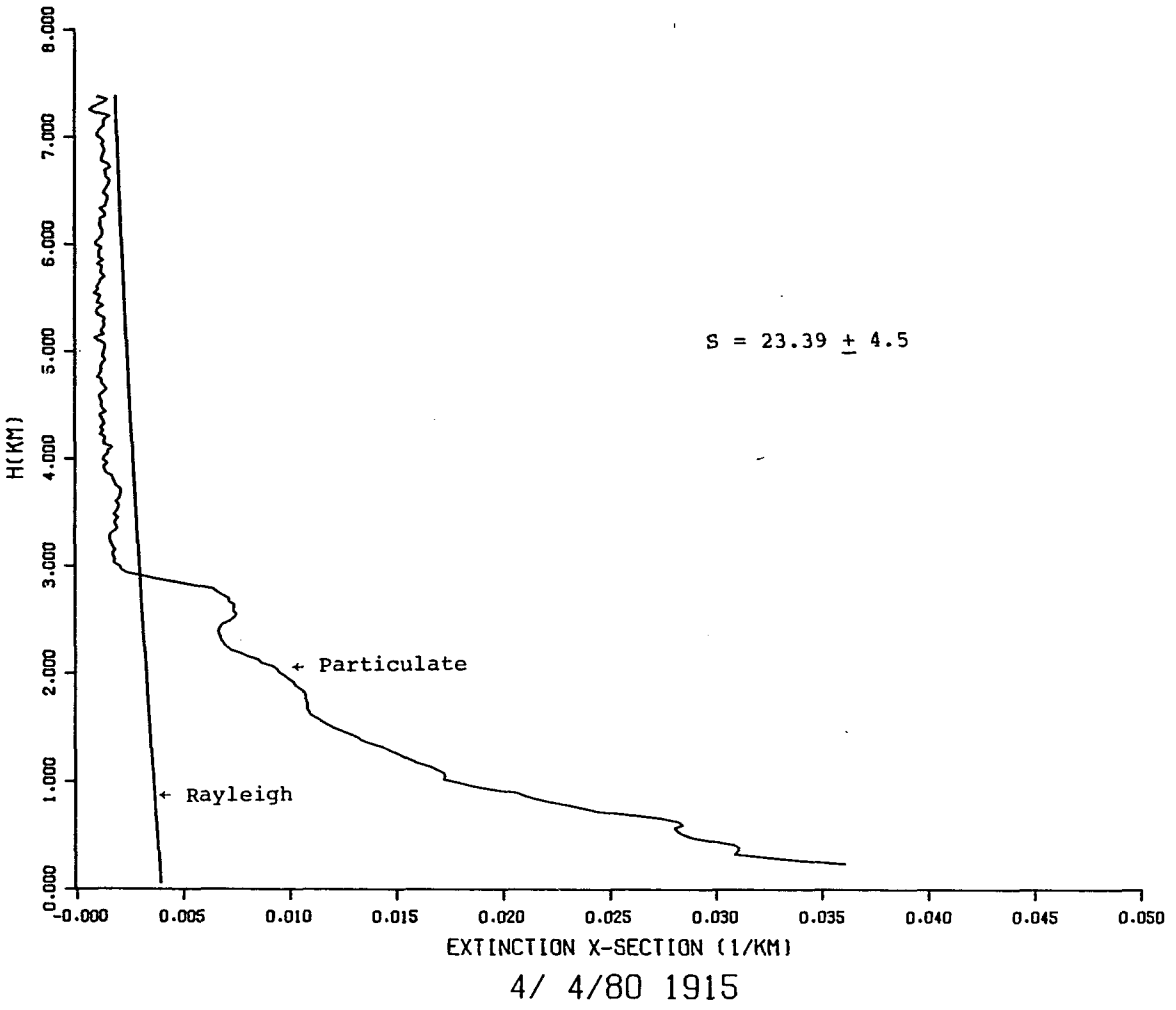

Figure 4.10. Extinction cross-section profile for 4 April 1980.

from the surface to 3 km. Above 3 km, the particulate extinction stayed smaller than Rayleigh all the way to 7.4 km. The total taup for this day was 0.0527, whereas the value of taup at HMIX was 0.04938, indicating that the majority of the contribution to the particulate optical depth occurred within the mixing layer.

Another variation in the shape of the particulate extinction profiles occurs when the particulate extinction coefficient begins at a value close to the Rayleigh extinction, becomes smaller than Rayleigh extinction as the height increases, and stays that way for the rest of the profile. In such cases, the value of HMIX can sometimes be difficult to estimate. An example of this is the case of 23 January 1980, shown in Figures 4.11 and 4.12. The PSIG profiles for this day, shown in Figure 4.11, indicate that the HMIX can not be clearly identified. A small jog in the returns can be seen at about 1.3 km, but it is neither distinct nor sufficiently above 1 km to be used in the AER3 solution. Returns for some angles can be seen deviating from the group as a whole at 3 points above 3 km; this is assumed to be due to noise. Indeed, program AIMLESS for this day indicated that the last gainstages for some of the angles were noisy. These portions of these angles were not used in the AER3 solution program. Barring the noise in the last gainstage, the %sd in PSIG for this day is quite acceptable, less than 10%. In

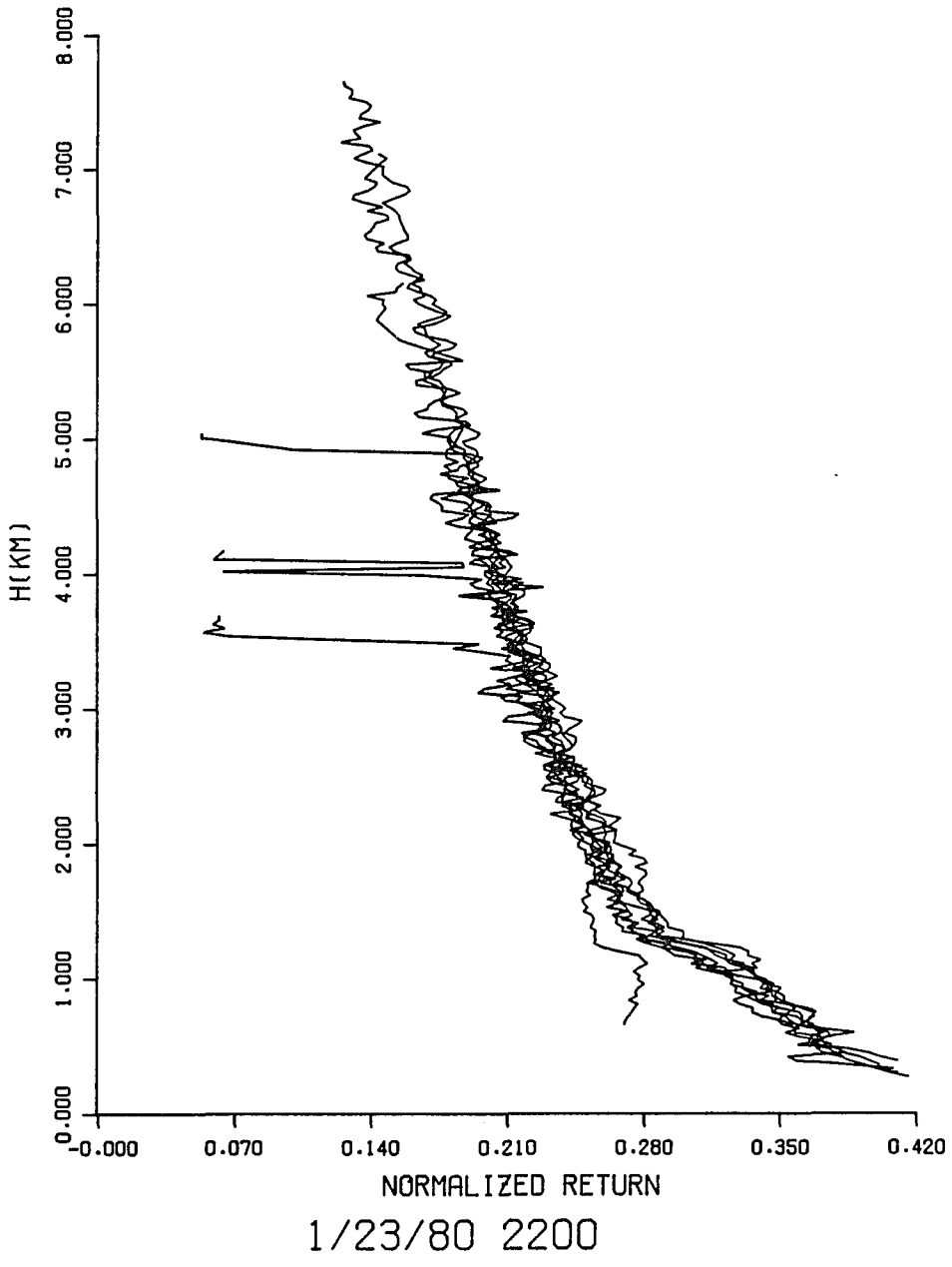

Figure 4.11. PSIG profiles for 23 January 1980.

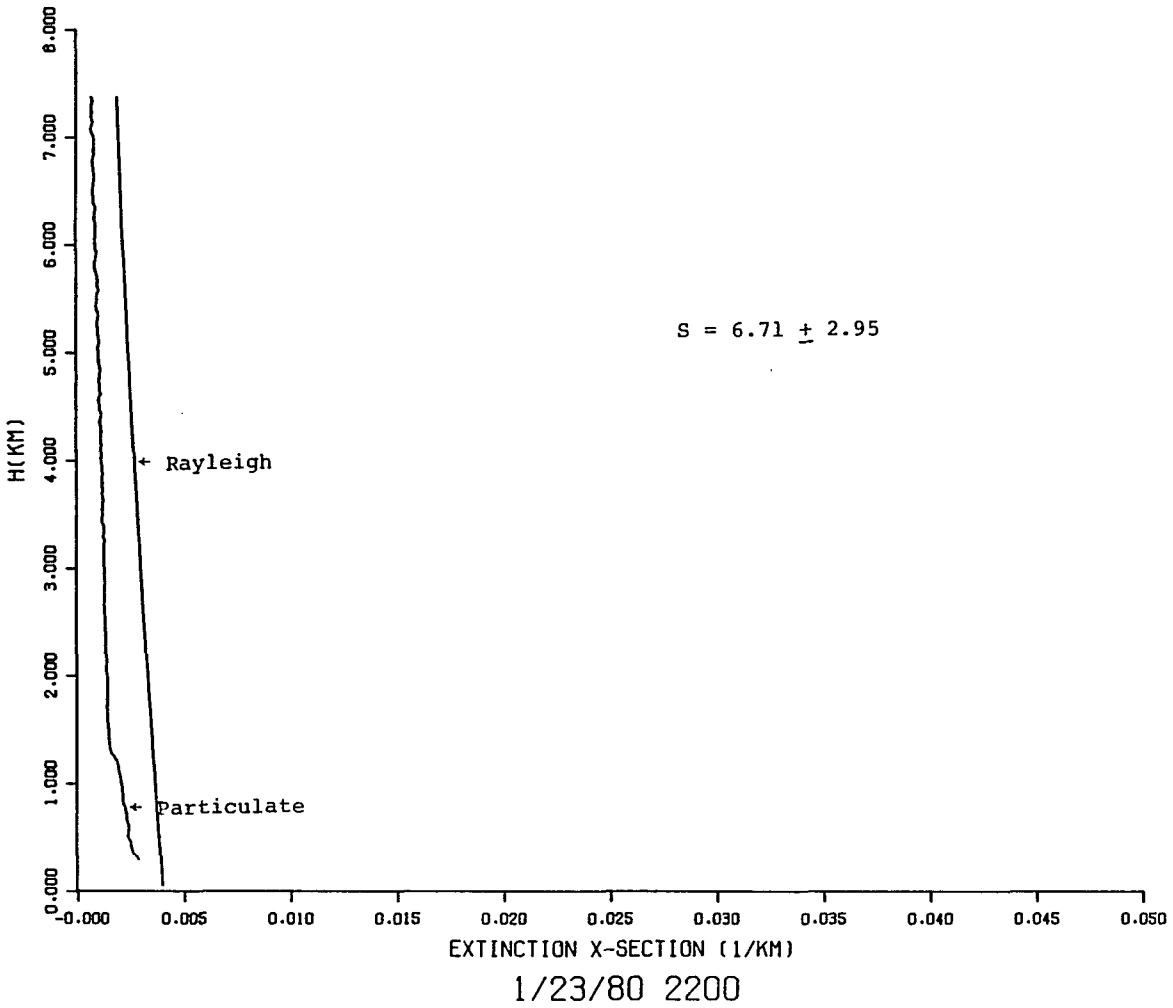

Figure 4.12. Extinction cross-section profile for 23 January 1980.

Figure 4.11, the return for secant angle 1.5 can be seen to deviate from the rest between 0.7 km and about 1.7 km, essentially driving the %sd out to 10% range. However, program AER3 was able to tolerate this. The sigmap profile, in Figure 4.12, shows that sigmap starts out at about 75 percent of the Rayleigh extinction, but gradually drops to about 36 percent of the Rayleigh extinction at 7.38 km.

The height of the mixing layer for 23 January 1980 is hard to judge, although there is a hint of one at 1.3 km. A solution was attempted using an HMIX of 1.3 km, but AER3 solution did not converge in this case. Mixing layer heights from 2 to 4 km were assumed, and they all yielded solutions, indicating that a larger value of HMIX was probably necessary to achieve a large enough optical depth for AER3 to run successfully. The solution shown in Figure 4.12, at an HMIX of 3 km, yielded the smallest error in the S ratio, 44%. The S ratio determined for this case was 6.71, the particulate optical depth at 3 km was 0.00522, with 70 percent error, and the total particulate optical depth was 0.0126. A profile like this indicates a very clean day, with very little aerosol loading. Typically the S ratio and the particulate optical depth obtained by AER3 for such a day are small, with above average percent errors.

4.3 Effects of Input Parameters on the Integrated Slant Path Solution

The slant path solution obtained by program AER3 generates a value of the S ratio subject to multiple constraints and input conditions. Thus, in the case of a successful solution, the results are subject to these same constraints and conditions. Studying the sensitivity of the solution to the various inputs can provide some insight as to the effect of these inputs on the solution results.

4.3.1 The effect of the Calibration Constant as an Input

It was noted in Chapter 3 that the lidar system calibration constant has been evaluated a number of times over the years. An accurate calibration constant value is important to the derivation of extinction profiles and the determination of the S ratio. The effects of changing the calibration constant (Calcon) are depicted by the example given in Table 4.2, which lists solutions obtained for 5/21/84 for Calcon values ranging from 340 to 300. Particulate extinction values are listed in 0.5 km increments, starting at 1.02 km. It can be seen that lowering Calcon resulted in an overall increase in the particulate extinction cross section, and, naturally, in the particulate optical depth, although the S ratio dropped slightly. (The particulate backscatter cross section also increased, since it is

Table 4.2. Effect of varying calibration constant as input to AER3 for 21 MAY 1984.

calcon ->	340		320		300	
height in km	sigp x10e-3	sigp/ sigr	sigp x10e-3	sigp/ sigr	sigp x10e-3	sigp/ sigr
1.02	7.15	1.96	7.26	1.99	7.07	1.93
1.5	6.79	1.95	6.90	1.98	6.70	1.92
2.01	4.61	1.39	4.78	1.44	4.78	1.44
2.52	2.43	0.77	2.67	0.85	2.85	0.91
3.00	0.942	0.31	1.22	0.41	1.54	0.51
3.51	0.151	0.05	0.443	0.16	0.830	0.29
4.02	1.11	0.41	1.42	0.53	1.70	0.63
4.50	0.852	0.43	1.10	0.43	1.39	0.54
5.01	0.494	0.20	0.740	0.30	1.05	0.43
5.52	0.554	0.24	0.786	0.34	1.07	0.46
6.00	0.767	0.35	0.982	0.45	1.23	0.56
6.51	0.531	0.25	0.741	0.36	0.996	0.48
7.02	0.258	0.13	0.463	0.23	0.727	0.37
S ratio	19.58 ±4		18.08 ±4		14.96 ±4	
Op.Dep @ hmix	0.01913 ±0.0061		0.01938 ±0.0061		0.01951 ±0.0060	
Op.Dep @ 7.02 km	0.01858 ±0.0061		0.01983 ±0.0064		0.02137 ±0.0069	

Note: Optical depth here is aerosol optical depth
Height of the mixing layer was 3.15 km.
sigp = particulate extinction
sigr = Rayleigh extinction

related to the extinction within the mixing layer by the S ratio.) It has been repeatedly observed that a decrease in the value of Calcon increases the particulate extinction cross section, and the particulate optical depth, along with a decrease in the S ratio. The basis for this can be discerned by examining Equation 2.6 for PSIG, which can be rewritten as

$$P(z,r) = C\beta_{TOT}(z,r)T_{TOT}^{r}(z,r) \qquad (4.3.1)$$

where

C = Calcon, the calibration constant

β_{TOT} = betat, total backscatter

T_{TOT} = trant, total transmission

r = 2 * secant theta, as before.

Equation 4.3.1 indicates that a lowering of C (Calcon) should increase the product betat*trant. Since transmission (trant) is a slowly varying quantity, betat (and hence betap) should primarily reflect the increase, and sigmap should increase, as the two are connected through the S ratio. In the example shown in Table 4.2, the effects within the mixing layer, where the solution is obtained, appear to be small--i.e., little change in sigmap, and the change in the S ratio is within the AER3 uncertainty limits ($S = 18.08 \pm 4$). This indicates good stability in the retrieval of the quantities of interest, sigmap and betap, as

long as Calcon is known within reasonable limits of $\pm$ 10% or less. Above the mixing layer, where particulates are fairly sparse, changing Calcon has a more significant effect on sigmap. The issue of sigmap values above the mixing layer is will be discussed further in section 4.4 in connection with a method for cross checking the lidar system calibration constant.

Sometimes the particulate extinction profile is seen to "pivot," as it were, about a height in the mixing layer. By this it is meant that when Calcon is changed, the sigmap values decrease below a certain height, and increase above it. Table 4.3 shows this behavior for the data set of 12 May 1982. When the Calcon value changed from 500 to 400, the extinction cross section decreased below the mixing layer, but increased above it. This increase was sufficient to increase the total optical depth. Note that the changes in both the S ratio and the optical depth were within their respective uncertainty limits. The change in extinction profile above the mixing layer is more pronounced, because there the same S ratio as was derived for the mixing layer is applied above HMIX, but the particulate concentration is sparse.

Table 4.3. Effect of varying calibration constant as input to AER3 for 12 May 1981.

calcon ->	500	450	400
height in km	sigp x10e-2	sigp x10e-2	sigp x10e-2
1.02	3.47	3.36	3.34
1.5	3.11	3.10	3.09
2.01	2.92	2.91	2.90
2.52	2.79	2.78	2.77
3.0	2.58	2.57	2.57
3.51	0.869	0.928	0.982
4.02	0.884	0.942	0.995
4.5	0.861	0.918	0.97
5.0	0.720	0.779	0.833
5.5	0.700	0.757	0.808
6.0	0.691	0.746	0.795
6.51	0.575	0.629	0.678
7.02	0.604	0.654	0.700
S ratio	28.60 $\pm$3.0	24.77 $\pm$2.7	21.20 $\pm$2.4
Opt. Depth @ hmix	0.1032 $\pm$0.0119	0.1031 $\pm$0.0118	0.1029 $\pm$0.0118
Total Opt Depth	0.1389 $\pm$0.0136	0.1425 $\pm$0.0138	0.1458 $\pm$0.0139

Note: Optical depth here is aerosol optical depth.
Height of the mixing layer was 3.50 km.
sigp = particulate extinction

4.3.2 The Effect of HMIX and S Ratio Estimate as Inputs

The height of the mixing layer (HMIX) as an input to AER3 can be varied. If it is less than the actual mixing layer height, the solution may not succeed, especially if the input value is less than 2 km. This is very likely to occur because there is not enough particulate optical depth for the solution to work with when HMIX is small. If the height selected for HMIX is larger than the actual mixing layer height, then error may be introduced in the solution because the atmosphere is different above the mixing layer. Additionally, all the angles may not be available for a higher value of HMIX, and some useful data may be needlessly eliminated. For these reasons, the solution can be fairly sensitive to the value of HMIX assumed for the input to AER3. In case of a data set where the extinction cross section is slowly decreasing with height, without showing a sharp mixing layer top, different HMIX values can be tried without seriously degrading the solution. However, for sharply defined mixing layer heights, it is important to select a value of HMIX as close to the true mixing layer top as possible.

S ratio values ranging all the way from very small ($\simeq 5$) to very large ($\simeq 60$) have been obtained with an S ratio input (Sinit) of 20, as can be seen from Appendix 1.2. This would be expected in the case of a good solution. On the other hand, there have been occasions when a data set would

only yield a solution for a specific range of Sinit. Additional sensitivity studies are called for in this area, but it is beyond the scope of the work reported here. When a data set fails to run, the printout of the AER3 program shows the values of S ratio that the AER3 program was last trying before it failed. Using that value as a modified estimate for Sinit sometimes results in a successful solution.

4.4 Assessment of Particulate to Rayleigh Extinction Ratios above the Mixing Layer

In the region of the troposphere above the mixing layer, the particulate extinction cross section is generally small compared to that within the mixing layer. The system calibration constant has to be accurately known in order to differentiate between particulate and Rayleigh extinction. This has been noted previously by Spinhirne et al. (1980) and Reagan et al. (1984). The ratio of aerosol to Rayleigh extinction above the mixing layer (referred to hereafter in this section as simply "extinction ratio") is an indicator of the accuracy of the calibration constant. An estimation of the extinction ratio may be obtained as discussed below.

Under clear conditions and a well defined mixing layer in the lower troposphere, it can be inferred from the efforts of other investigators (Russell et al., 1981) that the particulate to Rayleigh backscatter ratio (betap/betar) in the atmosphere above the mixing layer typically ranges

from ≃ 0.05 to ≃ 0.15. The extinction ratio (sigmap/sigmar) can be computed using this information with other known relationships. The ratio of sigmar to betar can be determined theoretically and is 8*pi/3. In the program AER3, the S ratio derived for the mixing layer is used to solve for the extinction and backscatter profiles above the mixing layer. The S ratio is S = sigmap/betap. The relationships just mentioned are:

$$\frac{\beta_P}{\beta_R} \simeq 0.1$$

and

$$\frac{\sigma_R}{\beta_R} = \frac{8\pi}{3}$$

and

$$\frac{\sigma_P}{\beta_P} = S$$

From these equations, one can compute sigmap/sigmar, as:

$$\frac{\sigma_P}{\sigma_R} \simeq 0.012(S)$$

Assuming the S ratio ≃ 25, which is in the most frequent value range of the S ratio, a value for sigmap/sigmar is

$$\frac{\sigma_P}{\sigma_R} \simeq 0.3$$

If a value of sigmap/sigmar of 0.3 above the mixing layer is obtained repeatedly for a number of data sets acquired over a period of time during which the Calcon changed, it would indicate that the Calcon had been derived with acceptable accuracy for that time period. It was noted in section 4.3

that a change in the value of Calcon of about 10% will change sigmap appreciably above the mixing layer, but will not change the S ratio by more than the AER3 solution error margin for the S ratio. Referring again to Table 4.2 from section 4.3, it can be seen that sigmap/sigmar ratio above the mixing layer changed from about 0.25 to 0.45 for a Calcon change from 340 to 300. This indicates that a sigmap/sigmar ratio of less than ≈ 1.0 above the mixing layer is probably adequate to imply that the calibration constant was known within acceptable error limits (i.e., within ≈ 10%).

A tabulation of extinction ratios is shown in Table 4.4. Category "A" indicates that there were 54 data sets that had an extinction ratio of less than 1.0. The total in Category "D," which shows the data sets with an extinction ratio exceeding 1.0, is 28, or 34 percent of all data sets. Particulate extinction values above the mixing layer can be greater than Rayleigh extinction in cases where winds carry soil particles or dust into the upper atmosphere, and it can persist for some time. This can occur locally, or advection can bring in "dust storm" aerosols from far away (e.g., the California Santa Anna winds and the New Mexico dust storms). Other natural phenomena such as volcanic eruptions or forest fires can also create this type of a situation. As an example, there were 4 days in category "D" in May and June 1982, following the eruption of the El Chicon volcano. Thus,

Table 4.4. Particulate/Rayleigh extinction ratio results.

Category A => particulate extinction cross section became less than Rayleigh extinction at some point above the mixing layer

Category D => particulate extinction cross section remained greater than Rayleigh extinction above the mixing layer

Number of data sets in category A and D per generic month, with percentages:

Month	Cat A	%of Total	Cat D	%of Total	A+D
Jan	2	50	2	50	4
Feb	6	86	1	14	7
Mar	9	64	5	36	14
Apr	9	64	5	36	14
May	12	57	9	43	21
Jun	7	58	5	42	12
Jul	0	0	1	100	1
Aug	0	0	0	0	0
Sep	0	0	0	0	0
Oct	2	100	0	0	2
Nov	3	100	0	0	3
Dec	5	100	0	0	5
Total	55	66	28	34	83

there is reason to expect that some days will have to have extinction ratios greater than unity. The important point is that some, perhaps the majority, of the days should indeed display extinction ratios less than one (1) if the calibration constant has been properly determined.

For Tucson weather, spring and summer are the times of the year when the situation of higher aerosol loading in the upper atmosphere is most likely to occur. Table 4.4 shows that all of the data sets in category D were collected between January and July, with 86 percent occurring between March and June. The S ratios for the data sets in category D were seen to have an average error of 22 percent, which is similar to that for category A. Additionally, it should be noted that data sets in category A were spread throughout the year, including the period from January to June. On a per-month basis, the percentage of data sets in category A was always greater than or equal to 50 percent. The calibration constant values used for the data sets in category D were the same as those used for other data sets in identical time frames. This indicates that the calibration constant was generally known fairly accurately. Thus, the slant path solution results should generally be accurate within the uncertainty limits predicted by AER3.

CHAPTER 5

CONCLUSIONS AND RECOMMENDATIONS

5.1 Conclusions

The system of software originated by Spinhirne (1977) to process lidar slant path data acquired by the ARSL has been debugged, modified, and documented. The current system of software can successfully analyze lidar data and produce results in the form of paper printouts, paper plots, and files on electronic or magnetic media. A substantial amount of lidar data was analyzed using this software. It was demonstrated that the integrated slant path lidar solution procedure is a valid tool with which to obtain information regarding the presence of, and scattering by, the aerosols in the lower troposphere. The procedure ran successfully on data sets acquired under a variety of atmospheric conditions, spanning most of the seasons. Successful results were obtained for 83 out of 104 data sets for which analysis was attempted, a success ratio of 80 percent.

The parameters S ratio, TAUP and HMIX were seen to have a moderate seasonal dependence, but it was also evident that short-term perturbations in the atmosphere had an impact on their values. New routines have been introduced which have generated valuable information regarding the horizontal

inhomogeneity of the atmosphere, thereby assessing the assumptions made in the integrated slant path lidar solution procedure. It was illustrated that a high % sd in either PSIG or BETAP was not always sufficient to lead to large errors in the solution parameters such as the S ratio and TAUP. The results indicate that the procedure generates good results on days with moderate to high optical depth, but suffers from an increase in errors when the optical depth is low. The calibration constant was seen to have an impact on the particulate extinction coefficient values above the mixing layer. It was demonstrated that the calibration constant has been derived with sufficient accuracy for the time period spanning most of the data sets.

The database that was created and employed to store and access the results proved enormously helpful in retrieving information subject to a wide variety of conditions. Further, as shown in Chapter 3, it assisted in exploring the relationships between some of the lidar parameters. The database should continue to be a valuable tool for researchers who may wish to continue working with the collection of lidar data at ARSL.

5.2 Recommendations

The database can be expanded to include more parameters; for example, the errors in BETAP and SIGMAP as generated by program AER3. It would be helpful if one could

store entire profiles (SIGMAP, BETAP, PSIG) in the database. Unfortunately, it would be beyond the capability of the current database package (REFLEX) in that it would require large amounts of memory and seriously affect access time. The current setup for the database on the AT&T 6300 at ARSL, with 640 kilobytes of random access memory, is approaching the maximum size available in random access memory for which the software can run without disk access. In view of this, it may be necessary to obtain a more capable software package and/or add more random access memory.

The effectiveness of any software is dependent on the hardware facility that is being used. At ARSL, the lidar data processing is currently dependent on the CCIT facilities. It would be a significant improvement to remove this dependence, provided adequate replacement facilities were available. Data currently stored on magnetic tapes could then be transferred to 5-1/4" diskettes or other suitable media and processed at the ARSL facility. All of the lidar software is written in Fortran, and compilers for Fortran are now available for most personal computers and workstations.

The raw data available includes a small but significant number of data sets that were acquired at an elevation angle 90 degrees only. There is a need to develop software to process this data. Slower sampling rates at the 90 degree angle used in this data may yield significant information

above 8 km, although lidar data does have significantly more noise at such high altitudes. All the data discussed in this work has only 255 samples per shot. Bruhns (1985) had changed the hardware setup to acquire 600+ samples per shot. This substantially increases the lidar ranging capability. Since only a few data sets were available after this conversion, the software has not been changed to accommodate it. It would be interesting to see the type of results that could be obtained if this change were incorporated into the software.

APPENDIX 1

THE DATABASES

APPENDIX 1.1

LIDAR DATA BASE: LISTING OF NUMBER 1 RUNS FOR SUCCESSFUL DAYS

DATE	TIME	FPNUM	OURNUM	TRYNUM	FLAGS
5/21/79	2020	047b	1001	1	rs
6/06/79	1935	049b	1003	1	rs
6/10/79	2000	052d	1004	1	rs
6/11/79	2000	060a	1006	1	rs
6/25/79	2010	069a	1010	1	rs
10/19/79	525	023A	1021	1	rs
10/25/79	1908	024a	1022	1	rs
11/05/79	2000	025A	1024	1	rs
11/27/79	2110	038C	1025a	1	rs
11/28/79	1815	039A	1026	1	rs
12/04/79	1920	044b	1028	1	rs
12/05/79	1830	045b	1029	1	rs
12/07/79	1855	078	1031	1	rs
12/10/79	1825	077	1032	1	rs
12/19/79	1910	057a	1035	1	rs
1/02/80	1955			1	rs
1/23/80	2200			1	rs
1/25/80	2025			1	rs
1/27/80	1955			1	rs
2/05/80	2125	264a	1045	1	rs
2/07/80	2040	263A	1044	1	rs
2/10/80	1930			1	rs
2/26/80	1840			1	rs
2/27/80	2000			1	rs
2/29/80	1835			1	rs
3/05/80	1925	265a	1050	1	rs
3/12/80	2005			1	rs
3/13/80	1910			1	rs
3/14/80	1928			1	rs
3/17/80	1905	213	1054	1	rs
3/19/80	1920	212	1055	1	rs
3/20/80	1940			1	rs
3/23/80	1910			1	rs
3/27/80	2115	171A	1062	1	rs
3/28/80	1924	211		1	rs
3/29/80	1935	210		1	rs
3/30/80	1905	201		1	rs
4/03/80	1900	055	1067	1	rs
4/04/80	1915	133A	1068	1	rs
4/05/80	2110	139A	1069	1	rs

DATE	TIME	FPNUM	OURNUM	TRYNUM	FLAGS
4/07/80	528	152B	1070	1	rs
4/07/80	1915	159D	1071	1	rs
4/08/80	1915	161D	1073	1	rs
4/09/80	1900	168G	1074a	1	rs
4/10/80	1850	202B	1075a	1	rs
4/11/80	1755	219E	1076	1	rs
4/16/80	2100	222C	1077	1	rs
4/17/80	2000	224B	1078	1	rs
5/07/80	2000			1	rs
5/16/80	1930			1	rs
5/20/80	2000			1	rs
5/21/80	2000			1	rs
5/22/80	2000	276	1085	1	rs
5/28/80	1945	277	1086	1	rs
5/29/80	2000			1	rs
5/30/80	2000	278	1088	1	rs
6/03/80	2020			1	rs
6/11/80	2000			1	rs
6/12/80	2000			1	rs
7/02/80	2010			1	rs
2/23/81	1840	026A	1099	1	rs
3/23/81	2030	072a	1101	1	rs
3/31/81	1900	036A	1103	1	rs
4/01/81	1845	050a	1104	1	rs
4/07/81	1920	137	1105	1	rs
4/29/81	1855	056	11000	1	rs
5/11/81	1950	053	1108	1	rs
5/12/81	2010	079d	1109	1	rs
5/13/81	1945	083c	1110	1	rs
5/18/81	1935	086b	1112	1	rs
6/03/81	2045	089e	1114	1	rs
6/11/81	2055	092a	1117	1	rs
6/16/81	1950	140a	1118	1	rs
5/05/82	2130	040A	1210	1	rs
5/09/82	1950	129B	1213	1	rs
5/20/82	2000	145a	1217	1	rs
6/01/82	2220	138B	1221	1	rs
6/09/82	2010	166	1222	1	rs
5/21/84	430	410A		1	rs
5/22/85	320	031G		1	rs
5/23/85	350	015Q		1	rs
5/24/85	340	035D		1	rs
5/24/85	2330	053D		1	rs

APPENDIX 1.2

LIDAR DATA BASE: LISTING OF NUMBER 1 RUNS FOR SUCCESSFUL DAYS

DATE	TIME	CALC	Sin	HMli	PHMl	AHMl	Shml	TAUPl
5/21/79	2020	196	30	2.50	1.60	1.70	16.29	0.01703
6/06/79	1935	130	20	3.00		3.25	19.25	0.03388
6/10/79	2000	296	50	2.50		3.50	81.90	0.08760
6/11/79	2000	204	50	2.50		3.00	70.91	0.04510
6/25/79	2010	130	20	3.00		3.35	10.25	0.06003
10/19/79	525	500	20	2.00	1.35	1.30	17.72	0.02930
10/25/79	1908	486	20	3.00	2.20	2.30	3.12	0.00740
11/05/79	2000	500	20	2.50	2.50	2.50	52.16	0.05921
11/27/79	2110	500	20	2.20	2.20	2.20	39.82	0.06543
11/28/79	1815	500	20	2.40	1.80	1.80	28.87	0.04008
12/04/79	1920	450	20	2.20	1.30	1.30	16.21	0.01952
12/05/79	1830	500	20	2.40	2.30	2.30	34.68	0.06740
12/07/79	1855	450	20	2.40	2.20	2.25	38.03	0.06970
12/10/79	1825	505	20	2.07	2.20	2.40	36.05	0.05260
12/19/79	1910	452	20	3.09	-1.00	3.10	31.86	0.07350
1/02/80	1955	450	20	2.00	1.50	1.50	18.52	0.03565
1/23/80	2200	463	20	2.50	-1.00	1.30	7.52	0.00563
1/25/80	2025	452	30	2.50	2.00	2.10	97.33	0.03926
1/27/80	1955	463	20	1.90	2.00	2.00	59.15	0.07490
2/05/80	2125	452	20	2.50	2.60	2.60	21.38	0.03550
2/07/80	2040	450	20	2.70	2.70	2.70	16.62	0.02960
2/10/80	1930	452	20	2.50	2.00	2.00	24.63	0.03150
2/26/80	1840	452	20	2.50	2.70	2.60	46.06	0.04330
2/27/80	2000	452	20	2.50	2.90	2.90	19.82	0.02070
2/29/80	1835	452	20	2.50	2.00	2.00	27.93	0.01995
3/05/80	1925	452	20	2.50	2.70	2.70	28.23	0.02558
3/12/80	2005	452	20	2.50	1.70	1.70	65.31	0.08780
3/13/80	1910	452	20	2.50	2.70	2.70	34.00	0.06090
3/14/80	1928	452	20	2.50	3.20	3.20	29.81	0.05100
3/17/80	1905	452	20	2.50	2.50	2.50	21.53	0.02128
3/19/80	1920	452	20	2.50	2.35	2.45	61.09	0.05101
3/20/80	1940	452	20	2.50	2.20	2.20	28.13	0.02477
3/23/80	1910	452	20	2.50	2.10	2.10	5.51	0.00999
3/27/80	2115	422	20	2.40	2.30	2.40	26.23	0.02889
3/28/80	1924	452	20	2.50	2.30	2.30	23.46	0.02757
3/29/80	1935	452	20	2.50	2.30	2.30	25.87	0.02944
3/30/80	1905	452	20	2.50	3.45	3.50	48.86	0.03511
4/03/80	1900	450	20	2.00	2.00	2.00	27.44	0.04814
4/04/80	1915	450	20	3.20	3.00	3.00	23.09	0.04980
4/05/80	2110	450	20	2.80	2.70	2.80	10.85	0.01818

DATE	TIME	CALC	Sin	HMli	PHMl	AHMl	Shml	TAUPl
4/07/80	528	422	20	2.90	3.00	2.90	40.03	0.07920
4/07/80	1915	450	40	2.50	1.80	2.50	42.52	0.05244
4/08/80	1915	450	20	3.80	3.70	3.70	37.44	0.06260
4/09/80	1900	450	20	2.50	2.50	2.60	26.84	0.04337
4/10/80	1850	450	20	2.50	2.60	2.80	22.59	0.04020
4/11/80	1755	450	20	2.00	2.00	2.00	17.01	0.07150
4/16/80	2100	450	20	2.70	2.80	3.00	29.13	0.07610
4/17/80	2000	450	20	4.00	4.50	4.50	29.90	0.12040
5/07/80	2000	452	20	3.50	3.60	3.50	6.06	0.02850
5/16/80	1930	452	20	2.50	3.00	3.00	28.19	0.04750
5/20/80	2000	452	20	2.50	4.50	4.50	12.26	0.03322
5/21/80	2000	452	20	2.50	4.20	4.20	9.91	0.02670
5/22/80	2000	452	20	2.40	3.00	3.00	22.70	0.04960
5/28/80	1945	452	20	2.40	3.20	3.30	55.04	0.05890
5/29/80	2000	452	20	2.50	2.60	2.65	11.58	0.01972
5/30/80	2000	452	20	2.50	2.60	2.90	33.71	0.05866
6/03/80	2020	452	20	2.80	2.90	2.90	10.73	0.03166
6/11/80	2000	452	20	2.50	3.50	3.50	10.86	0.02804
6/12/80	2000	452	20	2.50	3.80	4.00	31.79	0.04592
7/02/80	2010	452	20	2.50	3.30	3.30	7.64	0.02346
2/23/81	1840	450	20	3.00	3.00	3.00	31.88	0.03184
3/23/81	2030	450	20	2.70	2.80	2.70	24.71	0.02304
3/31/81	1900	450	20	3.10	3.00	3.10	24.42	0.02752
4/01/81	1845	452	20	3.10	3.75	3.60	29.50	0.02539
4/07/81	1920	452	20	3.10	2.50	2.20	24.73	0.02463
4/29/81	1855	450	30	2.20	2.20	2.80	65.68	0.04920
5/11/81	1950	450	20	3.00	3.50	3.50	17.83	0.03357
5/12/81	2010	450	20	3.50	3.50	3.50	24.77	0.10310
5/13/81	1945	450	20	3.50	3.50	3.50	49.77	0.07519
5/18/81	1935	450	20	3.00	3.00	3.00	14.14	0.01240
6/03/81	2045	450	20	5.60	5.30	5.60	12.50	0.02148
6/11/81	2055	450	20	2.40	2.80	2.80	18.32	0.02620
6/16/81	1950	400	20	3.30	3.30	3.30	28.50	0.03855
5/05/82	2130	400	20	3.90	3.30	3.80	44.05	0.10250
5/09/82	1950	400	20	2.00	2.00	2.00	25.15	0.11490
5/20/82	2000	350	20	3.30	3.30	3.30	39.81	0.03480
6/01/82	2220	400	20	2.58	2.75	2.60	35.26	0.04480
6/09/82	2010	400	20	2.40	2.60	2.60	31.37	0.04100
5/21/84	430	250	30	3.10	3.20	3.20	11.35	0.02080
5/22/85	320	400	40	2.80	2.90	3.00	38.69	0.03650
5/23/85	350	450	35	2.30	3.60	3.30	34.36	0.01240
5/24/85	340	325	30	2.10	2.10	2.10	26.92	0.02560
5/24/85	2330	400	20	1.60	1.60	1.60	66.46	0.02003

APPENDIX 1.3

LIDAR DATA BASE: LISTING OF NUMBER 1RUNS FOR SUCCESSFUL DAYS

DATE	TIME	Shm1	%D	TAUP1	%D	TAUPT	%D
5/21/79	2020	16.29	43	0.01703	43		
6/06/79	1935	19.25	37	0.03388	40		
6/10/79	2000	81.90	7	0.08760			
6/11/79	2000	70.91	15	0.04510	25	0.15230	
6/25/79	2010	10.25	21	0.06003	18	0.10410	
10/19/79	525	17.72	25	0.02930	11	0.04871	9
10/25/79	1908	3.12	255	0.00740	155	0.01060	
11/05/79	2000	52.16	8	0.05921	7	0.08480	6
11/27/79	2110	39.82	8	0.06543	4		
11/28/79	1815	28.87	27	0.04008	23		
12/04/79	1920	16.21	48	0.01952	28		
12/05/79	1830	34.68	18	0.06740	14		
12/07/79	1855	38.03	34	0.06970	25		
12/10/79	1825	36.05	40	0.05260	28		
12/19/79	1910	31.86	11	0.07350	8		
1/02/80	1955	18.52	163	0.03565	62	0.05430	55
1/23/80	2200	7.52	55	0.00563	71	0.01430	
1/25/80	2025	97.33	10	0.03926	22	0.07930	
1/27/80	1955	59.15	20	0.07490	17	0.12190	
2/05/80	2125	21.38	21	0.03550	16	0.05490	
2/07/80	2040	16.62	58	0.02960	70	0.04980	64
2/10/80	1930	24.63	21	0.03150	20	0.05140	
2/26/80	1840	46.06	31	0.04330	37	0.05670	
2/27/80	2000	19.82	21	0.02070	25	0.03440	
2/29/80	1835	27.93	21	0.01995	24	0.02970	
3/05/80	1925	28.23	6	0.02558	6	0.04300	
3/12/80	2005	65.31	6	0.08780	5	0.19660	
3/13/80	1910	34.00	22	0.06090	18	0.09370	
3/14/80	1928	29.81	13	0.05100	10	0.08870	
3/17/80	1905	21.53	29	0.02128	33	0.03390	
3/19/80	1920	61.09	10	0.05101	14	0.10290	
3/20/80	1940	28.13	31	0.02477	39	0.04170	
3/23/80	1910	5.51	109	0.00999	88	0.01430	
3/27/80	2115	26.23	14	0.02889	14	0.03890	14
3/28/80	1924	23.46	20	0.02757	21	0.04270	
3/29/80	1935	25.87	41	0.02944	42	0.04450	
3/30/80	1905	48.86	8	0.03511	12	0.08600	
4/03/80	1900	27.44	28	0.04814	18	0.07600	16
4/04/80	1915	23.09	18	0.04980	15	0.06640	13
4/05/80	2110	10.85	57	0.01818	50	0.02750	38
4/07/80	528	40.03	15	0.07920	17	0.10020	17

DATE	TIME	Shml	%D	TAUPl	%D	TAUPT	%D
4/07/80	1915	42.52	37	0.05244	32	0.10570	26
4/08/80	1915	37.44	22	0.06260	35	0.09920	27
4/09/80	1900	26.84	22	0.04337	16	0.06544	14
4/10/80	1850	22.59	18	0.04020	14	0.06190	12
4/11/80	1755	17.01	34	0.07150	16	0.09490	15
4/16/80	2100	29.13	16	0.07610	13	0.13490	10
4/17/80	2000	29.90	5	0.12040	4	0.17330	3
5/07/80	2000	6.06	79	0.02850	63	0.03980	
5/16/80	1930	28.19	18	0.04750	16		
5/20/80	2000	12.26	22	0.03322	17	0.07440	
5/21/80	2000	9.91	56	0.02670	41	0.04690	
5/22/80	2000	22.70	16	0.04960	12	0.09800	9
5/28/80	1945	55.04	12	0.05890	14	0.16510	9
5/29/80	2000	11.58	36	0.01972	29	0.03370	
5/30/80	2000	33.71	8	0.05866	6	0.09860	
6/03/80	2020	10.73	12	0.03166	10	0.05520	
6/11/80	2000	10.86	46	0.02804	31	0.04910	
6/12/80	2000	31.79	54	0.04592	57	0.09140	
7/02/80	2010	7.64	40	0.02346	29	0.04840	
2/23/81	1840	31.88	16	0.03184	22	0.03915	21
3/23/81	2030	24.71	15	0.02304	18	0.03450	14
3/31/81	1900	24.42	9	0.02752	12	0.04380	10
4/01/81	1845	29.50	22	0.02539	40	0.05518	28
4/07/81	1920	24.73	33	0.02463	49	0.04817	35
4/29/81	1855	65.68	46	0.04920	60	0.11810	53
5/11/81	1950	17.83	58	0.03357	63	0.04950	50
5/12/81	2010	24.77	11	0.10310	11	0.13520	10
5/13/81	1945	49.77	12	0.07519	20	0.11060	16
5/18/81	1935	14.14	41	0.01240	63	0.03583	36
6/03/81	2045	12.50	50	0.02148	95	0.02873	76
6/11/81	2055	18.32	68	0.02620	74	0.05442	55
6/16/81	1950	28.50	40	0.03855	61	0.05050	48
5/05/82	2130	44.05	16	0.10250	22	0.24200	14
5/09/82	1950	25.15	33	0.11490	17	0.19780	13
5/20/82	2000	39.81	16	0.03480	31		
6/01/82	2220	35.26	18	0.04480	20	0.12300	12
6/09/82	2010	31.37	34	0.04100	34	0.09500	23
5/21/84	430	11.35	29	0.02080	29	0.02900	25
5/22/85	320	38.69	28	0.03650	40		
5/23/85	350	34.36	80	0.01240	160		
5/24/85	340	26.92	39	0.02560	37	0.09460	18
5/24/85	2330	66.46	21	0.02003	30	0.05399	27

APPENDIX 1.4

LIDAR DATA BASE: LISTING OF NUMBER 1 RUNS FOR SUCCESSFUL DAYS

DATE	TIME	RAWP	AIMP	EDTP	PITP	PITG	AERP	AERG
5/21/79	2020	y		y	y	y	y	y
6/06/79	1935	n	n	n	n	n	y	y
6/10/79	2000	n	n	n	n	n	y	y
6/11/79	2000						y	n
6/25/79	2010	n	n	n	n	n	y	y
10/19/79	525	n	y	y	y	y	y	y
10/25/79	1908	y	y	y	y	y	y	y
11/05/79	2000	n	n	n	y	y	y	y
11/27/79	2110	n	y	n	y	y	y	y
11/28/79	1815	y	y	y	y	y	y	y
12/04/79	1920	n	y	y	y	y	y	y
12/05/79	1830		y	y	y	y	y	y
12/07/79	1855	n	y	y	y	y	y	n
12/10/79	1825	n	y	y	y	y	y	n
12/19/79	1910		y	y	y	y	y	n
1/02/80	1955		y		y	y	y	y
1/23/80	2200	n	y	n	y	y	y	y
1/25/80	2025	n	y	n	y	y	y	y
1/27/80	1955	n	y	n	y	y	y	y
2/05/80	2125		y	y	y	y	y	y
2/07/80	2040		y	y	y	y	y	y
2/10/80	1930	y	n	n	y	y	y	y
2/26/80	1840		y	y	n	y	y	y
2/27/80	2000	y	y	n	y	y	y	y
2/29/80	1835	y	y	n	y	y	y	y
3/05/80	1925	y	y	n	y	y	y	y
3/12/80	2005		y		y	y	y	y
3/13/80	1910	n	y	n	y	y	y	y
3/14/80	1928	n	y	n	y	y	y	y
3/17/80	1905	n	y	n	y	y	y	y
3/19/80	1920	n	y	n	y	y	y	y
3/20/80	1940	n	y	n	y	y	y	y
3/23/80	1910	n	y	n	y	y	y	y
3/27/80	2115	y	y	y	y	y	y	y
3/28/80	1924	y	y	n	y	y	y	y
3/29/80	1935	n	y	n	y	y	y	y
3/30/80	1905	y	y	n	y	y	y	y
4/03/80	1900	n	y	y	y	y	y	y
4/04/80	1915	n	y	n	y	y	y	y
4/05/80	2110		y		y	y	y	y

DATE	TIME	RAWP	AIMP	EDTP	PITP	PITG	AERP	AERG
4/07/80	528	y	y	n	y	y	y	y
4/07/80	1915	n	y	n	y	y	y	y
4/08/80	1915	n	y	n	y	y	y	y
4/09/80	1900	y	y	n	y	y	y	y
4/10/80	1850		y		y	y	y	y
4/11/80	1755	y	y	n	y	y	y	y
4/16/80	2100		y		y	y	y	y
4/17/80	2000	n	y	n	y	y	y	y
5/07/80	2000		y		y	y	y	y
5/16/80	1930		y		y	y	y	y
5/20/80	2000		y		y		y	y
5/21/80	2000		y		y	y	y	y
5/22/80	2000	n	y	y	y	y	y	y
5/28/80	1945	n	y	n	y	y	y	y
5/29/80	2000	n	y	n	y	y	y	y
5/30/80	2000	n	y	n	y	y	y	y
6/03/80	2020	n	n	n	n	y	y	y
6/11/80	2000	y	y	n	y	y	y	y
6/12/80	2000	n	y	n	y	y	y	y
7/02/80	2010	y	y	n	y	y	y	y
2/23/81	1840		y	y	y	y	y	y
3/23/81	2030	n	y	n	y	y	y	y
3/31/81	1900	n	y	n	y	y	y	y
4/01/81	1845	n	y	y	y	y	y	n
4/07/81	1920	n	y	y	y	y	y	n
4/29/81	1855	n	n	n	y	y	y	y
5/11/81	1950	n	n	y	y	y	y	y
5/12/81	2010	n	y	n	y	y	y	y
5/13/81	1945	n	y	y	y	y	n	y
5/18/81	1935	n	y	n	y	y	y	y
6/03/81	2045	n	y	n	y	y	y	y
6/11/81	2055	n	y	y	y	y	y	y
6/16/81	1950	n	y	n	y	y	y	y
5/05/82	2130			y	y			
5/09/82	1950		y	y	y	y	y	n
5/20/82	2000	n	y	n	y	y	y	y
6/01/82	2220		y	y	y	y	y	y
6/09/82	2010		y	y	y	y	y	y
5/21/84	430	n	y	n	y	y	y	y
5/22/85	320	y	y	n	y	y	y	y
5/23/85	350		y		y	y	y	y
5/24/85	340	y	y	y	y	y	y	y
5/24/85	2330	n	y	n	y	y	y	y

APPENDIX 1.5

LIDAR DATA BASE: LISTING OF NUMBER 1 RUNS FOR SUCCESSFUL DAYS

DATE	TIME	8473G	8413G	8449K	8462H	8433D	3283D
5/21/79	2020	y1				y46	
6/06/79	1935	y2				y47	
6/10/79	2000	y3				y48	
6/11/79	2000	y4				y49	
6/25/79	2010	y9				y54	
10/19/79	525						y52
10/25/79	1908	y12					y53
11/05/79	2000			y38			y54
11/27/79	2110						y56
11/28/79	1815	y13					y57
12/04/79	1920						y58
12/05/79	1830						y59
12/07/79	1855						y61
12/10/79	1825						y62
12/19/79	1910						y65
1/02/80	1955			y27		y32	
1/23/80	2200				y6	y33	
1/25/80	2025				y7	y34	
1/27/80	1955			y28	y8	y35	
2/05/80	2125		y2	y23		y20	
2/07/80	2040		y1	y24		y21	y66
2/10/80	1930		y21	y25		y43	
2/26/80	1840			y29	y11	y24	
2/27/80	2000	y14		y26		y22	
2/29/80	1835	y15				y23	
3/05/80	1925		y3	y11		y1	
3/12/80	2005			y7	y9	y36y44	
3/13/80	1910			y8	y10	y37y45	
3/14/80	1928		y13	y12		y2	
3/17/80	1905		y14	y15		y3	
3/19/80	1920		y15	y1		y4	
3/20/80	1940		y22	y2		y5	
3/23/80	1910		y17			y6	
3/27/80	2115		y23	y3		y7	
3/28/80	1924		y18	y4		y8	y69
3/29/80	1935		y19	y5		y9	y68
3/30/80	1905		y20	y6		y10	y67
4/03/80	1900		y24	y36y48		y11	
4/04/80	1915		y25	y49		y12	
4/05/80	2110		y26	y37y50		y13	

DATE	TIME	8473G	8413G	8449K	8462H	8433D	3283D
4/07/80	528		y8	y39y51		y14	
4/07/80	1915		y9				
4/08/80	1915		y11	y53		y15	
4/09/80	1900		y4	y42y54		y16	
4/10/80	1850		y5	y43y55		y17	
4/11/80	1755		y12	y58y59		y18y55	
4/16/80	2100		y6	y18		y19	
4/17/80	2000			y60y61	y15	y40y56	
5/07/80	2000		y34	y20		y25	
5/16/80	1930		y33	y31		y26	
5/20/80	2000		y35	y32	y1	y27	
5/21/80	2000			y30	y14	y39	
5/22/80	2000			y33	y2	y28	
5/28/80	1945				y3	y29	
5/29/80	2000				y4	y30	
5/30/80	2000			y35	y5	y31	
6/03/80	2020				y12	y41	
6/11/80	2000		y27				
6/12/80	2000		y28				
7/02/80	2010		y31			y42	
2/23/81	1840			y45y56			y29
3/23/81	2030			y46y57			
3/31/81	1900			y47			y32
4/01/81	1845						y33
4/07/81	1920						y34
4/29/81	1855						y36
5/11/81	1950						y37
5/12/81	2010			y62y63		y57	y38
5/13/81	1945						y39
5/18/81	1935						y47
6/03/81	2045						y41
6/11/81	2055						y43
6/16/81	1950						y44
5/05/82	2130						y12
5/09/82	1950						y15
5/20/82	2000						y17
6/01/82	2220						y19
6/09/82	2010						y20
5/21/84	430						y70
5/22/85	320					y61	y74
5/23/85	350					y62	y75
5/24/85	340					y63	y76
5/24/85	2330					y64	y77

APPENDIX 1.6

LIDAR DATA BASE
CONDITION: FLAGS = FS (FAILED SLANT PATH)

DATE	TIME	FPNUM	OURNUM	TRYNUM	FLAGS
6/12/79	1945	059d	1005	1	fs
6/16/79	2225	063h	1007	1	fs
6/18/79	1940	064f	1008	1	fs
6/19/79	2000	068b	1009	1	fs
12/06/79	1850	046b	1030	1	fs
12/13/79	2015	076	1033	1	fs
12/14/79	2050	067a	1034	1	fs
4/08/80	1630	160d	1072	1	fs
4/24/81	1915	073a	1106	1	fs
6/09/81	2155	119	1115	1	fs
6/10/81	2100	091a	1116	1	fs
11/24/81	1900	143a	1127	1	fs
2/02/82	1830	142a	1123	1	fs
4/24/82	1000	019b	1204	1	fs
4/25/82	630	021b	1205	1	fs
5/03/82	2000	114c	1208	1	fs
5/06/82	500	043B	1212	1	fs
5/15/82	1630	120A	1214	1	fs
6/12/82	2030	167	1223	1	fs
2/16/84	2100	393		1	fs
3/09/84	1930	394		1	fs

APPENDIX 1.7

LIDAR DATA BASE
CONDITION: FLAGS = ES (EQUIPMENT ERROR)

DATE	TIME	FPNUM	OURNUM	TRYNUM	FLAGS
6/07/79		041b	1027	0	es
8/27/79		117	1013	0	es
10/14/79		004e	1020	0	es
2/07/80		262a	1040	0	es
4/09/80		165d	1074	0	es
4/10/80		170g	1075	0	es
4/10/80		207d	1075b	0	es
5/05/81		074d	1107	0	es
11/02/81		141a	1120	0	es
5/19/82		116a	1215	0	es
7/01/82		189	5009	0	es

APPENDIX 1.8

LIDAR DATA BASE
CONDITION: FLAGS = S (SLANT PATH, NOT PROCESSED)

DATE	TIME	FPNUM	OURNUM	TRYNUM	FLAGS
6/01/79	2005	048b	1002	1	s
6/16/80	2000			1	s
3/22/81	2045	071a	1100	1	s
3/24/81	2000	031A	1102	1	s
10/06/82	1900	103k		0	s
10/27/82	2020	058h		0	s
11/01/82	2000	217A		1	s
11/03/82	1940	215A		1	s
6/09/83	2000	075g		0	s
2/10/85	1950	068F		0	s
2/12/85		069D		0	s
5/13/85	405	041F		1	s
5/15/85	315	048F		1	s
5/18/85	410	052I		1	s

APPENDIX 1.9

LIDAR DATA BASE
CONDITION: FLAGS = V (VERTICAL DATA ONLY)

DATE	TIME	FPNUM	OURNUM	TRYNUM	FLAGS
6/11/80	2020			1	v
7/02/80	2040			1	v
4/25/82	830	033B	1206	1	v
5/03/82	2000	130b	1209	1	v
5/05/82	2215	042e	1211	1	v
5/24/82	1945	144A	1218	1	v
11/03/82	2010	214A		1	v
5/21/84	720	394		1	v

APPENDIX 1.10

LIDAR DATA BASE
CONDITION: FLAGS = Z (SIMULATION DATA ONLY)

DATE	TIME	FPNUM	OURNUM	TRYNUM	FLAGS
11/23/81		065C	1119	1	z
1/06/82		111b	1121	1	z
3/09/82	2100	147a	1200	1	z
3/09/82	2130	148a	1201	1	z
5/13/84	0	393		1	z
6/07/84	1510	393		1	z

APPENDIX 1.11

LIDAR DATA BASE
CONDITION: FLAGS = C (CALIBRATION DATA ONLY)

DATE	TIME	FPNUM	OURNUM	TRYNUM	FLAGS
6/26/79	1610	070a	1011	1	c
9/07/79	1130	118	1000	1	c
11/05/79		016a	1023	0	c
11/05/79	1845	017a	1025	1	c
3/20/80	1850	018a	1058	1	c
3/21/80	1015	054	1060	1	c
1/23/81	1030	001b	1098	1	c
5/26/81	1145	061	1113	1	c
1/06/82	1200	110b	1122	1	c
3/12/82	1000	199	1202	1	c
4/23/82	1600	200	1203	1	c
5/10/84	900	394		1	c
7/06/85	1040	034G		1	c

APPENDIX 1.12

CALIBRATION DATA BASE: PARTIAL LISTING

DATE	FPYNUM	OURNUM	AVGCALCON
6/26/79	070A	1011	0
9/07/79	118	1000	600.5
11/05/79	016A	1023	0
11/05/79	017A		505
3/20/80	018A	1058	448
3/21/80	054	1060	438
1/23/81	001B	1098	452.5
5/26/81	061	1113	443.5
1/06/82	110B	1122	0
3/12/82	199	1202	348.5
4/23/82	200	1203	397.5
5/10/84	394		236.5
7/06/85	034G		587

APPENDIX 1.13

CALIBRATION DATA BASE: PARTIAL LISTING

Date	Time	OURNUM	3283D	8413G	8433D	8449K	8462H	8473G
6/26/79	1610	1011	y					
9/07/79	1130	1000	y					y
11/05/79		1023						
11/05/79	1845		y					y
3/20/80	1850	1058						
3/21/80	1015	1060		y				
1/23/81	1030	1098	y					
5/26/81	1145	1113	y					
1/06/82	1200	1122	y					
3/12/82	1000	1202	y					
4/23/82	1600	1203	y					
5/10/84	900							
7/06/85	1040		y				y	

APPENDIX 1.14

CALIBRATION DATA BASE: PARTIAL LISTING

Date	Time	Rsub	Tubrs	GrIB	GrIIB	GrICa	GrIICa	AvgCa
6/26/79	1610							0
9/07/79	1130	1000	3.7456	2	2	622	579	600.5
11/05/79								0
11/05/79	1845	1000	3.7456	2	2	498	512	505
3/20/80	1850	1000	3.7456	2	5	444	452	448
3/21/80	1015	1000	3.7456	2	5	454	422	438
1/23/81	1030	1000	3.7456	5	10	484	421	452.5
5/26/81	1145	1000	3.7456	5	10	489	398	443.5
1/06/82	1200							0
3/12/82	1000	1000	3.7456	5	10	355	342	348.5
4/23/82	1600	1000	3.7456	2	5	396	399	397.5
5/10/84	900	1000	3.7456	10	5	264	209	236.5
7/06/85	1040	1000	3.7456	5	10	549	625	587

APPENDIX 2

FLOWCHARTS OF PROGRAM AER3

APPENDIX 2.1

FLOWCHART OF PROGRAM AER3

declaration of variables and arrays

call READIN - read data input from AIMLESS and control file

call NORM - range normalize the signal

call RAYLEE - determine Rayleigh X-section parameters

call GROUND - extend the signal to ground (surface)

call SOLVE - solve the integrated slant path lidar equations

call VERTPRF(1) - obtain extinction and backscatter profiles

call TOPLYER - extend the solution above 7 km, obtain X-sections above 7 km

call PRINTF - print final results, obtain particulate backscatter profiles of individual angles, plot extinction profile

APPENDIX 2.2

Flowchart of subroutine READIN

begin

initialize variables

open random access file for future "write" operations

read control inputs
- switches to decide plotting information
- solution inputs: lidcal, tprad, hnurd, hmix, sinit
- number of solution layers
- heights of solution layers
- mcut array

print data set-related numbers, e.g. month, day, year, time.

end

APPENDIX 2.3

Flowchart for subroutine NORM

Begin

Set maximum number of angles, and maximum number samples per shot.

Count strings of non-initial, contiguous data points that are zero. If > 9 zeroes per string are found, that angle is zeroed out; it is assumed that the shot is bad from this point on.

Ensure that data points are zero for the initial non-overlap range of Lidar for each angle.

Set vertical height resolution to 0.03 km.

Normalize all slant path signal to vertical height intervals of 0.03 km.

If mcut values are specified, zero out the appropriate angles above the heights specified.

Interpolate the signal over the zeroes at spots where the gainswitches were.

end

APPENDIX 2.4

Flowchart for subroutine RAYLEE

```
Begin
- Declare data statements for pressure (in mB) and
temperature (in degree Celsius) values as a function of
height
- Initialize variables and constants (SIGMAR = extin.
Rayleigh, ZSURF= ht of Tucson from sea level in kilometers,
TR(1) = Rayleigh transmission at ground level in Tucson.)
- Compute BRAOB (raylee extin.) values at 1 km. from sea
level, up to 26 km., using the formula
Rayleigh extin. = 1.2833 (10 E-3) *
                  Pressure(mb)/Temp(deg.K)
- set up ZTEMP (height differential from ground level to
1st BRAOB value available). Calculate the slope of the 1st
two BRAOB values, assuming extinction is of an exponential
form. HR = (1/ slope).
   Loop:
     At each height Z(i),
     if z(i) .lt. next ht for BRAOB,
           then calculate BR (Rayleigh extin.) by
           exponential interpolation.
           and BETAR = (3/8pi) * BR; where BETAR =Rayleigh
           backscatter.
     else if z(i) .eq. next ht for BRAOB
           then BR = BRAOB
           and BETAR = (3/8pi) *BR; as above.
     else
           recompute HR, and ZTEMP
     endif
     if (just computed a new BR)
           then get DTAUR (incremental Rayleigh optical
           depth by
           DTAUR = (BR(i-1) - BR(i))/ HR, where
           HR = (1/slope) of Rayleigh extinction curve.
     endif
     get new TR (Rayleigh transmission).
     If switch nfac is zero then
           print out value BR, TR, BETAR
   End Loop.
End
What gets computed:
From height 1 to 255 ( 0 to 7.65 km)
BR = Rayleigh  extinction values
TR = Rayleigh transmission values
BETAR = Rayleigh backscatter value
```

APPENDIX 2.5

Flowchart for subroutine GROUND

Declare arrays JN and TAU. JN is an array to hold indexes of angles in descending order of zenith values, TAU holds particulate optical depth values for an assumed low altitude atmosphere for now, later it will hold recomputed values of particulate optical depth from 0 km to 7.65 km.

Order the 6 largest zenith angles in descending order of magnitude, using JN to hold indexes into PSIG, the signal array.

Extrapolate the 3 largest zenith angles to ground, using the lidar equation and an assumed low altitude atmosphere TAU values.

Begin Loop:

Select an angle that has nonzero psig values in the first 50 steps.

print out pertinent data about selected angle, selected height, etc.

compute (lidcal * total beta) product for the angle at the first available height, and at a height 9 levels above; then compute average (lidcal * total beta) product over the 9 values.

use the (lidcal * total beta) product just computed to calculate psig values from the lowest available signal to ground.

get PSINT, the sum of psig from ground to 1 km.

End loop.

Get PSL, the sum of PSINT for all three angles.
Compute BRT, the ratio of integrated signal in the lowest 60 meters to the integrated signal from ground to 1 km. (BRT is later used in subroutine SOLVE).

APPENDIX 2.6

Flowchart for subroutine SOLVE

```
Begin
Call INT (using an initial guess of S and particulate optical
depth at ground = 0), get particulate optical depth at 1 km.
   For each layer to be solved for:
      determine which angles to use (data must be present
      throughout the layer).
      MEASUREMENT INTEGRAL CALCULATIONS START.
         For each angle
            integrate from bottom to top of layer
            add contribution to the coefficient matrix
         end for
      solve for alpha(prime), tau(prime) according to eq.
      2.23 and 2.24 (Spinhirne).

      check for value of determinant. If too small, stop.
      adjust alpha(prime) and tau(prime), check gtau, adjust
      alpha(prime) and tau(prime) again if necessary.
      compute AO, and TO.
      check for -ve transmission and adjust TO.
      If alpha (prime) or tau(prime) are too large, redo the
      measurement integral above.
      Call ERRORS; get the errors in (1/S), particulate
      optical depth, and S.

      If this is the first layer then
         call INT; get parti. optical depth at 0 km.
            REPEAT until TAU(1) condition is met as below:
               compute BTAU, a tau(1) value by scaling tau
               (at 1 km) value by the ratio BRT (previously
               computed in GROUND).
               If this tau(1) is not within 0.0005 of BTAU,
               then adjust tau(1e) and toi, and redo the
               measurement integral
               Call INT; get TAU values from 1 km through to
               0 km.
               Extend PSIG to ground using the new values of
               TAU.
            end REPEAT
      end IF

      print results: height of new layer, S ratio, etc.
      set up parameters at the top of current layer, to get
      ready for the next layer.
   end FOR
END
```

APPENDIX 2.7

Flowchart for subroutine INT

A subroutine to calculate TAU (particulate optical depth) between two heights, given the S ratio, the particulate optical depth at one of the heights, and the two height values. TAU can be computed either upward or downward, and either at all intermediate heights, or only at the boundary.

```
Begin

   Initialize variables

   Loop: for each height
      calculate various terms required in the equation
      2.27 of Spinhirne's dissertation: I(z prime, gamma),
      b, TsubO, gamma, Tsub*, etc.

      If (ISP .gt. 0), then skip the next part and repeat
      iteration for the next height. (ISP is a switch that
      allows calculation of TAU either at all intermediate
      heights in a layer, or at the end height only.)

      Repeat until:
         Evaluate tau(prime) according to equation 2.27,
         (Spinhirne).

         Modify TO (the new particulate transmission).

         If tau(prime) is .lt. 0.00001, then repeat the
         REPEAT loop.

      End Repeat.

      get new particulate optical depth, TAU(L) = -LN(TO)

   End Loop.

End
```

APPENDIX 2.8

Flowchart for subroutine ERRORS

Begin

Initialize variables: S (the new S ratio that has been computed, TAO, TAW (particulate optical depths at the bottom and the top of the current layer, respectively), X (3*s/8*pi), etc.

(Error calculations done using formulas in section 2.4 of Spinhirne's dissertation.)

If there are too few angles, results are zero, and skip to the end of the subroutine.

For each angle
  initialize variables
  For each height in the layer
    running sum of terms required for getting I(gamma) according to eq. 2.15

  compute I(gamma)
  compute the mean of the variance of the measurements for I(gamma), according to equation 2.43 (Spinhirne). This term is partially computed.

Compute DAO =std.dev. of AO (AO=1/s) according to eq. 2.29, using 2.37 and 2.43. Compute DTAU = std. dev. of particulate optical depth, using 2.38 and 2.43, in a fashion similar to 2.29. Compute DS = std. dev. of S ratio
Assign SR(ik) =S, SE(ik)= DS, and ERS=DS/S

End

APPENDIX 2.9

Flowchart for subroutine VERTPRF

```
Begin

call INT: get TAU(L), tau particulate values from 1 km
through to ground.

   For each level from the lowest available signal to 1 km
      calculate SIGP (particulate extinction) by
      differentiating TAU
      calculate BETP by using SIGP/BETP=S
   end For

   For each next solution layer
      Setup initial conditions
      Call INT: get TAU(L) at each level within this layer
         For each height level in this layer
            from bottom to top,
            calculate SIGP(L) by differentiating TAU
            calculate BETP(L) by using SIGP/BETP=S
            If switch prntopt = 1, print the results
         end For
   end For

End
```

APPENDIX 2.10

Flowchart for subroutine TOPLYER

```
Begin
-declare data statement for BETZ(37), values of Rayleigh
backscatter in 0.5 km steps, from 7 km to 25 km.
-setup initial conditions
-call INT: get TAU(L), particulate optical depth, from top of
the solution layer (z2) through to the top of the signal
(ztop)
   For each level from z2 to Ztop
      get SIGP by differentiating TAU (delta_TAU/hdelta)
      get BETP by using SIGP/BETP = S
      get BPI = sum of BETP
   end For
get BPI = BPI * hdelta = integral (BETP), from z2 to Ztop
   For each level from 200 (6km) to ztop
      calculate BRT = average (BETP/BETR) ratio
   end For
   For each km from 1, 2, or 3 km to 25 km
      get BSR = a ratio for betp/betr
      get BPINT = sum of particulate backscatter from 1 km to
         25 km
      get BETT = BSR * BETZ = particulate backscatter
      get SIGT = BETT * S ratio
      get TAUP = (integral of beta parti. from z2 to top of
         atmosphere * 0.5 km) * S ratio + TWR
      where TWR = particulate optical depth at z2
   end For
get BPI = integral of particulate backscatter from z2 to top
of atmosphere.
   If no radiometer optical depth (TPRAD) given, then
      get TPRAD = TWR + (S * BPI)
      print results
   Else if radiometer optical depth is given, then
      SN = new S for upper atmosphere = (TPRAD - TWR)/ BPI
      If SN is too much different from last S (S_top), then
         go back to top of routine to iterate.
      get SE, error in S ratio for the upper atmosphere
      print results
   endif
END
```

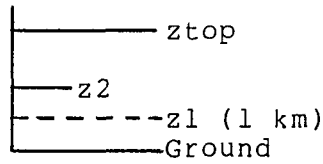

APPENDIX 2.11

Flowchart for subroutine PRINTF

```
Begin
   Setup initial conditions
   compute factor SMF for getting mass concentration from
   extinction cross section
   setup variables

   For each height from lowest available signal height
   to topmost available signal height
      setup conditions
      calculate taupt (taup + taur)
      For each angle
         solve lidar equation for the product c*betat
         get sum of c*betat

      get average c*betat
      get betat and betap

      calculate error quantities (equations 2.46, 2.47,
      2.48 in Spinhirne [1977], such as variance and
      standard deviation of c*betat, betap, and sigmap.
      calculate betap, and sigmap (from betap and S)

      print results

   call gtbeta(betp, bperr): gtbeta solves for betap
   values for individual angles using 2 different methods

   write results to array DIO (for an output file), using
   "writms" call.

   calculate and print error analysis at every 0.5 km,
   averaged over 5 height levels, for sigp, betp,
   taup, etc.

   call average: subroutine to set up data for monthly
   averages of parameters

   setup variables for plotting calls
   call profil (plot sigmap profile)
   call prfln (plot sigmar profile)
   call profil (call hi altitude profile if specified)

end
```

APPENDIX 2.12

Flowchart for subroutine AVERAGE

```
Begin
   Initialize variables

   For each 0.2 km, starting at 0.2 km to the top of
   available signal
      define error in taup (do this only once)

      compute save(i) through save(i+6): these are
      ht(km), betap, sdbetap, sigmap, sdsigmap, taup,
      and error in taup.  Each of these is an average of
      values at 3 heights, except the error in taup

   For every 0.5 km starting at 6.5 km,
      go to end of for loop if values already computed
      at this height

      compute save(i) through save(i+6), similar to the
      FOR loop above, except use values computed in
      TOPLYER subroutine

   Print save(i) values

   Write to logical file 1 the results (the avg file)

   Write a subset of results to logical file 2. (the ebt
   file)

End
```

LIST OF REFERENCES

Bruhns, T. V., 1985: University of Arizona Monostatic Lidar Data Acquisition System Software Manual. Tucson, Electrical Engineering Department, University of Arizona, 150 pp.

Bruhns, T. V., 1985: Hardware and Software for a Computer Controlled Lidar System. Ph.D. Dissertation, Department of Electrical and Computer Engineering, The University of Arizona, 192 pp.

Reagan, J. A., 1983: Measurements of Optical Properties of Particulates in an Arid Region, Final Report, submitted to the U. S. Army Research Office.

Reagan, J. A., Spinhirne, J. D., Byrne, D. M., Thomson, D. W., de Pena, R. G. and Mamane, Y., 1977: Atmospheric Particulate Properties Inferred from Lidar and Solar Radiometer Observations Compared with Simultaneous In Situ Aircraft Measurements: A Case Study, J. Appl. Meteor., Vol. 16, No. 9, September 1977, 910-928.

Reagan, J. A., Spinhirne, J. D., Bruhns, T. V. and Peck, R. L. 1976: Digital Detector for Monitoring Lidar Output Energy, Rev. Sci. Instrum., Vol.47, No. 12, December 1976, 1527-1530.

Reagan, J. A., Apte, M. V., Ben-David, A. and Herman, B. M., 1984b: Assessment of Aerosol Extinction to Backscatter Ratio Measurements made at 694.3 nm in Tucson, Arizona. Proc. 1984 CRDC Scientific Conference on Obscuration and Aerosol Research, 505- 516, CRDC, Aberdeen Proving Ground, MD, June 25-29, 1984; submitted to Aerosol Science and Technology, 1987.

Reagan, J. A., Apte, M. V., Bruhns, T. V. and Youngbluth, O., 1984a: Lidar and Balloon-Borne Cascade Impactor Measurements of Aerosols: A Case Study. Aerosol Science and Technology, 3, 259-275.

Russell, P. B., McCormick, M. P., Swissler, T. J., Chu, W. P., Livingston, J. M., Fuller, W. H., Rosen, J. M., Hoffman, D. H., McMaster, L. R., Woods, D. C. and Pepin, T. J., 1981: Satellite and Correlative Measurements of The Stratospheric Aerosol. II: Comparison of Measurements Made by Sam II, Dustsonde and An Airborne Lidar. Journal of the Atmospheric Sciences, Vol. 38, No. 6, June 1981, 1295-1312.

Spinhirne, J. D., 1974: Development of a Digital Data Acquisition System for Monostatic Lidar. M.S. Thesis, Department of Electrical Engineering, The University of Arizona, 54 pp.

Spinhirne, J. D., Reagan, J. A. and Herman, B. M., 1980: Vertical Distribution of Aerosol Extinction Cross Section and Inference of Aerosol Imaginary Index in the Troposphere by Lidar Technique. J. Appl. Meteor., Vol. 19, No. 4, April 1980, 426-438.

Spinhirne, J. D., 1977: Monitoring of Tropospheric Aerosol Optical Properties by Laser Radar. Ph.D. Dissertation, Department of Atmospheric Sciences, The University of Arizona, 176 pp.